Models for Thermal and Mechanical Monitoring of Power Transformers

Von der Fakultät
Informatik, Elektrotechnik und Informationstechnik
der Universität Stuttgart
zur Erlangung der Würde eines

Doktor-Ingenieurs (Dr.-Ing.)
genehmigte Abhandlung

vorgelegt von
Rummiya Vilaithong
aus Chiang Mai, Thailand

Hauptberichter: Prof. Dr.-Ing. Stefan Tenbohlen
Mitberichter: Prof. Dr.-Ing. Armin Schnettler, RWTH Aachen

Tag der mündlichen Prüfung:
01.07.2011

Institut für Energieübertragung und Hochspannungstechnik
der Universität Stuttgart

Acknowledgement

Finally, it is there. It is in your hand, the representation of my research work at Institute of Power Transmission and High Voltage Technology (IEH), University of Stuttgart.

I am deeply indebted to my supervisor Professor Dr.–Ing. Stefan Tenbohlen. His encouragement, suggestions and visions motivate me to reach the success.

It is an honour for me to Professor Dr.–Ing. Armin Schnettler from RWTH Aachen. He was the first one who opened the world of the German research system to me.

This thesis would not have been possible without the great cooperation work with Areva Energietechnik Mönchengladbach. I would like to thank all colleagues there.

It is a pleasure to thank also all of my colleagues and a number of students at the University of Stuttgart. Without their companion in work life and social life, my time would be more difficult.

Many thanks here to Dr. Matthew O.T. Cole for this professional scientific and language editing,

I owe very special thanks to the special one who always gives me a nice, warm support and many useful advices, Dr.–Ing. Stephan Pötschke.

To my family in Thailand, I am very grateful to them for their understanding that I have to spend time with my work instead of them. I would like to show my gratitude especially to the role model of my work life, my father, Dr. Thiraphat Vilaithong.

Lastly, I offer my regards and blessings to Germany for its well-organized academic system. It persuades me to believe that the opportunity in education is always opened for everyone who makes an effort.

In the name of an electrical engineer, I would like to dedicate my hard work along these years to the people who still live without the electricity.

Rummiya Vilaithong

Autumn in Düsseldorf, September 2011

Table of Contents

Abstract

At present, for economic reasons, there is an increasing emphasis on keeping transformers in service for longer than in the past. A condition-based maintenance using an online monitoring and diagnostic system is one option to ensure reliability of the transformer operation. The key parameters for effectively monitoring equipment can be selected by failure statistics and estimated failure consequences. In this work, two key aspects of transformer condition monitoring are addressed in depth: thermal behaviour and behaviour of on-load tap changers.

In the first part of the work, transformer thermal behaviour is studied, focussing on top-oil temperatures. Through online comparison of a measured value of the top-oil temperature and its calculated value, some rapidly developing failures in power transformers such as malfunction of the cooling unit may be detected.

Predictions of top-oil temperature can be obtained by means of a mathematical model. Long-term investigations on some dynamic top-oil temperature models are presented for three different types of transformer units. The last-state top-oil temperature, load current, ambient temperature and the operating state of pumps and fans are applied as inputs of the top-oil temperature models. In the fundamental physical models presented, some constant parameters are required and can be estimated using a least-squares optimization technique. Multilayer Feed-forward and Recurrent neural network models are also proposed and investigated. The neural network models are trained with three different Backpropagation training algorithms: Levenberg-Marquardt, Scaled Conjugate Gradient and Automated Bayesian Regularization.

The effect of varying operating conditions of the cooling units and the non-steady-state behaviour of loading conditions, as well as ambient temperature are noted. Results show a sophisticated temperature prediction is possible using the neural network models that is generally more accurate than with the physical models. The results are sufficient to justify applying the neural network model in the online monitoring system.

In the second part of this work, an acoustic measuring system for online condition monitoring of the tap changer operation is developed. Transformers with on-load tap-changer (OLTC) are important elements in modern power systems since they allow voltage to be maintained under load changes. Being a mechanical device that undergoes repeated operation, OLTCs have a high failure rate compared to other electricity distribution equipment. Failures of an OLTC may cause damage to other parts of the complete transformer unit. During the operation of an OLTC a series of mechanical and electrical events produce distinctive vibration and noise patterns. In principle, an analysis of these typical vibration signatures should reveal different aspects and phases of tap changer operation. The transition time interval during the tap change is expected to be constant as long as no fault appears.

In this work, the sequences of movable main contacts and transition contacts in the diverter switch during the transition phase are studied. Vibration signals through the tap change process are detected by a piezoelectric sensor coupled to an amplifier. The captured vibration signatures are analyzed. The tap change switching time interval is determined. This specific time interval is defined as a characteristic time of the tap change process. It is sent by means of an output current to an online monitoring system. Together with the statistical methods named control chart and Shewhart, the characteristic time is applied as a criterion of the tap changer monitoring. Results from on-site measurements show that the characteristic time under normal operation may be precisely obtained. Significantly, different vibration signals and different characteristic time during the tap change process under normal condition and fault conditions may also be seen. An acoustic monitoring system is thus suitable for detecting major defects in a tap changer.

In conclusion, both the top-oil temperature modelling and acoustic monitoring system for the tap changer have good potential to be part of a comprehensive condition monitoring system for power transformers.

Zusammenfassung

Leistungstransformatoren sind komplexe und damit kostspielige Betriebsmittel. Störungen können zur Zerstörung des Transformators sowie der angrenzenden Betriebsmittel führen. Zudem besteht dabei Gefahr für Mensch und Umwelt. Routinewartungen verringern das Störungsrisiko, sind allerdings sehr teuer. Die bessere Alternative ist die zustandsabhängige Wartung durch eine Online-Überwachung charakteristischer Transformatorkennwerte mittels Überwachungs- und Diagnosewerkzeugen. Das erlaubt eine Verlängerung seiner Laufzeit, seiner Erhaltung und Modernisierung sowie, wenn notwendig, eine rechtzeitige Auswechslung des Transformators.

Ein preisgünstiges Überwachungswerkzeug kann nur durch Fokussierung auf die wichtigsten Kennwerte des Transformators gewährleistet werden. Die Kennwertauswahl erfolgt durch Fehlerstatistik und durch Analyse der erwarteten Fehlerfolgen. Aktuelle statistische Untersuchungen an Leistungstransformatoren heben besonders die Wichtigkeit der Überwachung der Temperaturen in den Wicklungen, einschließlich Isolierung, sowie des Stufenschalters hervor. Demzufolge sind in der vorliegenden Arbeit verlässliche und preiswerte Möglichkeiten zur Online-Überwachung der Deckelöltemperaturen sowie der Stufenschalter untersucht worden.

Thermisches Modell zur Online-Überwachung der Deckelöltemperatur in Leistungstransformatoren

Die Temperatur im sogenannten Hot-Spot (Heißpunkt) der Wicklungen ist von großem Einfluss auf die Verlässlichkeit des Leistungstransformators, da sie die Lebensdauer der Isolation bestimmt. Die Erforschung der direkten Temperaturmessung im Heißpunkt ist derzeit noch nicht abgeschlossen. Gemäß dem internationalen Standard [IEC 60354, 1991] kann der Heißpunkt hingegen auch aus der Deckelöltemperatur (Temperatur im oberen Bereich des Transformatoröls) abgeschätzt werden. Die Deckelöltemperatur lässt sich unkompliziert oberhalb der Kühleinheiten messen. Der thermische Zustand wird wesentlich durch die Transformatorlast und der damit einhergehenden Zunahme der Wicklungsöltemperatur bestimmt. Wobei die Kühleinheiten, dass heißt die Lüfter und Pumpen, die Einhaltung einer zulässigen Deckelöltemperatur sicherstellen. Unregelmäßigkeiten der Kühleinheiten können bei guter

Modellierung der Deckelöltemperatur, durch die Differenz zwischen modelliertem und gemessenem Temperaturwert erkannt werden.

Wichtig ist demnach eine zuverlässige dynamische Modellierung der Deckelöltemperatur anhand von Messdaten aus längeren Versuchszeiträumen. Gegenwärtig werden diverse physikalische Modelle für die Abschätzung der Deckelöltemperatur verwendet, von denen einzelne in dieser Arbeit vorgestellt werden. Die ausgesuchten physikalischen Modelle beruhen auf den internationalen Standards IEC60354 und IEEE Std. C57.91. Da einige Konstanten der Modelle, von Herstellern nicht angegeben sind, werden diese anhand der Methode der kleinsten Quadrate abgeschätzt.

Seitdem künstliche neuronale Netzwerke in vielfältigen Einsatzgebieten verstärkt eingesetzt werden, existiert das Interesse diese für die Modellierung der Deckelöltemperatur zu verwenden. In dieser Arbeit werden derartige numerische Modelle basierend auf einem künstlichen neuronalen Netzwerk untersucht. Verwendet werden Multilayer Feed-Forward und Recurrent Netzwerkstrukturen. Erstere werden als One-Hidden-Layer und Two-Hidden-Layer Strukturen mit bis zu 20 Neuronen und verschiedenen Trainingsalgorithmen erprobt. Besonders erfolgreich waren die drei Backpropagation Algorithmen: Levenberg-Marquardt, Scaled Conjugate Gradient und Automated Bayesian Regularization. Die aufwendigeren Recurrent Netzwerkstrukturen wurden lediglich als One-Hidden-Layer konfiguriert. Die erzeugten neuronalen Netzwerke werden anschließend unter Berücksichtigung der optimalen trainierten Faktorgewichtung der Eingangsgrößen in mathematische Modelle zur Berechnung der Deckelöltemperatur überführt.

Die Deckelöltemperatur wird anhand physikalischer und neuronaler Netzwerkmodelle für drei unterschiedliche Kühlungsarten (ONAN, ONAF und ODAF) berechnet. Als Eingangsgrößen für das Netzwerk werden der letzte Zustand der gerechneten Deckelöltemperatur, des Laststroms, der Umgebungstemperatur sowie der in Betrieb befindlichen Kühleinheiten verwendet. Die notwendigen Messdaten für die Untersuchung wurden freundlicherweise von der AREVA Energietechnik GmbH zur Verfügung gestellt und mit herkömmlichen Überwachungssystemen über längere Zeiträume aufgenommen. Für die Bewertung der Modelle wurde die mittlere Differenz zwischen gemessener und errechneter Temperatur herangezogen.

Unter den physikalischen Modellen liefert das Modell aus dem IEEE Standard C57.91 mithilfe linearer Regressionen die besten Ergebnisse. Für die Transformatoren vom Typ ONAN und ONAF werden Abweichungen zwischen gerechneten und gemessenen Werten von 1,6 K und 1,3 K gefunden. Für den ODAF Transformatortyp liegen die Abweichungen bei etwa 3,3 K abhängig vom Betriebszustand der Kühleinheiten.

Die neuronalen Netzwerkmodelle dagegen liefern bessere Ergebnisse als die physikalischen Modelle mit Temperaturabweichungen kleiner 1,9 K für alle Transformatoren. Dem Multilayer Feed-Forward Netzwerk ist gegenüber dem Recurrent Netzwerk der Vorzug zu geben. Das Recurrent Netzwerk ist zusätzlich nachteilig, wegen der komplexeren Strukturen und der damit aufwendigeren Trainings- und Testphase. Die Multilayer Feed-Forward Netzwerke zeigen die besten Ergebnisse, wenn sie als One-Hidden-Layer mit geringer Anzahl Neuronen konfiguriert sind. Unter den verglichenen Trainingsalgorithmen ermöglicht der Bayesian Regularization Algorithmus die besten Ergebnisse, wegen der enthaltenen Methode zur Modellgeneralisierung. Die benötigte Trainingszeit hängt ab von der Anzahl Neuronen in den Hidden-Layer sowie der genutzten Datenmenge. Die geringste Trainingszeit benötigt der Lavenberg-Marquardt Backpropagation Algorithmus, da dieser ein Abbruchkriterium zur Verbesserung der Trainingszeit beinhaltet.

Der besondere Vorteil der neuronalen Netzwerke gegenüber den physikalischen Modellen ist ihre rasche Anpassung an neue Betriebszustände der Kühleinheiten. Problematisch stellen sich für die Modellierung stark wechselnde Umgebungstemperaturen dar, wogegen veränderte Lastzustände nur geringfügig die Genauigkeit der Ergebnisse beeinflussen.

In der vorliegenden Arbeit wird gezeigt, dass durch die hohe Genauigkeit der Deckelöltemperaturberechnung mit neuronalen Netzwerken, Fehlfunktionen der Kühlanlage detektiert werden können und demzufolge neuronale Netzwerkmodelle für Online-Überwachungssysteme der Deckelöltemperatur gut geeignet sind.

Vibrations-Messungen zur Online-Überwachung von Stufenschaltern in Leistungstransformatoren

Leistungstransformatoren mit Stufenschaltern spielen eine wichtige Rolle für den Betrieb elektrischer Energieversorgungsnetze, da sie eine gleichbleibende mechanische Netzspannung trotz wechselnder

Lastzustände erlauben. Der Stufenschalter ist aber insbesondere wegen der häufigen mechanischen Schaltvorgänge für Störungen anfällig. Es treten speziell mechanische Fehler an Federn, Lagern, Führungen und Antriebsmechaniken sowie elektrische Fehler wie Verkokung von Kontakten, Verbrennen von Übergangswiderständen und Isolationsprobleme auf. Eine hohe Zuverlässigkeit dieser Komponente ist jedoch für den Transformatorbetrieb unabdingbar.

Aufgrund der Überwachungsmöglichkeit der Mechanik ist die Überwachung mittels Vibrationsmessung besonders erfolgversprechend. Im zweiten Teil dieser Arbeit wird daher ein Vibrationsmesssystem für die Online-Zustandsüberwachung des Stufenschalterbetriebs beschrieben. Durch Vibrationsmessungen wird ein charakteristischer Zeitraum für den Schaltvorgang überprüft und als Kriterium für die Überwachung des ordnungsgemäßen Zustands des Stufenschalters verwendet. Der Ablauf der Hauptkontakte und Überschaltkontakte im Umschalter während des Schaltvorgangs werden untersucht.

In modernen Transformatoren mit Hochgeschwindigkeits-Überschaltwiderstand findet die Übertragung des Stroms von einem Hauptkontakt zum anderen entlang der Übergangswiderstände im Umschalter innerhalb von 40-70 ms statt und ist abhängig vom verwendeten Mechanismus. Im fehlerfreien Betrieb ist die Übergangszeit konstant. Während des Stufungsvorganges erzeugen die mechanischen und elektrischen Vorgänge charakteristische Vibrationen und Geräusche. Die Vibrationsanalyse kann folglich viele Aspekte der Schaltvorgänge aufdecken. Die mechanischen Vibrationen geben beispielsweise Auskunft über die Schaltzeit und die Rücksprungcharakteristik der Lichtbogenkontakte, inklusive deren Unversehrtheit. Auftretende Störungen können durch Abweichungen der dafür charakteristischen Zeiträume erkannt werden.

Die Vibrationen des Stufenschalters werden durch einen piezoelektrischen Sensor aufgenommen und einem Verstärker zugeführt. Die nachfolgende Messung der charakteristischen Zeit aus dem verstärkten Signal erfolgt in einem Messkreis. Die Implementierung eines Mikrocontrollers ermöglicht eine flexible Anpassung des Systems bei Änderungen der Messcharakteristik. Das Ausgangssignal des Messkreises wird an einen Digital/Analogwandler übergeben. Schließlich wird die charakteristische Zeit als 4-20mA Signal in das Online-Überwachungssystem eingespeist. Das Überwachungssystem wird automatisch durch das Vibrationssignal

getriggert. Die Unterdrückung betriebsbedingter Nebengeräusche kann durch zusätzliche Filter erfolgen.

Die Vorortmessungen wurden an einem Stufenschalter des Typs VACUTAP® VR 400Y-123/D-10191G durchgeführt. Die Bedienung des Stufenschalters erfolgte manuell im lastfreien Zustand. Die Ergebnisse aus 20 Messungen zeigen die Reproduzierbarkeit der charakteristischen Zeit im Normalbetrieb. Es ergeben sich für die charakteristische Zeit abhängig, ob eine ungerade oder gerade Stufe geschaltet wird, Standardabweichungen von 0,2 s beziehungsweise 0,4 s. Der Prozess ist unter statistischer Kontrolle, wie durch eine Kontrollkarte und die Shewhart Prozedur geprüft wird. Ferner wird aus Laborversuchen deutlich, dass bei fehlerhaften Zuständen, wenn sich beispielsweise Fremdkörper zwischen den Kontakten befinden oder bei fehlendem Kontakt, erheblich abweichende Vibrationssignale auftreten.

Die in dieser Arbeit dargestellten Untersuchungen belegen, dass die mittels Vibrationsanalyse gemessene charakteristische Zeit und ihre Standardabweichung als Überwachungsgrößen von Stufenschaltern geeignet sind. Die gesammelten Erkenntnisse stellen eine gute Basis für die Umsetzung und Weiterentwicklung unter betrieblichen Bedingungen dar.

1 Introduction

Power transformers are one of the most expensive components in electrical transmission systems. Failures in power transformers may cause serious damage to electrical equipment. Accordingly, optimized maintenance for power transformers is required. As routine maintenance is a major expenditure, a condition-based maintenance should be a better option. The information about the conditions may be used for optimising assets, lifetime, refurbishment strategy, upgrading and replacement of the transformer.

1.1 Background and Motivation

In order to obtain effective monitoring equipment at moderate cost, it is necessary to focus on essential key parameters. These key parameters may be obtained by inspection of failure statistics and estimated failure consequences. Studies on power transformer statistics suggest that the most important parts to be monitored are winding insulation and on-load tap changers [CIGRE, 1983].

Thermal model

The ageing behaviour of the oil/paper insulation is determined mainly through the thermal conditions inside the transformer. Overloading or local overheating may cause high temperatures in transformers. Even in the case of reduced load conditions, overheating may occur due to reduced cooling efficiency. Thus, monitoring of temperature, loading condition and fan/pump operations are the base information for thermal behaviour of the transformers.

Winding hot-spot temperature is a critical parameter affecting insulation life and safe loading practices. Measurement of the exact hot-spot temperature is still in a research stage. However, according to the international standards [IEC 60354, 1991], hot-spot temperature may be estimated from the top-oil temperature if load, ambient temperature and the winding oil temperature rise are also taken into consideration. Consequently, the thermal behaviour of transformers may be considered

from the top-oil temperature, which may be easily measured above the cooling unit. Transformer thermal characteristics also depend on the combination of fans and pumps operating during forced cooling conditions. Therefore, an online top-oil temperature modelling should lead to information about the thermal behaviour of the transformer and the ability to detect a malfunction of the cooling units.

On-load tap changer

On-Load Tap Changers (OLTCs) are the main components of power transformers and are responsible for maintaining a defined voltage band supplied to consumers under variable load conditions. Changing a tapping on the winding enables the turns ratio of the transformer and thus the level of output voltage to vary. An OLTC has two main switches: a selector switch and a diverter switch. The selection of tapping on the transformer winding is done via the selector switch. The load current is switched via the diverter switch. The on-load tap changer is more susceptible to failures than other components of a power transformer due to its complex mechanical nature [Gao, 2002].

High failure rates of OLTCs are direct consequences of mechanical malfunctioning such as springs, bearings, shafts, drive mechanisms, followed by electrical faults such as coking of contact, burning of transition resistors and insulation problems. These potential faults necessitate the assurance of the reliability of OLTCs [Handley, 2001].

According to the diverse mechanical and electrical functions of a tap changer, several physical and technical solutions are available for tap changer monitoring [Bengtsson, 1996]. Since most mechanical and electric parts are enclosed in the oil filled steel tank, vibration monitoring is promising for its non-invasive nature and its moderate cost.

During the operation of a tap changer, the series of mechanical and electrical processes produce distinctive vibrations and noise patterns. In principle, an analysis of these typical vibration signatures should reveal different aspects and phases of tap changer operation. Mechanical vibrations should include information about switching times and bouncing characteristics of the on-load switch’s arc contacts. Since all electric contacts are enclosed in oil filled steel tanks, an online

monitoring of the OLTCs with a non-invasive acoustic technique is proposed as a means to investigate the vibrating signals from a tap change process.

In modern high-speed resistor tap changers, the current transfer over the electric contacts via the transition resistors in the diverter switch during the tap-change process takes place in about 40-70 ms, depending on the type of mechanism used for switching. This transition time interval is expected to be constant as long as no mechanical problems are involved. Therefore, online monitoring of the tap-change transition time is a possibility to check the reliability of the tap changer.

1.2 Aim of the Work

The aim of this work is to evaluate suitable criteria for condition monitoring of cooling units and on-load tap changers in online power transformer monitoring systems.

Malfunctions of the cooling units or pollution of coolers should be detected by means of an online comparison of measured top-oil temperature and its predicted values, which depend on the number of operating fans and pumps. Firstly, a suitable model for top-oil temperature prediction must be developed by investigation of different physical and neural network models. By simulating the malfunction of the cooling, the relation between the top-oil temperature difference and the cooling capacity should be found. This should lead to monitoring criterions for the alarm setting in the power transformer online monitoring system.

Based on the assumption that the transition time during the transition process of an on-load tap changer should reveal the status of the mechanical part, a compact online vibration measuring system for the transition time measurement should be developed and tested on-site. The repeatability of the transition time should be confirmed before being taken as a criterion for indicating mechanical problems of an on-load tap changer.

1.3 Outline of the Thesis

The thesis is divided into three main parts. Power transformer monitoring and diagnosis is introduced in the first part (Chapter 2). The second part deals with the thermal model investigations (Chapter 3 – Chapter 6). The monitoring of on-load tap changers is covered in the third part of the thesis (Chapter 7 – Chapter 8).

In Chapter 2, common failures in power transformers are reviewed. Maintenance strategy, monitoring and diagnostic parameters are also considered.

The background information about thermal conditions in oil-immersed power transformers including transformer losses, transformer cooling and hot-spot temperature are studied in Chapter 3.

Chapter 4 presents long-term investigations of physical top-oil temperature models to be used in an online monitoring of power transformers. State of the art in top-oil temperature prediction and the investigated models are described. The parameter estimation procedure and top-oil temperature calculation are then explained. Finally, results from different models are compared and discussed in detail. The influence of starting points on the parameter estimation process and the results of using different sets of estimated parameters are investigated.

Models for transformer top-oil temperature prediction based on neural networks are given in Chapter 5. An introduction to neural networks including biological neurons and the history of neural networks is also included. The performance of different neural network structures for thermal modelling are compared and discussed.

Chapter 6 describes applications of the top-oil temperature prediction. First, the comparison between the performance of the physical model and the neural network model for the calculation of top-oil temperature is performed. The accuracy of the chosen top-oil temperature model in different loading conditions and the effect of transient-states of ambient temperature are investigated in detail. Finally, the potential of the model in detecting a malfunction of cooling units is confirmed.

The last part of the thesis begins with an introduction of tap changer characteristic including tap changer design schemes, switching methods, and motor drive mechanisms in Chapter 7. Failure mechanisms of on-load tap changers along with tap changers maintenance and diagnosis in general are studied.

In Chapter 8, a vibration measuring system for transition time monitoring of the tap changer process is introduced. The reliability of the measuring system is also investigated on-site. The results of the investigations for the transition process and mechanical failures in tap changers are shown. Statistical methods for monitoring criteria are suggested.

2 Monitoring and Diagnosis of Power Transformers

Power transformers are the most important and expensive components in the electric power system. In practice, the lifetime of a grid-coupling transformer may be as long as 60 years with appropriate maintenance. Generally, a transformer has sufficient electrical and mechanical strength to withstand unusual conditions. However, as transformers age, their insulation strength deteriorates to the point that they may not withstand certain malfunctions in regular performance, such as short-circuit faults or transient overvoltage, subsequently causing serious transformer failures.

2.1 Failures in Power Transformers

The term *Transformer Failure* may be defined [Kogan, 1988] as follows:

- any forced outage of the transformer due to its failure in service;
- trouble which requires the transformer to be returned to a factory for repair, or which requires extensive field repair.

In-service failures of transformers may be potentially dangerous to utility personal through explosion and fire and can potentially damage the environment through oil leakage. Furthermore, a transformer with catastrophic failure is costly to repair or to replace, and may result in significant loss of revenue (e.g., loss in produced energy, process downtime, penalties).

Transformer failures may occur because of different causes and conditions. Generally, the causes of failures may be divided into two groups: internal causes and external causes. Internal causes of failures are insulation deterioration from ageing of paper or transformer oil, damage to the winding or deformation of the winding under short circuit force, loss of winding clamping, overheating or vibration damage to the core, contamination of moisture and particles in the insulating oil, partial discharge, overvoltage due to winding resonances, manufacturing/design errors or handling during transportation, commissioning or maintenance. External causes of failures are lightning strikes, system switching

operation (switching transient), system overloads and system faults (short circuit). In addition to failures in the main tank, failures may also occur in the bushings, tap changers or transformer accessories [Wang 2002].

A CIGRE working group had earlier performed a survey on failures in large power transformers. These transformers were less than 20 years old and were for EHV and UHV networks. Typical failure modes were collected and tabulated from a population database with at least 5000 units. Shortened life due to accelerated deterioration of bushings and on-load tap changers were highlighted in this publication. Faults of mechanical origins in the active part of the transformer often resulted from short circuit force or from possible vibration of supporting parts of the windings or from the core itself. Dielectric faults in the winding insulation or the main insulation may occur due to mechanical winding displacement during a transport shock, a short circuit in the power network near the transformer, or a high voltage stress [CIGRE, 1983].

Transformer failure data from the Eskom network in South Africa has been reported [Minhas, 1999] in an extension of the earlier work [Minhas, 1997]. The failure analysis was based on 188 power transformers in the voltage range from 88 kV to 765 kV with power ratings from 20 to 800 MVA. The analysis showed that ageing related failures were dominant in smaller transformers. In the medium power rating class, tap-changer failures constituted the highest failure rate. Insulation design failure was the most common cause in the early service period of large transformers.

The percentage of different failure modes of large power transformers is shown in Figure 2.1. The results agree in a certain extent to those obtained in the earlier work [Minhas, 1997] in that major failures are due to tap changers, ageing and lightning/switching surges. Tap changers, bushings and windings contributed to about 79% of the severe and intermediate failures recorded during year 1996-2006. Recent information on failures of transformers from Eskom [Jagers, 2007] showed that tap changer related failures were the most prominent.

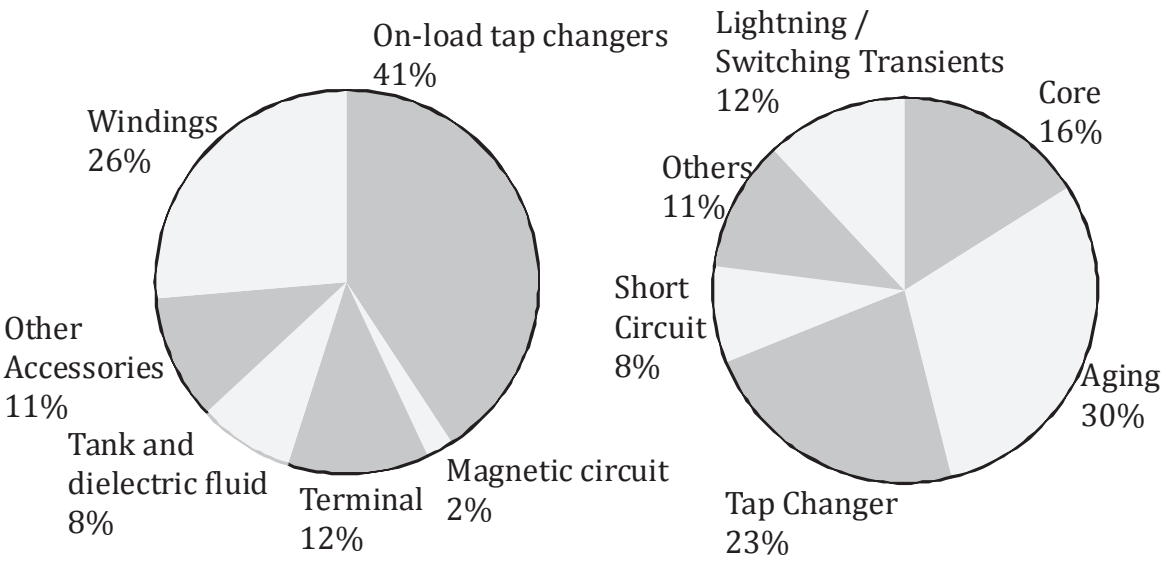

Figure 2.1 Percentage of failures of large power transformers from CIGRE (left) [CIGRE, 1983] and from Minhas (right) [Minhas, 1999]

2.2 Monitoring and Diagnosis

Nowadays, there is a trend in the industry to change from traditional *time-based maintenance (TBM)* to *condition-based maintenance (CBM)*. The CBM is more appropriate because the average age of the transformers in service is increasing and approaching the end of nominal design lifetime. Instead of doing maintenance at a regular interval, maintenance is carried out only under a certain condition indicated by the equipment. The need for better nonintrusive monitoring and diagnostic tools to assess the internal condition of transformers is thus very strong.

The terms monitoring and diagnosis must be clearly differentiated. *Monitoring* is here defined as a persistent *online* collection of raw data and warning signals from the equipment under supervision while the equipment is operating. Generally, a monitoring system includes sensor units for online application, data acquisition systems and data processing [Bengtsson C, 1996], [Leibfried, 1998], [Tenbohlen, 2000].

Development of new techniques and applications of condition monitoring have become one of the most important tasks for equipment manufacturers and utilities since the beginning of 1990s. Monitoring and diagnosis tools are mandatory to keep track of the power transformer's

operational levels. The monitoring system must be designed for long-term operation with a high reliability due to the lifetime of power transformers in the range of 30 years and more. It should be inexpensive and able to be retrofitted.

The time resolution of the online measurements provides the ability to determine the rate of change in the monitored parameters. It should be distinguished whether the change is gradual over a long period or sudden. The exact time of the change should be calculated. Then, the information may be used to determine the appropriate course of action.

One of the primary challenges to the online approach is the management of a tremendous amount of data. Today's microprocessor technology provides a sophisticated means to extract the essential information. The data acquisition system incorporates sensors, signal conditioning, timing and control, and memory to store data for a short period. The use of a true multitasking computing environment is pertinent to a monitoring system that performs a number of tasks simultaneously. Storage of data must be organized to be conveniently accessible to the user.

Diagnosis comprises interpretation of offline and online measured data. *Offline diagnosis* has served the industry well and it continues to play an important role in the reliability of power systems. The offline application provides management and strategy information. It identifies the serious changes that take place between test intervals and supports the decision as to which part needs to be removed from service.

Nowadays, engineers and researchers are seriously investigating the development of an *expert system* employing *artificial intelligence (AI)* modelling techniques for transformer diagnosis. Software expert systems should be able to access the condition of transformers and should allow a corrective action with an optimal time. However, this potential has not yet been realized [Leibfried, 1998], [Ward, 2000], [Stirl, 2006].

2.3 Online Monitoring Techniques

A power transformer has to withstand thermal, electrical and mechanical stress. This, in turn, results in a degradation of the oil/paper insulation system. Degradation means a reduced insulation quality. Local discharges lead to winding breakdowns and hot spots of oil temperature accelerate aging behaviour.

Monitoring a large number of parameters means high cost. The challenge is to balance the functions of a monitoring system and its cost and reliability with the value–added outcomes. In order to get effective monitoring equipment at moderate costs, it is necessary to focus on the key parameters, the selection of which is based on failure statistics and the estimated consequences of the respective failures.

2.3.1 Load and Operating Conditions

Continuous online monitoring of current and voltage together with temperature measurements provide a trace for thermal performance of a transformer and gives an individual load profile essential to distribution system planning. Measurements of voltages and currents, together with the tap changer position, allow the calculation of the power transmitted through the transformer. In addition, some other quantities like oil level in the compensator and the tap changer tank, as well as the oil pressure in the bushings, are measured in order to provide more information about the transformer condition.

Voltages may be measured using the measuring tap of the bushings, in the case of capacitor bushings. If there are no capacitor bushings available, voltages may be picked up by any kind of external voltage transformers. Current transformers may be either mounted in the bushing domes for newly designed transformers or else an external current transformer may be used for current measurements [Leibfried, 1999].

2.3.2 Thermal Performance

The degradation of transformer insulation depends on the hot spot temperature inside the transformer winding. The hot spot temperature may be measured by fibre optic temperature sensors installed inside the transformer winding. The development of fibre optic devices to monitor hot-spot temperature directly is the beginning of the monitoring technology [Kirtley 1996]. However, there are several drawbacks of this technique. First, the exact location of the hot spot has to be known. Moreover, optical sensors have to be placed inside the transformer and can weaken the insulation system. Consequently, only new transformers may be equipped with these sensors.

Another way to determine the hot spot temperature is to measure certain parameters such as top-oil temperature, ambient temperature, and load current combined with a thermal model for calculating the hot spot temperature. Hot-spot temperature is consequently used for determining the aging behaviour of the oil/paper insulation.

2.3.3 Insulating Oil

Thermal and electrical faults such as overheating, arcing, partial discharges or local breakdown in power transformers are always related to the formation of gases dissolved in the oil. Thus with the analysis of gasses dissolved in the oil, such faults may be distinguished from each other. The method of *gas-in-oil analysis* is based on analyzing the types, concentration and production rates of generated gasses. If a certain generation rate is exceeded, gas bubbles can arise. These gas bubbles may cause a local breakdown if they come into regions of the insulation system with high electric field strength.

Different types of faults produce different key gases and different combinations of gases. The evaluation of gases in oil tests commonly considers the concentration of hydrogen (H_2), methane (CH_4), acetylene (C_2H_2), ethane (C_2H_4), carbon monoxide (CO), carbon dioxide (CO_2), nitrogen (N_2), and oxygen (O_2). The relative ratios and the amount of gas detected in the sample are used to predict problems with the insulation structure. For instance, arcing leads to the generation of acetylene (C_2H_2)

and carbon oxides (CO, CO_2) that are formed by overheated cellulose. Heating the oil produces ethylene (C_2H_4).

It is also necessary to take into account not only the absolute concentrations but also the production rates of the different gases. Moreover, the type of transformer under investigation should be considered when making the analysis: a generator step-up unit shows a different pattern than a system transformer or a HVDC transformer. Traditionally, the gases are extracted from oil samples, which are taken manually at regular intervals, normally every one or two years depending on the transformer.

For on-line monitoring, the Hydran combustible gas sensor, manufactured by GE Syprotec Inc. is one type of commercially available gas sensors [Bengtsson C, 1996], [Leibfried, 1998], [Tenbohlen, 2000]. The sensor measures the cumulative gas quantity based on a fuel cell and in relation to a proportional distribution formula (H_2 (100%), CO (18%), C_2H_2 (8%), C_2H_4 (1.5%)) in ppm. The increase in the quantity of gas may be used as a starting point for a conventional gas analysis to draw conclusions about the type of the fault. Sensors that are more complex (e.g. based on infrared technology or gas chromatography) may detect several or all of these gases.

Recently, applications of artificial intelligence (AI) combined with the dissolved gas-in-oil analysis have been quite promising in detecting thermal faults, low-energy discharge (partial discharge), high-energy discharge (arcing) and cellulose degradation [Wang[1], 2000].

2.3.4 Partial Discharge Measurement

The properties of the insulating materials in transformers may degrade by partial discharge (PD) which may lead to eventual failures. Abnormal levels of PD may indicate conditions such as voids in the insulation, de-lamination at insulation interfaces, cracking or fissures in brittle insulation, contamination in the insulation, “electrical trees” in the insulations, abnormal electrical stress areas due to improper manufacture or application. The acceptable PD limits for new transformers depend on the voltage and size of the transformer. The maximum charge may range from 100 to 500 pC [Wang, 2002].

PD causes high-frequency currents that can be detected electrically. The electric PD measurements have certain drawbacks and limitations for on-site/online measurements, e.g. the low applicability of sensors and receptivity for several disturbances. The use of electromagnetic ultra high frequency (UHF) signals (typically 1-2 GHz) has been developed to detect PD in gas-insulated substations and has been applied to transformers. The advantages are that the sensors do not need any electric connection to the high voltage circuit and the measurements are independent from the outer disturbing signals such as corona [Markalous, 2006].

Acoustic PD measuring methods have been developed to detect the mechanical stress waves which are generated by PD pulses that propagate through the surrounding oil (in the range of 100 to 300 kHz). The acoustic emission sensors can be mounted on the transformer tank wall. The PD may be located three-dimensionally based on the arrival time of the pulses at different sensors. Due to the attenuation of the signal by the oil and winding structure, the sensitivity of the measurements depends on the location of the PD. Thus, the deeper the PD is located inside the winding the greater the attenuation [Großmann, 2002].

PD may also be detected indirectly, using chemical techniques such as measuring the degradation products produced by the PD, mainly hydrogen [Küchler, 1996].

2.3.5 HV Bushing Monitoring

Capacitive high voltage bushings are critical components of the power transformer. The two most common bushing failure mechanisms are moisture contamination and partial discharge.

Moisture usually enters the bushing via deterioration of the gasket material or cracks in terminal connections resulting in an increase in the dielectric-loss and insulation power factor. Tracking over the surface or burning through the condenser core or a breakdown between two adjacent layers of a capacitor bushing is typically associated with partial discharge. These problems increase the power factor. As the deterioration progresses, increases in capacitance will be observed.

Thus, measurement of dissipation factor (tanδ) and capacitance are widely used as methods for detecting the early stage of insulation defects of capacitive apparatus with multi-layer insulation like a bushing. A classical Schering bridge technique may be used, particularly to measure capacitance for offline measurement. This usually requires a standard low loss capacitor at the voltage rating of the equipment under test.

Online tanδ measurement of HV capacitive equipment in substations is mainly based on comparative methods. The tanδ is measured by comparing the phase angles between the measured current of the tested object and a reference voltage.

A HV bushing online monitoring method is the current summation method. The basic principle is that if the system voltages in a three-phase system are perfectly balanced and the bushings are identical, the vector sum of the bushing currents will be zero. In reality, bushings are never identical and system voltages are never perfectly balanced. As a result, the sum current is a non-zero value and is unique for each set of bushings. The initial sum current may be obtained and the condition of the bushings may be determined by evaluating changes in the sum current phasor. Thus, the online monitoring on a single-phase transformer is not possible with this method [Lachman, 2000].

The capacitive controlled bushings can also be monitored online in a simple manner based on the use of a capacitive voltage sensor that is installed at the measurement tap of the bushing. The monitoring of the change in the bushing capacitances is achieved by means of a three-phase voltage measurement. The output signal of a voltage sensor is compared with the two remaining phases. The detection and evaluation of the overvoltage is the basis for the evaluation of the bushing insulator reliability [Stirl 2004].

3 Thermal Behaviour of Power Transformers

The transformer thermal performance is one of the basic criteria which limit the transformer's load ability and usable life. Aging or deterioration of insulation is a function of time and depends on temperature, moisture, and oxygen content of the oil. The moisture and oxygen contributions to insulation deterioration can be minimized. However, the insulation temperature is still the controlling parameter. Experimental evidence indicates that the relation of insulation deterioration to time and temperature follows an adaptation of the Arrhenius reaction rate theory that has the following form [IEC 60354, 1991].

$$\text{Life duration} = e^{\left[\alpha + \beta / T\right]} \tag{3.1}$$

Where α and β are constants and T is the absolute temperature.

The relation can be used to make meaningful comparisons based on *rate of ageing* via the following simpler exponential expression of Montsinger:

$$\text{Rate of ageing} = \text{constant x } e^{\left[-\rho\theta\right]} \tag{3.2}$$

Where ρ is a constant and θ is a temperature in degrees Celsius.

The constant in the equation depends on many factors, such as the original quality of the cellulose products (raw material composition, chemical additives) and environmental parameters (moisture content, free oxygen in the system). The coefficient for temperature variation ρ may be taken as a constant over the actual range of temperature between 80 °C and 140 °C. The rate of ageing is doubled for every increment of approximately 6 K.

The rate of ageing prediction is based on the winding hot-spot temperature. For transformers designed in accordance with IEC 76, a usual reference value (rate of ageing = 1.0) at rated load and normal ambient temperature is 98 °C. The temperature distribution in most apparatus is not uniform. The part, which is operating at the highest temperature, will ordinarily undergo the greatest deterioration. Therefore, the highest (hottest-spot) temperature is considered for the aging effect.

3.1 Hot-spot Temperature

The most important factor limiting the loading capacity and the service life of an oil-paper-insulated power transformer is the highest temperature in the winding area, the so-called *hot-spot area*. This is because the principal factor determining the ageing of a transformer is the thermally activated chemical process deteriorating the insulation in the winding hot-spot area. In the international standard [IEC 60354, 1991], a linear transformer temperature behaviour diagram is assumed as depicted in Figure 3.1.

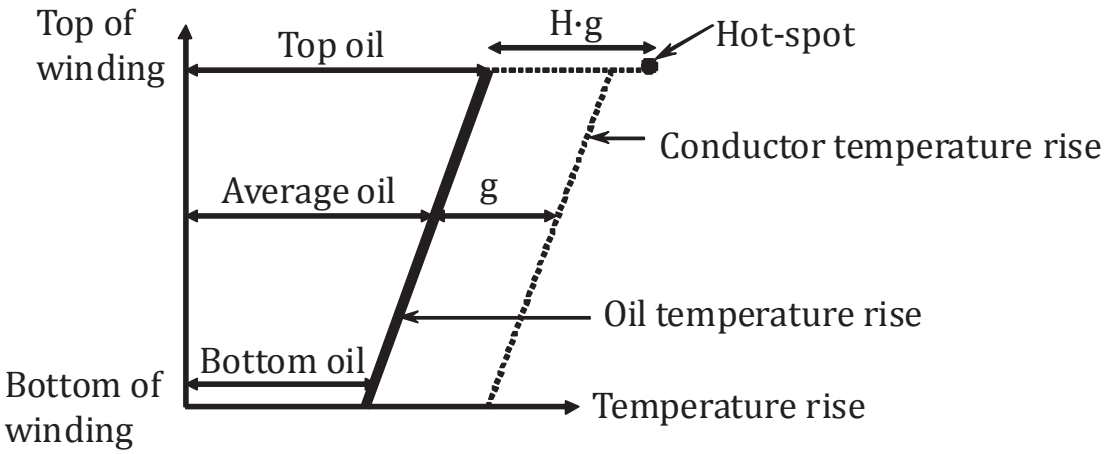

Figure 3.1 Transformer temperature behavior based on IEC 60354

This diagram is a simplification of a more complex distribution based on the following assumptions:

Oil temperature rise inside the windings increases linearly from the bottom to the top;

Temperature rise of the conductor at any position up the winding increases linearly parallel to the oil temperature rise, with a constant difference g between the two straight lines (g is the difference between the average winding temperature rise and the average oil temperature rise);

Hot-spot temperature rise is higher than the temperature rise of the conductor at the top of the winding because of the increase in stray losses. To take account of this non-linearity, the difference in temperature between the hot spot and the oil at the top of the winding is

made equal to $H \cdot g$. This H factor varies from 1.1 to 1.5 depending on transformer size, short-circuit impedance and winding design. The suggested H factors are given in Table 3.1 [IEC 60354, 1991].

	Distribution transformers	Medium and large transformers		
	ONAN	ON...	OF...	OD...
H factor	3.0	2.5	1.5	1.5

Table 3.1 Hot-spot factor (H)

3.2 Transformer Losses

No-load losses (P_N) and load losses (P_S) are the two significant sources of heating considered in the thermal modelling of power transformers. Both loss components combined can be defined as the total loss (P_T) of the transformer. Load losses or short-circuit losses are proportional to the square of the load factor (K) flowing in the windings, as seen from Eq. (3.3).

$$P_T = P_S K^2 + P_N \tag{3.3}$$

No-load losses are hysteresis losses and eddy losses in the transformer core occurring during the energization of the transformer. The magnitude of the no-load losses is influenced by various factors such as core design, quality of core plate material, induction and mass of core [Tenbohlen, 2001].

Hysteresis loss is due to the elementary magnets in the material aligning with the alternating magnetic field. The energy used to turn each domain is dissipated as heat within the iron core. When a magnetic field is passed through a core, the core material becomes magnetized. To become magnetized, the domains within the core must align themselves with the external field. If the direction of the field is reversed, the domains must turn so that their poles are aligned with the new direction of the external field. This loss, called hysteresis, may be thought of as resulting from molecular friction. Hysteresis loss may be held at a small value by proper choice of core materials.

Eddy currents are induced in the core by the alternating magnetic field. The core of a transformer is usually constructed of some type of ferromagnetic material because it is a good conductor of magnetic lines of flux. Whenever the transformer is energized by an alternating-current source, a fluctuating magnetic field is produced. This magnetic field cuts the conducting core material and induces a voltage into it. The induced voltage causes random currents to flow through the core, which dissipates power in the form of heat. These undesirable currents are called eddy currents.

The amount of hysteresis and eddy loss is dependent on the exciting voltage of the transformer. To minimize the loss resulting from eddy currents, transformer cores are laminated. Since the thin, insulated laminations do not provide an easy path for current, eddy-current losses are greatly reduced.

Load losses or short-circuit losses consist of copper loss due to the winding resistance and stray load losses due to eddy currents in other structural parts of the transformer. The copper loss consists of DC resistance loss and winding eddy current loss. The resistance of a given winding is a function of the diameter of the wire and its length. Using the proper diameter wire may minimize copper loss.

Table 3.2 shows the loss characteristics of different on-site power transformer types, which depend on the power of the transformers.

Transformer type	Rated power (MVA)	Cooling type	Short-circuit loss (kW)	No-load loss (kW)
Generator	850	ODAF	2060	370
Grid Coupling	600	OFAF	1666	313
Generator	600	OFWF	1520	290
Grid Coupling	300	ODAF	850	179
Generator	273	OFWF	640	205
Grid Coupling	150	ONAF	414.2	67.52
Grid Coupling	40	ONAN	135	20

Table 3.2 Losses from different types of transformers

3.3 Transformer Cooling Systems

Cooling in the transformers involves the transfer of heat from the core and windings to the insulating oil. The oil circulation in the winding may be associated with different types of cooling. The cooling systems *ONAN* (**O**il **N**atural **A**ir **N**atural) and *ONAF* (**O**il **N**atural **A**ir **F**orced) use radiators for heat exchange. The heat resulting from the losses is transferred to the oil in the tank and the natural circulation of the oil transfers the heat to external radiators. The radiators increase the cooling surface area of the transformer tank. Forced air-cooling is commonly applied on large power transformers, where fans are used to blow air over the surface of the radiators, which can double the efficiency of the radiators.

In the case of very large radiators, additional special oil pumps are sometimes used to increase the flow of oil. Consequently, the efficiency of the radiators is increased. With the cooling type *OFAF* (**O**il **F**orced **A**ir **F**orced), the circulation of the oil is forced by additional pumps and the pumped oil flows freely through the tank. The transformers supplied with this cooling type are called non-directed oil flow transformers. In directed oil flow transformers (*ODAF* – **O**il **D**irected **A**ir **F**orced), the pumped oil is forced to flow through the windings. The radiator design on *OFAF* and *ODAF* transformers can differ substantially to the radiator design on *ONAF* transformers. Radiators are sometimes called coolers instead.

For some large power transformers, water-cooling may replace large radiators (*ODWF* – **O**il **D**irect **W**ater **F**orced). Large power transformers may also have additional ratings for multiple stages of forced cooling.

4 Top-oil Temperature Prediction Based on Physical Models

Currently, there are various proposed types of physical models to determine the top-oil temperature in power transformers. The top-oil temperatures predicted from some of these models are suitable for applying in the power transformer on-line monitoring system.

4.1 State of the Art

The IEC60354-Loading Guide for Oil-Immersed Power Transformers has suggested a model for top-oil temperature calculation [IEC 60354, 1991]. The model captures the basic characteristics that the top oil is a mixture of various oil flows, which have circulated along and/or outside the windings. The different types of cooling are treated separately in the calculation because of the differences in the oil flows. It is assumed that the oil circulation in the winding for ON-cooled (**O**il **N**atural) and OF-cooled (**O**il **F**orce) transformers is caused by thermal convection. However, for OD-cooled (**O**il **D**irected) transformers the rate of flow of the oil is mainly governed by the pump and thus is not dependent on the oil temperature.

The IEEE Std. C57.91 Guide for Loading Mineral-Oil-Immersed Transformers [IEEE Std. C57.91, 1995] has proposed another top-oil rise temperature model for top-oil temperature prediction. This model is based on the concept that the change in top-oil temperature rise over ambient temperature is caused by the change in loading condition. However, the temperature calculations assume a constant ambient temperature. Thus, this fundamental model has the limitation that it does not accurately take account of the effect of daily variations in ambient temperature.

Lesieutre from Massachusetts Institute of Technology [Lesieutre, 1997] has proposed a modification model of the IEEE top-oil rise temperature model by taking account of ambient temperature variations, oil viscosity, winding dynamics, and various types of thermal losses in the calculations. The model parameters were estimated from manufacturer's

data and off-line tests. The model predicts top-oil temperature more accurately and can be implemented in an on-line system. Good results were found using data from a transformer operating in the forced-oil, -air cooling state.

Tylavsky has later modified the model of Lesieutre. In his work, some sources of error that affected top-oil temperature predictions were investigated [Tylavsky, 2000]. The result showed that the input error caused by database quantization, remote ambient temperature monitoring and low sampling rate account for about 2/3 of the errors from the field data. Nevertheless, only some cooling types were considered in this simplified model.

Tenbohlen has presented a top-oil temperature model, calculated under consideration of the one-body system, which represents the thermal behaviour of a transformer. The model assumes that, under stationary conditions, all losses are transferred to the environment via the thermal resistance of the cooling equipment. In case of fluctuations in ambient temperature or load, the thermal capacity of the transformer has also been taken into consideration. This, together with the thermal resistance, results in the thermal time constant of the transformer. The reliability of the model is proved so that it is possible to detect failures of the cooling system, such as failures of pumps or fans, by comparison of measured and calculated top-oil temperature [Tenbohlen[2], 2000].

A fundamental thermal model based on thermal-electric analogy, heat transfer theory and definition of non-linear thermal resistance was another competing choice [Swift, 2001]. The key feature of this model is the use of a current source analogy and a non-linear resistor analogy to represent heat input due to losses and the effect of air or oil cooling convection currents respectively. A 250 MVA transformer was used as a sample model test. The results were shown very positive. However, the tests were carried out in a relatively short measuring period (<3days) during the steady state of ambient temperature.

Another thermal model of an oil-immersed power transformer based on thermal-electric analogy was also proposed. The model was based on the principles of heat exchange and electric circuit laws [Tang, 2004]. A set of differential equations was derived to calculate both the transient-state temperatures and the stationary-state equilibrium in the main parts of a

transformer. For the problem of thermal parameters identification, a genetic algorithm was employed to find global solutions for thermal parameters using on-site measurements.

The next attempt for more accurate calculations of hot-spot and top-oil temperature was introduced in 2005. The investigations were done during transient conditions based on data received in a normal heat run test (i.e., the top-oil in the tank of the transformer and the average winding-to-average oil gradient). Oil viscosity changes and loss variation with temperature are taken into account. However, complex constant parameters are necessary in these physical models. Furthermore, the first-order differential equations of the models themselves are rather complicated. On the other hand, it has been shown that these thermal models yield good results for a short period of examination [Susa, 2005].

4.2 Top-oil Temperature Physical Models

From the references mentioned above, four different physical models for top-oil temperature calculation were chosen to be investigated in this work.

4.2.1 IEEE Std. C57.91 Top-oil Temperature Rise Model

As a thermal model for an on-line monitoring system, the IEEE/ANSI C57.115 standard top-oil temperature rise model was chosen as a fundamental model for the prediction of top-oil temperature [from here on **Model A**]. This model predicts that an increase in the load (current) of the transformer will result in an increase in the losses within the device and thus an increase in the overall temperature [IEEE Std. C57.91, 1995]. The temperature model is governed by the following first-order differential equation.

$$\tau_{TO} \frac{d\theta_{TO}}{dt} = -\theta_{TO} + \theta_{TO,\infty} \tag{4.1}$$

The top-oil temperature rise at a time after a step load change is given by the following exponential expression Eq. (4.2) containing an oil time constant. The derivation of this equation may be found in Appendix A.

$$\theta_{TO} = \left(\theta_{TO,\infty} - \theta_{TO,I}\right)\left(1 - e^{\frac{-\Delta t}{\tau_{TO}}}\right) + \theta_{TO,I} \tag{4.2}$$

The ultimate temperature rise depends upon the ratio of actual load to rated load (K) and ratio of total loss to no load loss (R) as in Eq. (4.3).

$$\theta_{TO,\infty} = \theta_{TO,R}\left(\frac{K^2 R + 1}{R + 1}\right)^n \tag{4.3}$$

The exponent (n) in the temperature rise equation depends upon the cooling state. The suggested exponents in the temperature rise equations are given in Table 4.1 [IEEE Std. C57.91, 1995].

Cooling type	Oil exponent (n)
ONAN	0.8
ONAF	0.9
OFAF	0.9
ODAF	1.0

Table 4.1 Oil exponent values from different cooling types

The original top-oil time constant is given as

$$\tau_{TO} = \theta_{TO,R}\frac{C_{th}}{P_T} \tag{4.4}$$

The thermal capacity (C_{th}) is given by the following equation for the ONAN and ONAF cooling modes:

$$\begin{aligned} C_{th} &= 0.0272 \text{ x (weight of core and coil assembly in kilograms)} \\ &+ 0.01814 \text{ x (weight of tank and fittings in kilograms)} \\ &+ 5.034 \text{ x (litres of oil)} \end{aligned} \tag{4.5}$$

For either directed or non-directed forced-oil cooling modes the thermal capacity is given by the following equation:

C_{th} = *0.0272 x (weight of core and coil assembly in kilograms)*
+ 0.0272 x (weight of tank and fittings in kilograms)
+ 7.305 x (litres of oil) (4.6)

The top-oil temperature is then given by

$$\vartheta_{TO} = \theta_{TO} + \vartheta_{amb} \tag{4.7}$$

4.2.2 Semi-physical Model

This modified top-oil temperature model is based on the concept originally developed from the IEEE top-oil temperature rise model. The ambient temperature is directly considered in the first-order differential equation of the model [Lesieutre, 1997].

$$\tau_{TO} \frac{d\vartheta_{TO}}{dt} = -\vartheta_{TO} + \vartheta_{amb} + \vartheta_{TO,\infty} \tag{4.8}$$

Using forward Euler approximation for the time derivative:

$$\frac{d\vartheta_{TO}[i]}{dt} = \frac{\vartheta_{TO}[i] - \vartheta_{TO}[i-1]}{\Delta t} \tag{4.9}$$

The linear regression technique is applied to the model. When the oil exponent (*n)* is assumed to be 1 in this state, Eq. (4.9) may be expressed in the following discretized form:

$$\begin{aligned}\vartheta_{TO}[i] &= \frac{\tau_{TO}}{\tau_{TO} + \Delta t}\vartheta_{TO}[i-1] + \frac{\Delta t}{\tau_{TO} + \Delta t}\vartheta_{amb}[i] \\ &+ \frac{\Delta t \vartheta_{TO,R} R}{(\tau_{TO} + \Delta t)(R+1)}(K[i])^2 + \frac{\Delta t \vartheta_{TO,R}}{(\tau_{TO} + \Delta t)(R+1)}\end{aligned} \tag{4.10}$$

The derivation of this equation may be found in Appendix B. The simplified model can be found as the following:

$$\vartheta_{TO}[i] = J_1 \vartheta_{TO}[i-1] + (1 - J_1)\vartheta_{amb}[i] + J_2 K[i]^2 + J_3 \tag{4.11}$$

The parameter J_1, J_2 and J_3 are obtained from the parameter estimation method.

Tylavsky modified the linear semi physical model in Eq. (4.11) later. The term (1-J_1) is replaced with an arbitrary coefficient J_4 [Tylavsky, 2000]. The modified model in Eq. (4.12) is defined in this work as **Model B**.

$$\vartheta_{TO}[i] = J_1 \vartheta_{TO}[i-1] + J_4 \vartheta_{amb}[i] + J_2 K[i]^2 + J_3 \tag{4.12}$$

4.2.3 IEC60354 Steady-state Temperature Equations

The IEC model [from here on **Model C**] distinguishes between different types of cooling modes. The basic idea of the model is that the top oil is a mixture of various oil flows, which have circulated along and/or outside the various windings [IEC 60354, 1991].

Normally, the temperature difference between the main windings is not important for ON cooling. The oil temperature at the top of the winding is, for all windings, taken as the temperature of the mixed top oil in the tank. For OF and OD cooling, on the other hand, the oil temperature at the top of a winding is taken to be the bottom oil temperature plus twice the difference between the average oil temperature inside that particular winding and the bottom-oil temperature. Therefore, top-oil temperature may be calculated as below.

ON cooling

$$\vartheta_{TO} = \vartheta_{amb} + \theta_{TO,R}\left(\frac{K^2 R + 1}{R + 1}\right)^x \tag{4.13}$$

OF and OD cooling

$$\vartheta_{TO} = \vartheta_{amb} + \theta_{BO,R}\left(\frac{K^2 R + 1}{R + 1}\right)^x + 2\left(\theta_{MO,R} - \theta_{RO,R}\right)K^y \tag{4.14}$$

The exponents x and y in temperature rise equations depend upon the cooling state and the type of transformers. The suggested exponents used

in the temperature rise equations for medium and large power transformers are given in Table 4.2 [IEC 60354, 1991].

Cooling type	Oil exponent (x)	Winding exponent (y)
ON…	0.9	1.6
OF…	1.0	1.6
OD…	1.0	2.0

Table 4.2 Oil exponents and winding exponent from different cooling types

4.2.4 One-body Model

The thermal behaviour of the whole transformer can be explained by a one-body equivalent circuit as show in Figure 4.1. The thermal losses in the active part are presented here as a current source (P_T). In stationary state, these losses are transferred to the surrounding via the cooling equipment (R_{th}). However, because of the temporary change of heat flows or fluctuations in ambient temperature, the thermal capacitance (C_{th}) of the transformer must be additionally taken into account [Tenbohlen, 1999].

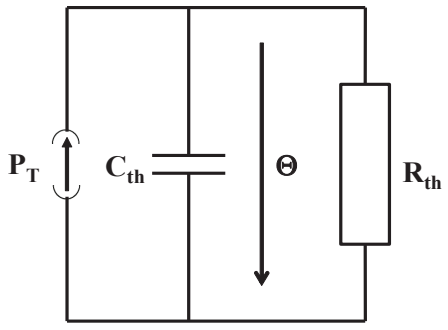

Figure 4.1 One-body diagram of the transformer

The temperature drop over the parallel circuit between the thermal capacity (C_{th}) and the thermal resistance (R_{th}) corresponds to the temperature rise of oil in the transformer. The neutral of the circuit is provided as the ambient temperature. Based on an assumption that all losses are transferred to the environment via a thermal resistance of the

cooling equipment and by taking the variation of ambient temperature into consideration, the model is shown as below [from here on **Model D**].

$$\vartheta_{TO} = \left(\vartheta_{TO,\infty} - \vartheta_{TO,I}\right)\left(1 - e^{\frac{-\Delta t}{C_{th}R_{th}}}\right) + \vartheta_{TO,I} \tag{4.15}$$

Where

$$\vartheta_{TO,\infty} = \vartheta_{amb} + \left(P_S K^2 + P_N\right)R_{th} \tag{4.16}$$

The losses in the individual components during the operation of a transformer increase the temperature of the active part. The losses are the no-load loss and load loss.

The approximated range of thermal capacitance C_{th} may be expressed in terms of the specific heat capacity (c_p) and the mass (m) of the observed parts of the transformer. In a transformer, materials in different quantities and with various specific thermal capacitances are used. The thermal capacitance may be calculated from:

$$C_{th} = m_{oil}c_{p,oil} + m_{cu}c_{p,Cu} + m_{Fe}c_{p,Fe} + m_{steel}c_{p,steel} \tag{4.17}$$

Table 4.3 shows the specific thermal capacitance of the different components of a transformer.

Material	c_P [Wh/g·K]
Oil	0.5360
Copper [*Cu*]	0.1066
Iron [*Fe*]	0.1288
Steel	0.1332

Table 4.3 Specific thermal capacities

4.3 Top-oil Temperature Models Investigation

The four models mentioned above (Model A, B, C and D) are chosen to be examined in this work. The investigations are done using a database collected from different types of three phase transformer units for a period of at least one year. Due to an uncertainty associated with some manufacturer-supplied parameters and the complicated transformer configuration, some model parameters have to be optimized by means of parameter estimation. Based on these model parameters the top-oil temperature is then calculated and the performances of the models are compared. The performance of the model is defined as the deviation of calculated top-oil temperature from the measured top-oil temperature.

4.3.1 Parameter Estimation

Least square technique is the optimization technique, which was used in this work for the parameter estimation. Parameter estimation is the process of finding the values of the unknowns of a mathematical model for simulating a complex system. A model is generally given by differential equations or a system of equations or inequalities. Interval computations are numerical computations over a set of real numbers.

Least square Techniques (Regression Analysis)

In statistics, least-squares techniques can be used as an approach for assigning values to unknown quantities in a statistical model, based on observed data. It is a mathematical procedure, which attempts to find a function, which closely approximates a series of measured data. The least-squares technique is commonly used in curve fitting.

The best-fitting curve is found by minimizing the sum of the squares of the ordinate differences (called residuals) between points generated by the function and corresponding points in the data, with the smallest operations (per iteration). However, it requires a large number of iterations to converge. An implicit requirement for the least squares method to work well is that errors in each measurement be randomly distributed. The collected data should be well chosen, to allow visibility into the variables to be solved for (and possibly giving more weight to particular data, referred to as weighted least-squares).

When a function $f(x_i) = y_i$ must be found for a dataset that consists of the points (x_i, y_i) with $i = 1, 2...n$, it is firstly supposed that the function $f(x)$ is of a particular form that contains some parameters which need to be determined. For instance, suppose that the function is quadratic: $f(x) = ax^2 + bx + c$, where a, b and c are not yet known. The values of a, b and c may be found by minimizing the sum of the squares of the residuals (S):

$$S = \sum_{i=1}^{n} (y_i - f(x_i))^2 \tag{4.18}$$

The problem is more difficult if $f(x)$ is not linear, but then an algorithm like Newton's method or gradient descent can be used. Another possibility is to apply an algorithm that is developed especially to tackle least squares problems, for instance the Gauss-Newton algorithm or the Levenberg-Marquardt algorithm.

4.3.2 Software Development

Two programs for top-oil calculation were developed in MATLAB. First, the input data from different data sources are put in one file. This process is performed in a data preparation program. In the second step, the necessary parameters are estimated and the top-oil temperature is calculated.

Data Preparation

The required measured data are obtained from an online monitoring system MS 2000 supplied by AREVA Energietechnik GmbH. The original data of different input variables are available in different sampling periods and in individual text files. The specific software is developed in order to combine all the input data with different sampling time intervals into one input file.

Moreover, the information of the states of operating pumps and fans are indicated only by the status *"on"* and *"off"* in an individual file for each pump and each fan. The software calculates the total number of operating pumps and fans in each period. This combined input file may be written either in the format of Matlab or Excel, depending on the required application.

Parameter Estimation

The function for nonlinear curve fitting (*lsqcurvefit*) in the *MATLAB Optimization Toolbox* is applied in the parameter estimation process. Function *lsqcurvefit* solves the nonlinear curve-fitting (data-fitting) problems in the least-squares sense. This function may be expressed in Eq. (4.19). It is an attempt to find the coefficients x that best fit the equation to the given input data *xdata*, and the observed output *ydata*, where *xdata* and *ydata* are vectors of length m and *F(x, xdata)* is a vector-valued function.

$$\min_x \frac{1}{2}\left|F(x, xdata) - ydata\right|_2^2 = \frac{1}{2}\sum_{i=1}^{m}\left(F(x, xdata_i) - ydata_i\right)^2 \qquad (4.19)$$

Results from [Vilaithong, 2005] indicate that the estimated parameters are not constant values. They vary according to the different operating states of pumps and fans in different periods of the year. However, in order to simplify the model to be used in an online monitoring system, one set of estimated parameters for each state of operating pumps and fans should be applied for the whole year.

In this work, the whole dataset is divided into different periods depending on the operating states of pumps and fans. In each period, the parameters will be estimated when the operating state of pumps and fans in that period remains constant for more than 2 hours and the load factors are larger than 0.02. Consequently, for one operating state, there are different sets of estimated parameters from different periods. In each period, these estimated parameters are used to calculate the top-oil temperature, then, the temperature deviation between the measured and the calculated top-oil temperature is determined.

The estimated parameters from the periods with temperature deviation less than 2K are selected to determine the average estimated parameters of each operating state of pumps and fans (n). The time interval of different periods (Δt_n) is used for weighting the estimated parameters in that period (P_{n1}, $P_{n2...}$). The calculation of the average estimated parameter ($\overline{P}_n$) for any state of operating pumps and fans is shown as the following equation.

$$\overline{P}_n = \frac{\left(P_{n1} \cdot \Delta t_{n1}\right) + \left(P_{n2} \cdot \Delta t_{n2}\right) + \left(P_{n3} \cdot \Delta t_{n3}\right) + \ldots}{\Delta t_{n1} + \Delta t_{n2} + \Delta t_{n3} + \ldots} \tag{4.20}$$

4.3.3 Investigated Transformer Characteristics

The characteristics of the three different investigated power transformers (Tr1, Tr2, and Tr3) are shown in Table 4.4. Three different cooling types are considered. They are ONAN, ONAF and OFAF.

As the aim of this work is to detect malfunction of pumps or fans using the top-oil temperature prediction, the main criteria for the calculation is the number of operating pumps and fans. The operating states of the cooling units of Tr2 remain constant during the investigated period (number of operated fans = 2). The cooling operating states of Tr3 vary as seen in Table 4.5. The total number of pumps is 8 and the total number of fans is 8.

Transformer	**Tr1**	**Tr2**	**Tr3**
Type	Grid coupling	Grid coupling	Generator
Rated power [kW]	40	150	840
Rated voltage [kV]	110	245/36/6	21/233 ±5%
Short-circuit loss [kW]	135	414.2	2060
No-load loss [kW]	20	67.52	370
Type of cooling	ONAN	ONAF	OFAF
Total number of pumps	0	0	8
Total number of fans	0	2	8

Table 4.4 Main characteristics of the investigated power transformers

State	Number of pumps	Number of fans
1	8	0
2	8	2
3	8	4
4	8	6
5	8	8

Table 4.5 States of pumps and fans in operation of Tr3

To apply a thermal model in an online monitoring system, the set of estimated parameters should be able to apply in different periods of input data. Thus, in this work, by using the parameters estimated from one period of data to calculate the top-oil temperature in other period of input data, the reliability of the estimated parameters is also examined. Table 4.6 shows the different periods of the input data used for the parameter estimation process and the top-oil temperature calculation process.

	Parameter estimation	Top-oil temperature calculation
Tr1	January 2004 – May 2004	June 2004 – December 2004
Tr2	January 2003 – May 2003	June 2003 – December 2003
Tr3	January 2003 – December 2003	January 2004 – December 2004

Table 4.6 Sets of investigated data

4.3.4 Required Input Data

All model parameters are classified as seen from Table 4.7. The input constants P_S and P_N for Model A, B and D may be obtained from the data sheets of transformers. The input constant C_{th} from Model A and Model D are obtained from calculation according to Eq. (4.18).

	Model A	Model B	Model C	Model D
Input constant	P_S P_N C_{th}	-	P_S P_N	P_S P_N C_{th}
Input variable	K ϑ_{amb} $\#Fans$	K ϑ_{amb} $\#Fans$	K ϑ_{amb} $\#Fans$	K ϑ_{amb} $\#Fans$
Estimated input parameter	$\theta_{TO,R}$	J_1 J_2 J_3 J_4	$\theta_{BO,R}$ $\theta_{MO,R}$	R_{th}

Table 4.7 Model parameters classification

The results of calculated thermal capacities from Eq. (4.17) and Table 4.3 can be seen in Table 4.8. Masses of transformer parts and transformer oil are required in the calculation. These values are obtained from the data sheet of the transformers.

	m_{oil} [Kg]	m_{cu} [Kg]	m_{Fe} [Kg]	m_{steel} [Kg]	C_{th} [W·h/K]
Tr1	17000	11845	20550	7820	14063
Tr2	48555	27800	60000	41200	42509
Tr3	71000	282000		58000	82106

Table 4.8 Thermal capacities of investigated transformers

4.4 Application of Physical Thermal Models

The parameters of the above mentioned transformers are estimated for all models. Long-term investigations at varying load currents and ambient temperatures are performed; results are shown in section 4.4.1. The influence of the starting values in the parameter estimation process and the variation of top-oil time constant are later discussed in section 4.4.2 and section 4.4.3 respectively. Further, the comparison of the performances between the models is dealt with in the last section.

4.4.1 Results of Parameter Estimation

The estimated parameters for different models obtained from Trl and Tr2 are shown in Table 4.9. In order to approximate an acceptable range of the estimated top-oil rise temperature $\theta_{TO,R}$ of Model A and Model C, the most frequently measured top-oil temperature [*FO*] and ambient temperature [*FA*] in the investigated period are also calculated. The *FO* and *FA* of Trl, Tr2 and Tr3 are measured during June 2004 - October 2004, June 2003 - December 2003 and January 2004 -December 2004, respectively.

The estimated $\theta_{TO,R}$ from Model A is 22 K for Trl and 29 K for Tr2. They are in the acceptable range. However, the estimated $\theta_{TO,R}$ of Trl (79 K) and Tr2 (61 K) obtained from Model C are not reasonable. They are much higher than the estimated $\theta_{TO,R}$ from Model A. The set of estimated parameters from Model B show no obvious relation between each parameter.

The acceptable range of R_{th} from Model D is estimated from the Eq. (4.15). It should be in the order of 10^{-4} K/W. The results in Table 4.9 show a seemingly acceptable value for R_{th}, both from Trl ($6.0907*10^{-4}$ K/W) and Tr2 ($1.3532*10^{-4}$ K/W).

Table 4.10 shows the estimated parameters from Tr3 with different operating states of fans *[F].* The estimated $\theta_{TO,R}$ of Model A, $\theta_{BO,R}$ and $\theta_{MO,R}$ of Model C and R_{th} of Model D decrease when numbers of operating fans increase. However, in all models, there is no obvious relation between each estimated parameter for different states of operating fans.

	FO (°C)	*FA* (°C)	Model A	Model B				Model C	Model D
			$\theta_{TO,R}$ *(K)*	J_1	J_2	J_3	J_4	$\theta_{TO,R}$ *(K)*	R_{th} *(K/W)*
Tr1	34	16	22	0.966	1.350	0.619	0.028	79	$6.0907*10^{-4}$
Tr2	46	21	29	0.951	1.877	0.947	0.046	61	$1.3532*10^{-4}$

Table 4.9 Estimated parameters from different models for Tr1 and Tr2

	Model A	Model B				Model C		Model D
	$\theta_{TO,R}$ (K)	J_1	J_2	J_3	J_4	$\theta_{BO,R}$ (K)	$\theta_{MO,R}$ (K)	R_{th} (K/W)
P 8 *F* 0	165	-0.747	2.668	35.361	4.877	244	346	8,2435*10^{-5}
P 8 *F* 2	87	0.593	7.854	15.916	0.043	188	141	7,6752*10^{-5}
P 8 *F* 4	75	0.425	0.596	23.308	0.245	186	112	2,6405*10^{-5}
P 8 *F* 6	58	0.269	-0.070	30.005	0.279	159	111	2,3369*10^{-5}
P 8 *F* 8	38	0.591	3.188	14.657	0.171	120	95	1,6919*10^{-5}

Table 4.10 Estimated parameters from different models for Tr3

4.4.2 Influence of Starting Values in Parameter Estimation

In the first step of the parameter estimation process, the starting values of the estimated parameters must be set. In this section, the influence of these starting values is investigated.

Different starting values: 1 K, 10 K and 100 K for the top-oil temperature rise $\theta_{TO,R}$ were employed in the model A and C. Results show that the different starting values have no influence on the parameter estimation process, in both models. The same values of the estimated parameters were obtained from all different starting values.

For Model D, the starting values of the thermal resistance R_{th}: 10^{-9} K/W, 10^{-4} K/W, 10^{-2} K/W, 1 K/W and 100 K/W were applied. In Table 4.11, results from the calculations with Tr1 show that the different starting values do have an influence in some manner on the parameter estimation process. Results show the same values of the estimated parameters were obtained when the starting values were set below 1.

Starting Value R_{th} (K/W)	10^{-9}	10^{-4}	10^{-2}
Estimated R_{th} (K/W)	2.7187*10^{-3}	2.7187*10^{-3}	2.7187*10^{-3}

Table 4.11 Estimated parameters from different starting value for Model D

4.4.3 Variation of Top-oil Time Constant Values

The top-oil time constant (τ_{TO}) of Model A may also be considered when varying the starting value. It should be remarked that when an investigated transformer is subjected to a step variation of load, the top-oil temperature rise does not behave exactly as an exponential function and the oil time constant may therefore not be treated as a fixed value [IEEE Std. C57.91, 1995]. The time constant is found to vary according to the top-oil rise over ambient temperature at different time and may be calculated as shown in Eq. (4.21).

$$\tau_{TO} = \tau_{TO,R} \frac{\left(\frac{\theta_{TO,\infty}}{\theta_{TO,R}}\right) - \left(\frac{\theta_{TO,I}}{\theta_{TO,R}}\right)}{\left(\frac{\theta_{TO,\infty}}{\theta_{TO,R}}\right)^{\frac{1}{n}} - \left(\frac{\theta_{TO,I}}{\theta_{TO,R}}\right)^{\frac{1}{n}}} \tag{4.21}$$

Where the top-oil time constant at rated load is given by the following:

$$\tau_{TO,R} = \theta_{TO,R} \frac{C_{th}}{P_T} \tag{4.22}$$

In this section, the variation of τ_{TO} with varying starting values of $\theta_{TO,R}$: 1 K, 10 K and 100 K were considered in the parameter estimation process. Results also show that the temperature deviation for all transformers obtained from the model with the varied τ_{TO} has no significant difference from the temperature deviation obtained from the fixed τ_{TO}.

4.4.4 Performance of Different Top-oil Temperature Models

To evaluate the performance of the investigated thermal models, the following discussions focus on the calculated time evolution of top-oil temperature for all models. Due to the influence of the ambient temperature on the capability of the models, two different time periods are analyzed. The first considered period involves an average ambient temperature above 20 °C and is referred to as “summer period”. The

second period, termed as “winter period”, during which the average ambient temperature is around 10 °C.

Ambient temperature, load factor and calculated top-oil temperature courses in the summer period are shown in Figure 4.2, 4.3 and 4.4 for Trl, Tr2 and Tr3, respectively. Ambient temperature, load factor and calculated top-oil temperature courses in the winter period are shown in Figure 4.5, 4.6, 4.7 for Tr1, Tr2 and Tr3, respectively.

In the summer period, the load levels of observed transformers are different. For Trl, a low load factor is found with daily fluctuations within a range of 0.2. The load factor of Tr2 is constant high at 0.7. A high fluctuation of load factor between 0.2 and 0.6 is found in Tr3. There is also a shutdown State in Tr3 from 9 August until 11 August. The ambient temperature in this period is found in a range of variation of 20 °C for all transformers.

In Tr1 and Tr2, Model B and Model D can reasonably capture the measured temperature courses better than Model A and Model C, in average. The top-oil temperature deviations of both Model B and Model D are on average 2 K. The calculated temperature from Model B is always 1 K lower than the measured temperature for both transformers. The calculations temperature from Model A and Model C for both transformers during the increasing of either load or ambient always show a temperature that is on average 5 K higher than the measured temperature. This delay in temperature change might be an effect of an oil time constant, which is calculated from the inaccurate thermal capacitance in Eq. [4.5].

In Tr1, during the period of constant ambient temperature on the 11 August, Model A also presents a similar constant top-oil temperature. However, the calculated top-oil temperatures from other models still decrease. This implies that the ambient temperature has a strong influence on the top-oil temperature calculation of Model A. Conversely, the other models react slowly on an ambient temperature change. The short period of constant top-oil temperature is also presented in Model C. Thus, the ambient temperature may also have an influence on the top-oil temperature calculation of Model C.

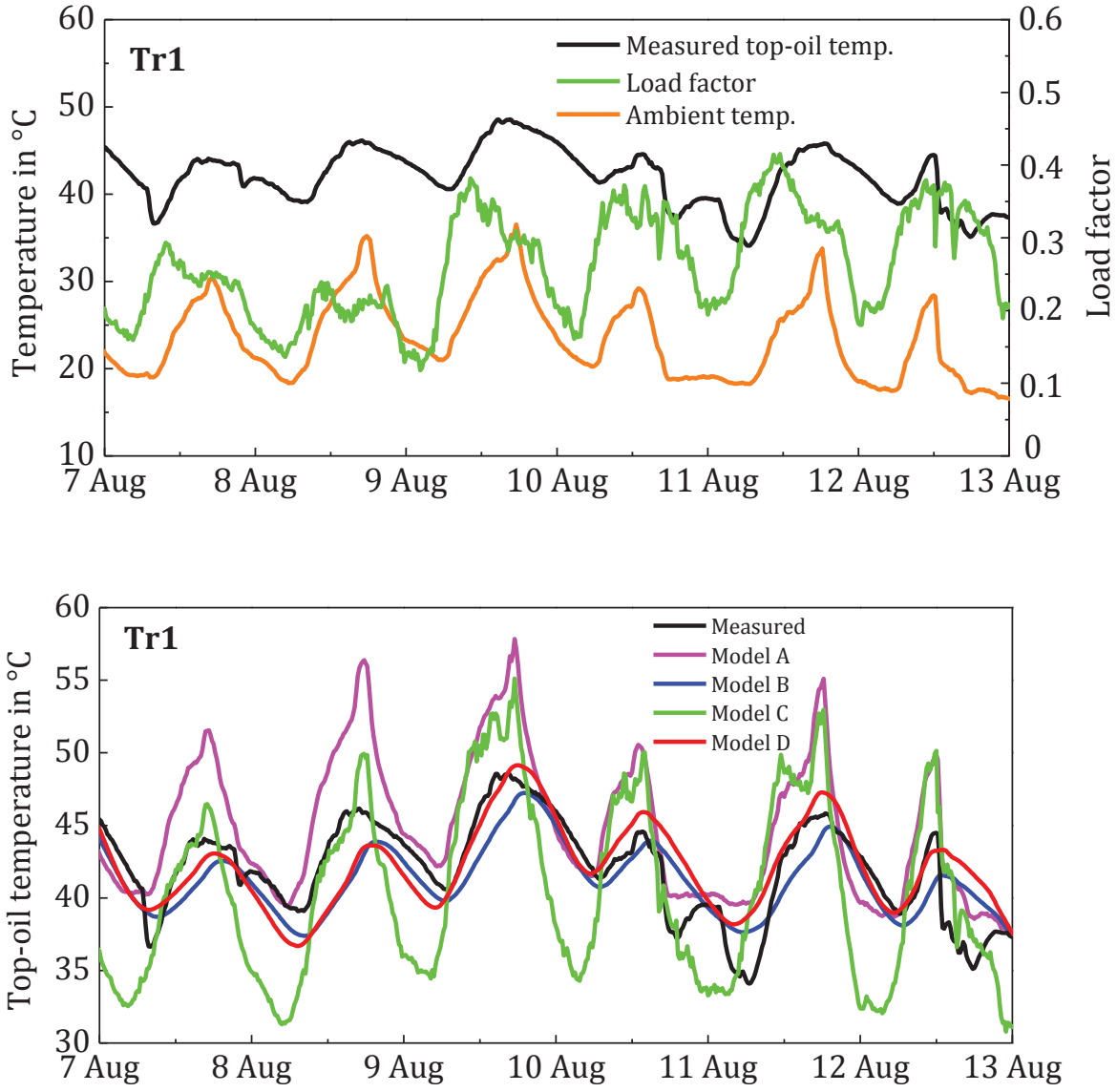

Figure 4.2 Results of Tr1 during the summer period

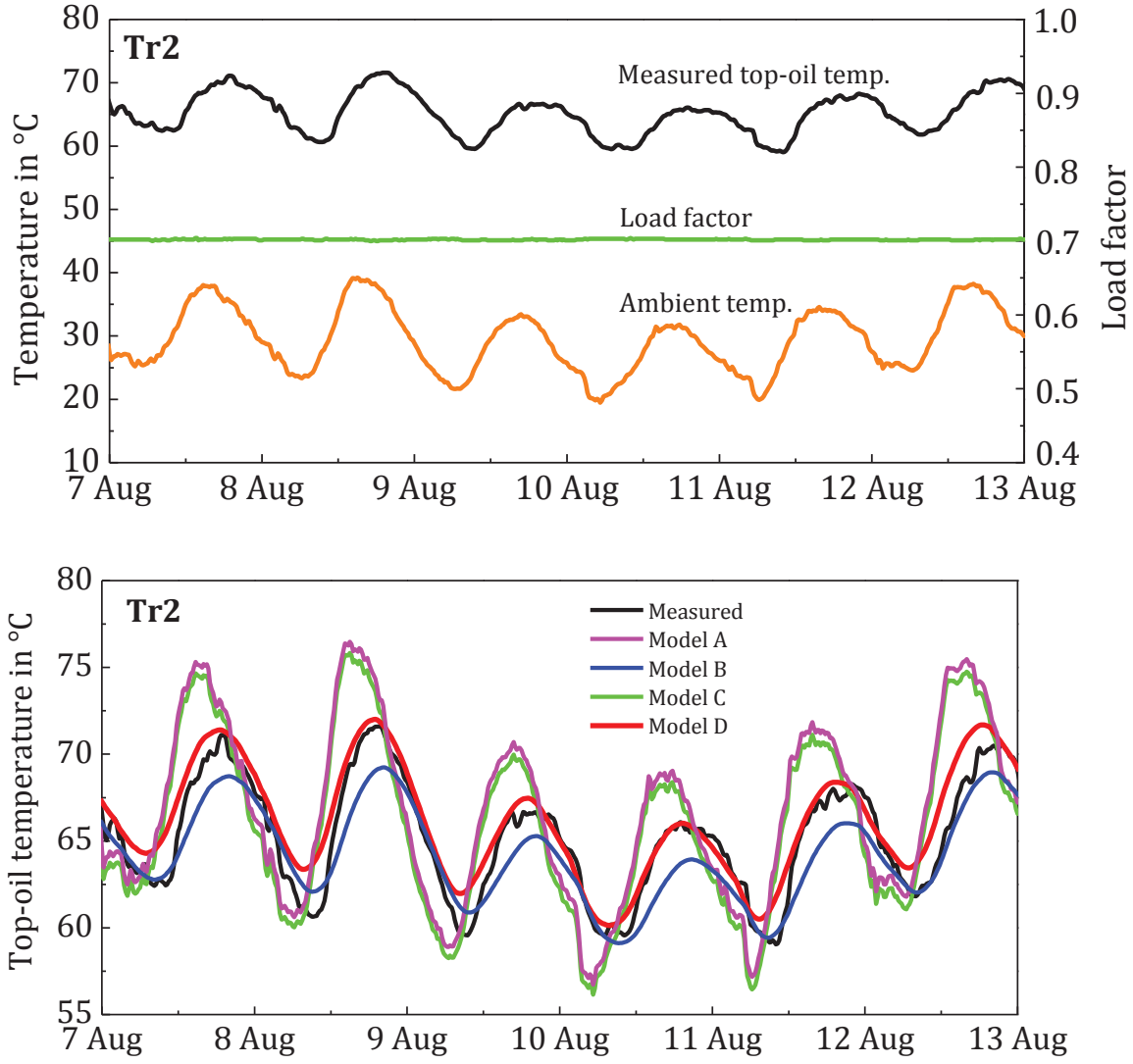

Figure 4.3 Results of Tr2 during the summer period

The calculated top-oil temperature courses of Tr3 from all models in this period are very unstable due to the frequent changes in the number of fans. A long period of the shut-down state can be seen. It has a strong effect on the top-oil temperature calculated from Model B. The temperature deviations between measured and calculated top-oil temperature for Model C and D are very high compared to the measured temperature. The top-oil temperature courses of Model A and Model B run at a similar level as the measured temperature. Model A shows the most stable top-oil temperature course. However, Model B sometimes shows the transients in calculated top-oil temperature. Thus, Model A and Model B have more ability than the others to calculate the top-oil temperature during the changes of pumps and fans operation.

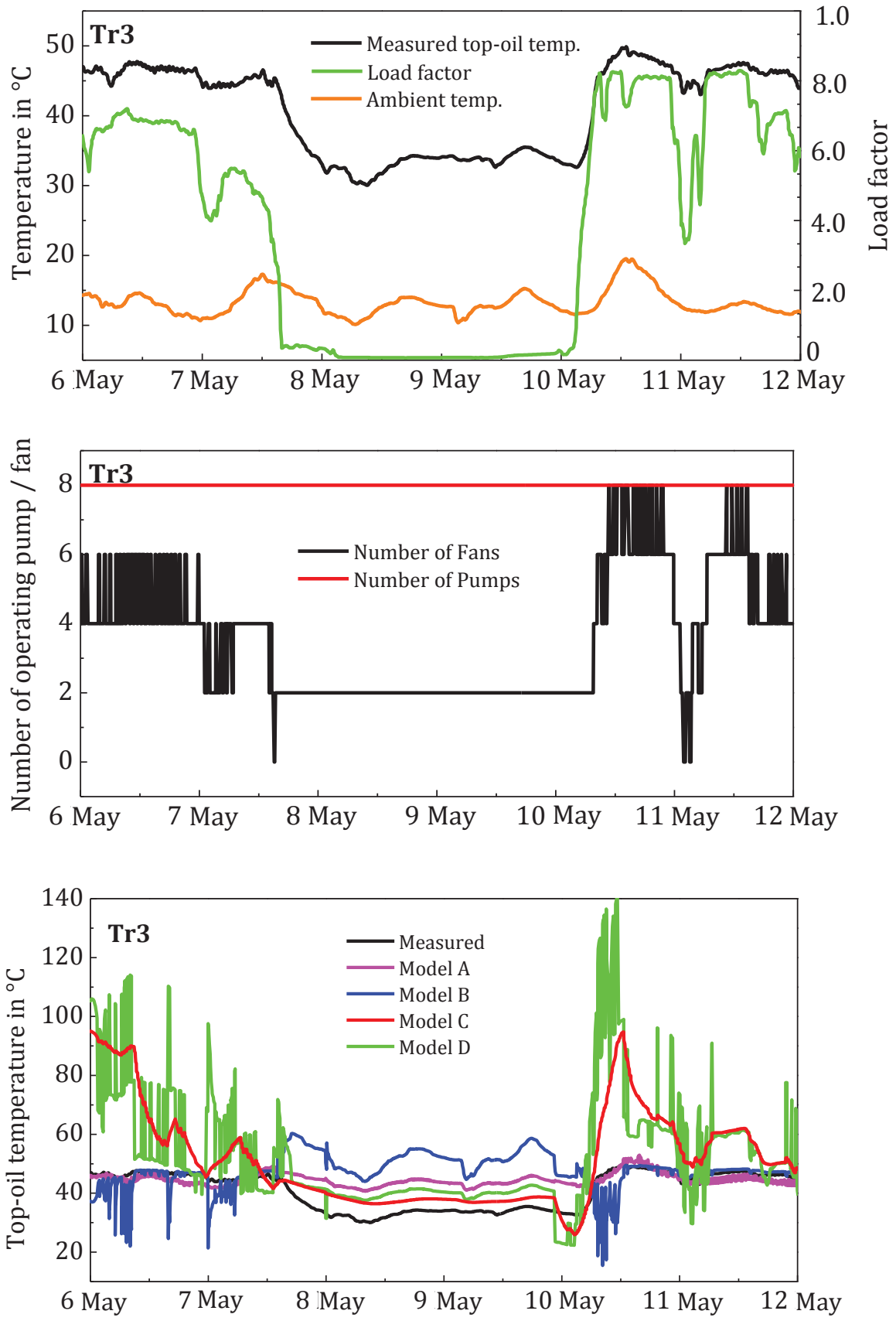

Figure 4.4 Results of Tr3 during the summer period

In winter, the load conditions, as shown in Figure 4.5, are similar to the load conditions in summer. A low load factor is found in Tr1, and it fluctuates strongly. It varies normally from factor 0.2 to 0.4. In some stage, it rises up to a factor of around 1.0. The load factor of Tr2 is higher and quite constant at 0.7. A high fluctuation in load factor between 0.3 and 0.7 is found for Tr3. The variation of ambient temperature in this winter period is lower than in summer and occurs in a range of variation of 10 °C for all transformers.

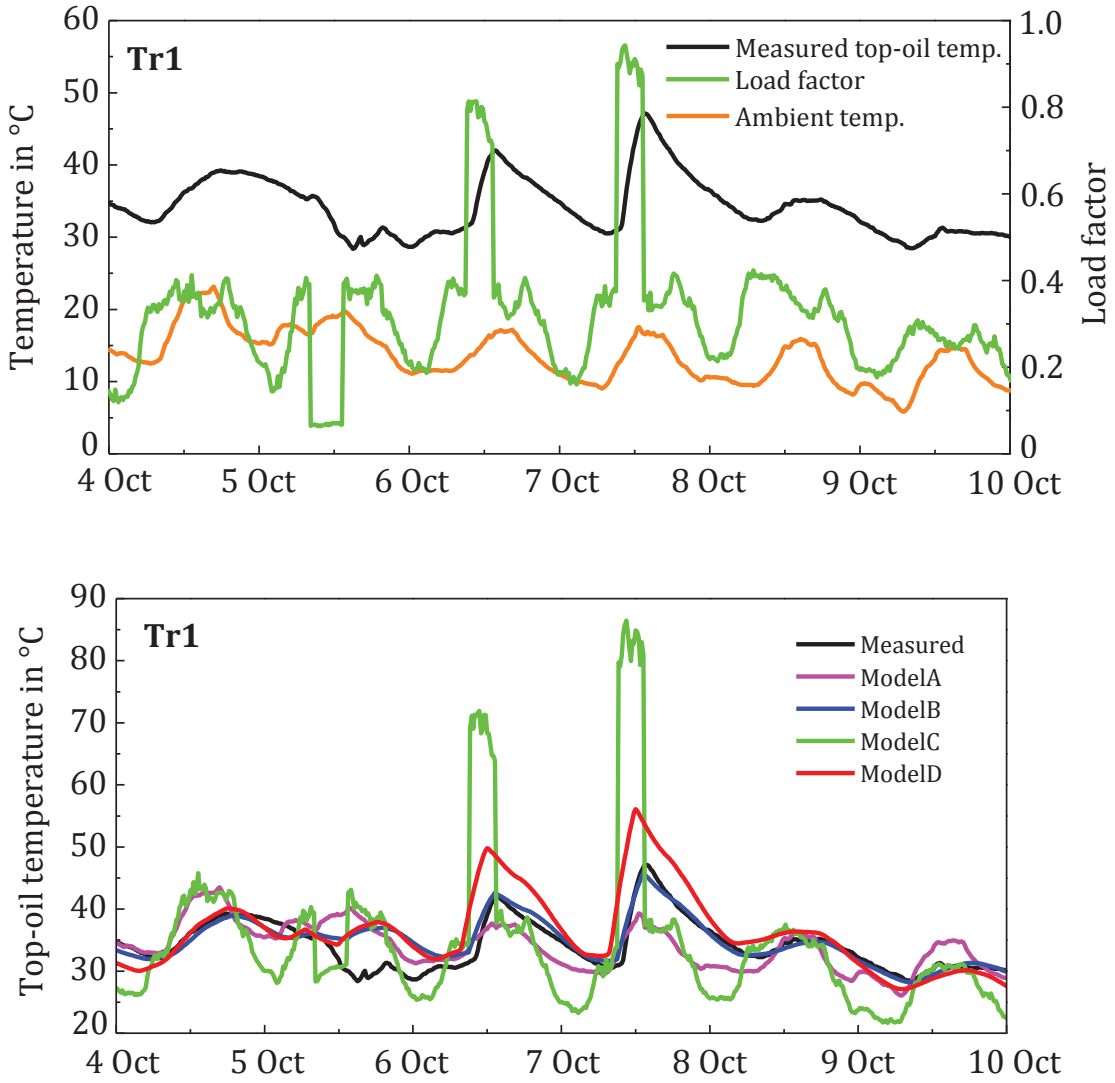

Figure 4.5 Results of Tr1 during the winter period

Model A and Model C produce fairly in consistent results. The calculated temperature courses from both models fluctuate clearly due to the fluctuation of the load. During the transient of the increasing load on 6 October and 7 October up to a factor of over 0.8, an increase in calculated top-oil temperature from Model C is clearly observed. The calculated top-oil temperature rises up to over 80 °C, which is more than a 40 K deviation from the measured temperature. Model B in Tr1 can reasonably capture the measured temperature courses over most of this winter period. The average temperature deviation between calculated and measured temperature in this period is 1 K. However, during the transient of decreasing load on 5 October, the calculated temperature still increases, while the measured temperature decreases after the transient state. The average temperature deviation of more than 5 K can be observed in this stage. Model D also gives reasonable results over the period of low fluctuation of the load. The higher calculated top-oil temperature from model D is also observed in this transient period. The temperature deviation between calculated and measured top-oil temperature of around 10 K can be noticed.

Figure 4.6 shows the calculations for the winter period of Tr2. All models produce calculated top-oil temperature values that are around 5 K lower than the measured top-oil temperature. However, all models can still capture the measured temperature courses. Model A and Model D present better results than the others. Strong transients of the load factor have been observed two times within one week (2 December and 4 December). They fall down to the load factor of 0.4. Results from Model C show explicit decreasing calculated top-oil temperature below 30 °C in this transient period. This result confirms the observation in the last paragraph that the influence of load on Model C is extremely strong.

Results from Tr3 are illustrated in Figure 4.7. Most of models present highly fluctuating top-oil temperature courses, but especially model C. In this winter period, the transients of decreasing loads can be found very often. Fluctuations occur between load factors of 0.3 and 0.7. Model D also shows very low top-oil temperature courses during these periods.

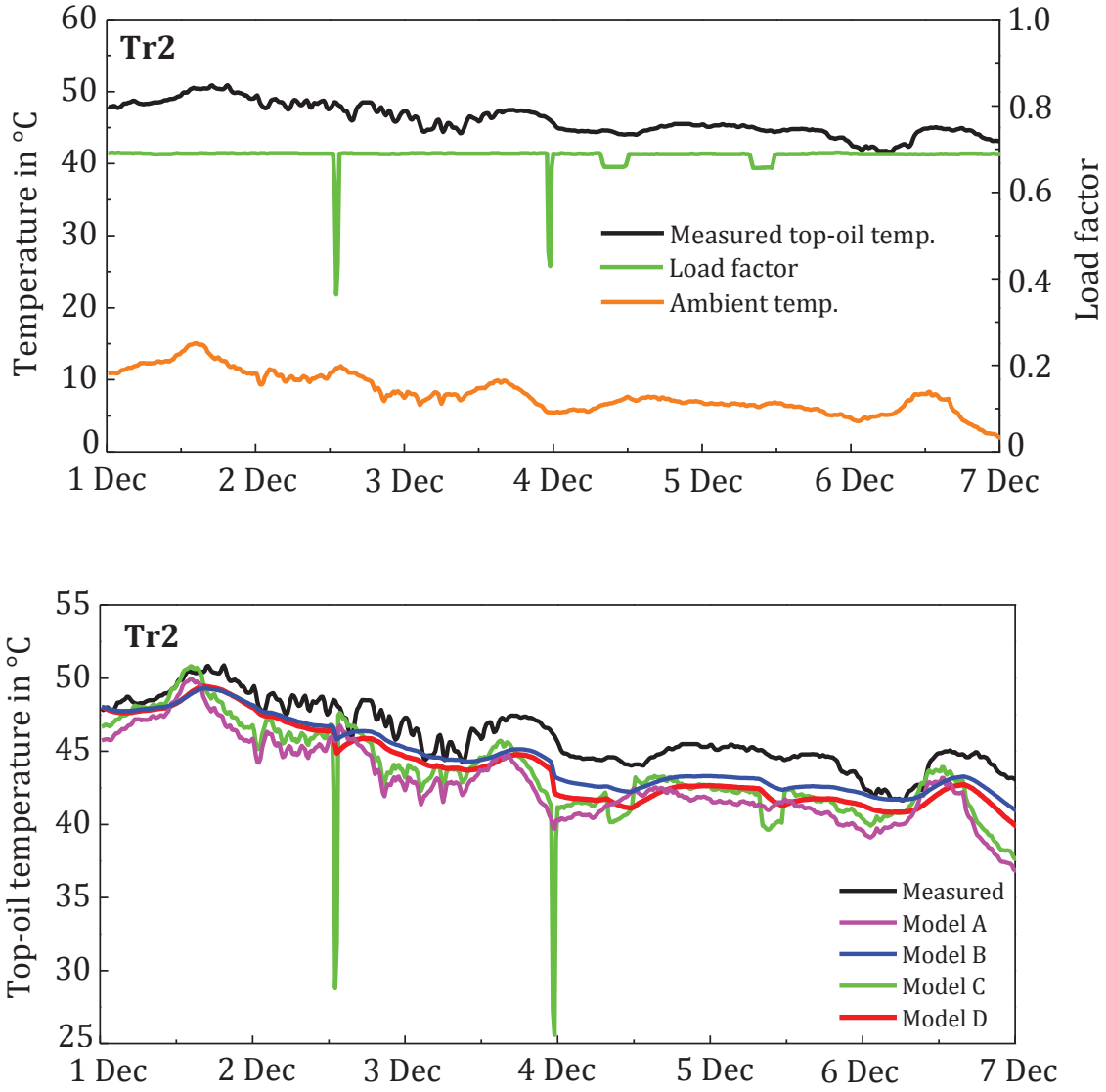

Figure 4.6 Results of Tr2 during the winter period

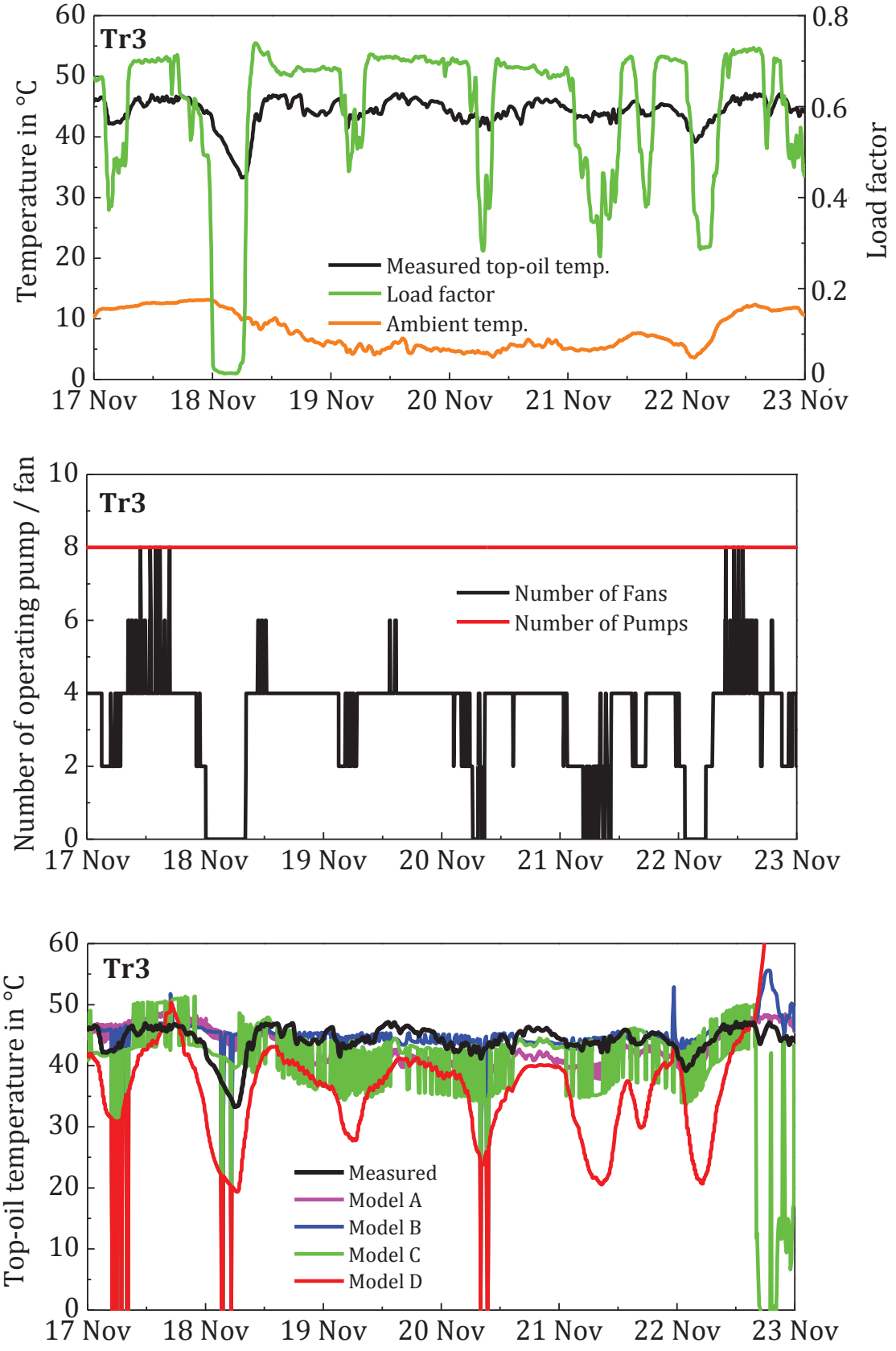

Figure 4.7 Results of Tr3 during the winter period

4.4.5 Conclusion

The comparison of all model performances is summarised in Table 4.12. Results are compared by means of the arithmetic average temperature deviations over the whole calculated period, as shown in Table 4.6. The arithmetic average is applied in order to show the sensitivities of certain models, such as the high average temperature deviations from Model C and Model D, which may be caused by the influence of transient load factor or transient ambient temperature in some periods.

	Model A	Model B	Model C	Model D
Tr1	3.0 K	1.6 K	4.4 K	1.9 K
Tr2	4.4 K	1.3 K	2.4 K	1.7 K
Tr3	4.5 K	3.3 K	12.4 K	13.7 K

Table 4.12 Average temperature deviations from different models

Results for the monthly average temperature deviation are illustrated in Figure 4.8. The temperature deviations from Model B are found to be the lowest of all transformers. The average temperature deviation of Model B for Tr1 (ONAN) is 1.6 K, for Tr2 (ONAF) is 1.2 K. and for Tr3 (ODAF) is 3.3 K. The temperature deviations by other models are almost in the same range of 2 - 4 K, except the results for Tr3 from Model C and Model D. Model D produces the highest temperature deviation in case of Tr3 (13.7 K).

In general, it can be observed that the fluctuation of ambient temperature has more influence on the measured top-oil temperature than the fluctuation of the load. It has a strong influence on the top-oil temperature calculation of Model A and Model C. When Eq. [4.7] of model A and Eq. [4.13] of model C are considered, it can be noticed that the ambient temperature is involved as a final state in the calculation in both models.

Model D considers the ambient temperature in the first-order differential equation of the model, thus the strong fluctuation of ambient temperature has less influence than in other models.

In Eq. [4.13] of model C, the variation of load is directly considered without the time derivative after a step load change. Thus, a strong fluctuation of load has also a direct influence on calculated top-oil temperature from Model C.

The accuracy of the top-oil temperature calculation still cannot be expected when the rapid change of the cooling units is taken into account. The set of estimated parameters of each state of the operating cooling units must be accurately established.

In conclusion, under the scope of this investigated database, Model B is the most accurate physical model for top-oil temperature prediction for transformers with all cooling types. This might be due to the consideration of all input variables as coefficients in the model equation. Also, all coefficients are estimated from the actual measured data. Whereas, the calculated specific thermal capacitance is required as the input constant of the Model A and Model D. Thus, the accurate data of the masses of materials is necessary.

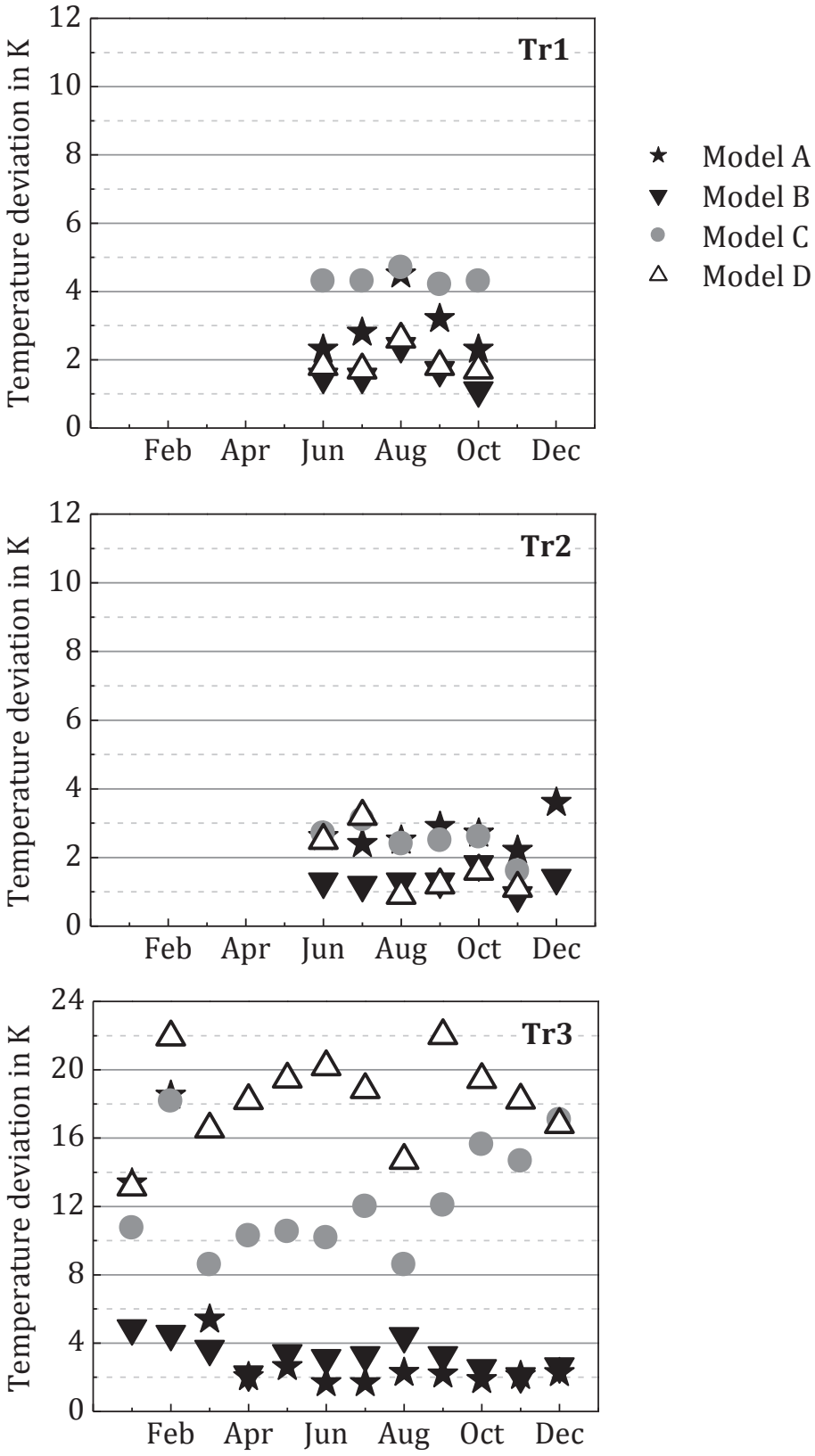

Figure 4.8 Average deviations compared between different mo

5 Top-oil Temperature Prediction Based on Neural Networks

Neural networks may be used to set up complex relationships between inputs and outputs or to find patterns in data. They are also considered by many researchers due to their great similarity to the structure of the brain, a characteristic not shared by more traditional computational systems. Artificial neural networks present a growing new technology as indicated by a wide range of applications that includes transformer top-oil temperature prediction.

5.1 State of the Art

An attempt to estimate the top-oil temperature and hot-spot temperature using neural networks began 10 years ago. In He's work; the uses of static neural networks, temporal processing networks and recurrent networks have been explored for predicting the top-oil temperature of transformers. The Levenberg-Marquardt algorithm has been used in the training. The Recurrent network provided the best performance in terms of both the mean squared error and peak error, compared with the auto regression linear model [He 2000].

Pradhan has shown that the theoretical framework presented in his work is applicable to the estimation of both top-oil temperature and hot-spot temperature under dynamic loading and dynamic ambient conditions. The generalization capability of the neural network model has been increased due to the incorporation of Bayesian Regularization and by the optimal combination of several networks [Pradhan 2004].

Pylvänäinen has shown that, to evaluate temperature values for a transformer supplying loads with severe harmonics, the effects of current harmonics should be taken into account [Pylvänäinen, 2007].

Another paper has introduced an alternative hybrid Recurrent Neurofuzzy network to model the thermal condition of power transformers [Hell, 2007]. Simulations indicated that the Neurofuzzy model is more effective than the multilayer perceptron, radial basis function, and a deterministic

model. That is because it approximates and generalizes transformer dynamics properly and is able to manage imprecise data.

Most publications show the results for short measuring periods (< 2 weeks). Some results are achieved from data of less than 500 samples. However, it is important to consider a long-term period for investigation of dynamic top-oil temperature models for further application in online monitoring and diagnostic systems for power transformers. The variation of loading condition and ambient temperature should be also addressed.

5.2 Introduction to Neural Networks

Neural network or ***A**rtificial **N**eural **N**etwork (ANN)* refers to an interconnecting group of artificial neurons that uses mathematics or a computational model designed to reproduce some properties of biological neural networks. In more practical term, ANNs are non-linear statistical data modelling tools. An advantage of neural networks is that they are well suited to solve the problems that are most difficult to solve by traditional computational methods [Garson, 1998].

5.2.1 Biological Neurons

The human brain is principally composed of about 10 billion neurons; each connected to about 10,000 other neurons. A typical neuron receives electrochemical inputs from other neurons through a host of fine structure called *dendrite*. If the sum of these electrical inputs is sufficiently powerful to activate the neuron, it transmits an electrochemical signal along the *axon* that splits into thousands of branches, and passes this signal to the other neurons whose dendrites are attached at any of the axon terminals. At the end of each branch, a structure called a *synapse* converts the activity from the axon into electrical effects that inhibit or excite in the connected neurones. When a neuron receives excitatory input that is sufficiently large compared with its inhibitory input, it sends a spike of electrical activity down its axon. Learning occurs by changing the effectiveness of the synapses so that the influence of one neuron on another changes. Figure 5.1 depicts a biological neuron (the cell body, or Soma) and its connections *(www.neuralpower.com)*.

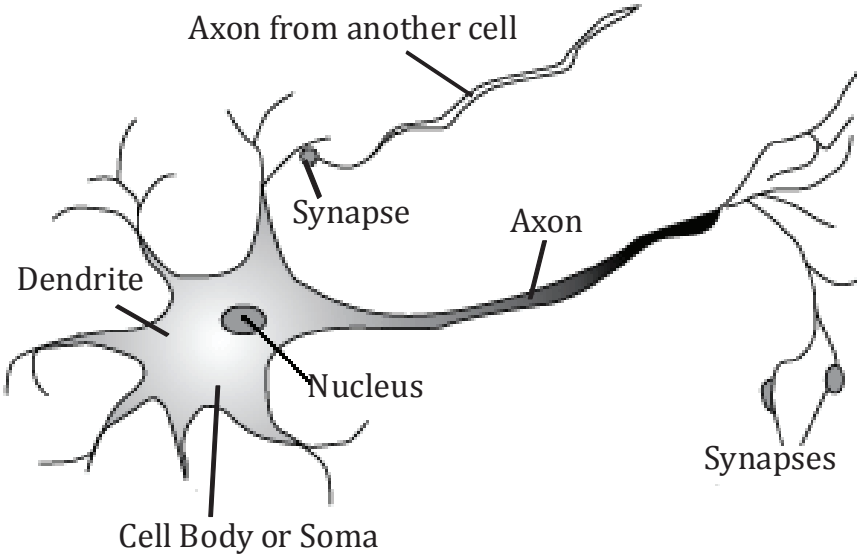

Figure 5.1

Biological neuron

5.2.2 Structure of Artificial Neural Networks

A neural network is a structure involving weighted interconnections among units (or *neurons*). They may be linear or nonlinear scalar transformations, but most often nonlinear. Input neurons, which represent raw information, are fed into a network and connected to an output layer through other neurons in *hidden layers*. The number of hidden layers and number of neurons in each hidden layer are user design parameters. The general rule for network design is to choose these parameters so that the best possible model with as few parameters as possible is obtained [Garson, 1998].

Neurons are connected to each other very specifically, each connection having an individual *weight* (described by a single number). Each neuron generates an output signal based on its activation. It sends its output value to all other neurons to which they have an outgoing connection. Through these connections, the output of one neuron may influence the activations of other neurons. Figure 5.2 shows a sample of the structure of neural network.

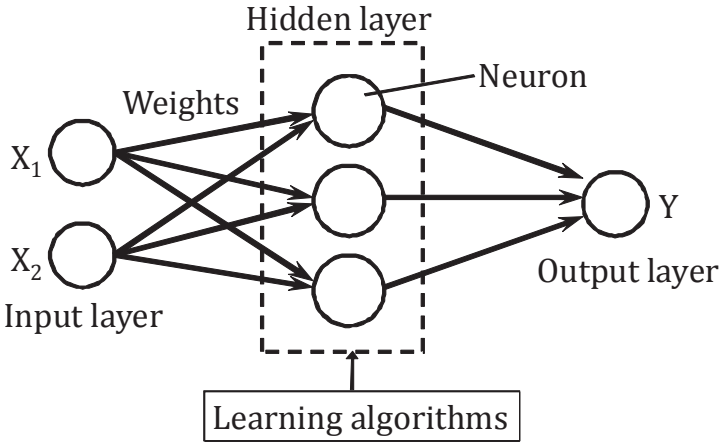

Figure 5.2

Feed-forward Neural Network

The behaviour of an ANN depends on both weights and the input-output function so called *activation function* (or transfer function). The outputs may be obtained from taking a linear combination of input signals and their weights, then transform them with a transfer function. The neuron calculates its activation by taking a weighted sum of the input signals. The activation function determines how and when the summed weighted input values merit the sending of an input signal or firing. Firing occurs when the activation level is above the threshold level set by the learning rule. A signal called input bias may be added to raise or lower the threshold level of a neuron.

The network weights are adjusted by *training* the network. The training (or *learning*) process involves adjusting the weights until an aim is obtained. The aim involves minimizing the sum of squares of the differences between desired and actual outputs. One complete entire training set is called an epoch. The learning process falls into three groups with respect to the sort of feedback that the learner has access to as the following.

Supervised learning: involves learning with some supervision from an external source (teacher signal). It requires the correct output answer for each input pattern to be learned. That is, the desired target which is the response for the vector of training cases is also presented to the network. It allows network weights to be adjusted not only in response to the training vector but also based on an error signal defined by the target vector.

Unsupervised learning: There is no explicit teacher signal in this kind of learning. The network's task is to re-represent the inputs in a more efficient way, as clusters or categories or using a reduced set of dimensions. Unsupervised learning is based on the similarities and differences among the input patterns. It does not result directly in the behaviour of the network because its "outputs" are internal representations. However, these representations may then be used by other parts of the system in a way that affects behaviour. The researcher specifies the number of clusters and the algorithm attempt to identify that number of clusters by assessing their proximity in n-dimensional space. Such models are also called self-organizing networks. The purpose of unsupervised learning might be to discover an underlying structure of the data, to encode the data, to compress the data or to transform the data.

Reinforcement learning: combines the fields of dynamic programming and supervised programming to yield powerful machine-learning system. An agent learns by interacting with its environment and observing the results of these interactions. Supervised learning lets the learner know exactly what it should have done, while reinforcement learning learns by receiving a reward or reinforcement signal from its environment indicating that if the behaviour was inappropriate and (usually) how inappropriate it was for a given input by its own decision making policy [Garson, 1998].

5.3 Training Algorithms

There are a number of learning rules or training algorithms available for neural network models. *Backpropagation* is the best-known training algorithm for the supervised learning process. It is based on the *delta rule*, which was one of the most commonly used learning rules. The delta rule is also called the ***L**east **M**ean **S**quare (LMS)* method. For a given input vector, an output vector is compared to a correct answer. If the difference is zero, no learning takes place; otherwise, the weights are adjusted to reduce this difference. The change in weight Dw_{ij} from output u_i to u_j is given in Eq. (5.1), where r is the learning rate, a_i represents the transfer function of u_i and e_j is the difference between the expected output and the actual output of u_j.

$$\Delta w_{ij} = r \cdot a_i \cdot e_j \tag{5.1}$$

Backpropagation is an algorithm that extends the analysis of the delta rule to the applied networks with hidden nodes. It was created by generalizing the Widrow-Hoff learning rule to multiple-layer networks and non-linear differentiable transfer functions.

Generalization is a group of techniques that allows the amount of information to be retained even when the amount of data is reduced. Input vectors and corresponding target vectors are used to train a network unit. It computes the error term for the output units using the observed error. The model repeat propagating the error term back from output layer to the previous layer and updating the weights between the two layers until the earliest hidden layer is reached.

The weights between neurons of successive layers are initially assigned in random. The speed and accuracy of the learning process (updating weights process) depends on a learning rate. Typically, a new input only leads to an output that is nearly similar to the target. This generalization property makes it possible to train a network on a representative set of input/target pairs and get good results without training the network on all possible input/output pairs.

5.3.1 Levenberg-Marquardt Backpropagation

The Lavenberg-Marquardt algorithm uses an early stopping criterion to improve network training speed and efficiency. To determine the criterion, all data are divided into three sets. The first set is the training set for determining the weights and biases of the network. The second set is the validation set for evaluating the weights and biases and for deciding when to stop training. The validation error normally decreases at the beginning of the training process. When the network starts to over-fit the data, the validation error begins to increase. The training is stopped when the validation error begins to increase and the weights and biases will then be derived at the minimum error. The last data set is for validating the weights and biases to verify the capability of the stopping criterion and to estimate the expected network operation on new data sets.

5.3.2 Scaled Conjugate Gradient Backpropagation

The Scaled Conjugate Gradient is based on a well-known optimization technique in numerical analysis called the Conjugate Gradient method. It was designed to avoid the line search per learning iteration by using a Levenberg-Marquardt approach in order to scale the step size. Unlike many other standard Backpropagation algorithms, this technique does not require any user-specified parameters and its computation is faster [Moller, 1993].

5.3.3 Automated Bayesian Regularization

During the training period, an overfitting problem or poor *generalization* capability may occur. Overfitting is when the model is allowed to draw too many characteristics specific to the training data set. Bayesian regularization is a modification of the Levenberg-Marquardt training algorithm to improve the model's generalization [Mackay[1], 1992]. Generalization means how well the network will make classification of patterns that are not in the training set. This approach involves modifying the performance function, which is normally chosen to be the sum of the squares of the network errors on the training set (*MSE* or E_d).

$$F = E_d = \frac{1}{N}\sum_{i=1}^{N}(e_i)^2 \tag{5.2}$$

The objective function in Eq. (5.2) can be generalization improved as shown in Eq. (5.3) by a term E_w that is the sum of squares of the network weights.

$$F = \beta E_d + \alpha E_w \tag{5.3}$$

The β and α parameter are optimized in Bayesian framework [MacKay[2], 1992]. It is assumed that the weights and biases of the network are random variables following Gaussian distributions and the parameters are related to the unknown variances associated with these distributions. This performance function results in smaller weights and biases of the network. Accordingly, the network response will be smoother and less prone to over-fitting.

5.4 Neural Network Topologies

The topologies of a neural network describe how a network transforms its input to an output. They show the pattern of connections between the units and the propagation of data. In this work, Feed-forward neural networks and Recurrent neural networks were considered.

5.4.1 Feed-forward Neural Network

Feed-forward neural networks are the most popular and most widely used in many practical applications. They have been applied successfully to solve some complex problems including nonlinear system identification and control, finance analysis, signal modelling, power load forecasting, etc. Feed-forward neural networks comprise many neurons working in parallel. Every neuron in the layer is connected with all neurons in the next layer by different strengths or weights. These weights are allowed to be adapted through a learning process, which encodes the knowledge of a network. Data enter at the inputs and pass through the network, layer by layer to the next, until they arrive at the outputs. There is no feedback between layers. No neuron is linked between the same layer, back to the previous layer or skipping the layer. This is why they are called feed-forward neural networks.

5.4.2 Recurrent Neural Network

Recurrent neural networks have a closed loop in the network topology. They are developed to deal with the time varying or time-lagged patterns and are usable for the problems where the dynamics of the considered process is complex and the input data is noisy. Compared to Feed-forward networks, Recurrent neural networks are models with feedback connections. While a Feed-forward network propagates data linearly from input to output, Recurrent network also propagates data from later processing stages to earlier stages. Contrary to Feed-forward networks, the dynamical properties of the recurrent network are important. The values, which are computed as outputs of the network are in the recurrent connections, and may be regarded as extra inputs to the network.

A simple Recurrent neural network, also called an “Elman network”, is a variation on the Feed-forward neural network. Elman networks are commonly one-hidden layer networks with the addition of a feedback connection from the output of the hidden layer to its input. This feedback path allows Elman networks to learn to recognize and generate temporal patterns (time-varying patterns), as well as spatial patterns since the network stores information for the future reference.

At each time step, the input is propagated in a standard Feed-forward structure and a Backpropagation learning rule is applied. The values stored at the previous time step is used to compute for the values at the current time step. The network can maintain a sort of state, allowing it to perform such tasks as sequence-prediction.

5.5 History of Artificial Neural Networks

The concept of neural networks started in the late-1800s as an effort to describe how the human mind performed. The modern era of neural network research is credited with the work done by Warren McCulloch and Walter Pitts in 1943. They published "A logical calculus of the ideas immanent in nervous activity" which was the earliest work in neural computing. They proposed that the modelling brain could be represented mathematically. These models made several assumptions about how neurons worked.

In the late 1940s, Donald Herb made one of the first hypotheses for a mechanism of neural plasticity (i.e. learning), *Hibbing learning*. He presented how learning may take place in a network of perceptrons. Hebbian learning was considered a 'typical' unsupervised learning rule and it (and variants of it) was an early model for long-term neural memory. However, the first significant step of the progression from the biological neural studies took place in 1950’s when Frank Rosenblatt introduced the first concrete neural model, the *perceptron,* which was capable of learning certain classifications by adjusting connection weights.

In 1960 Widrow & Hoff had developed the least mean square theory of linear perceptron and *Widrow-Hoff learning rule*, which was later applied in the *delta rule*. It was the first time for real word applications of neural

network. At first, the use of the Multi-Layer Perceptron (MLP) was complicated by the lack of a suitable learning algorithm. In 1974, Werbos introduce a so-called *backpropagation algorithm* for the three-layered perceptron network. The application area of the MLP networks remained rather limited until the breakthrough in 1986 when a general backpropagation algorithm for a multi-layered perceptron was introduced by Rummelhart and McClelland.

In the early 1980's, researchers showed renewed interest in neural networks. Recent work includes multilayer networks, Hopfield network, Boltzmann machines, competitive learning models, and adaptive resonance theory models. The ability for bi-directional flow of inputs between neurons/nodes was produced with the *Hopfield network* (1982). Unlike the neurons in MLP, the *Hopfield network* consists of only one layer whose neurons are fully connected with each other.

Radial Basis Function (RBF) networks were first introduced by Broomhead & Lowe in 1988. Although the basic idea of RBF was developed 30 years ago under the name method of potential function, the work by Broomhead & Lowe opened a new frontier in the neural network community. A unique kind of network model is the *Self-Organizing Map (SOM)* introduced by Kohonen in 1982. SOM is a certain kind of topological map that organizes itself based on the input patterns in the training process. The SOM originated from the Learning Vector Quantization network the underlying idea of which was also Kohonen's in 1972 [Garson, 1998].

5.6 Top-oil Temperature Prediction with Neural Networks

First, an efficient network structure related to the investigated transformer is designed. Fundamentally, there are no fixed rules to follow for the network design. The core design parameters, which have to be considered, are network topologies, number of hidden layers, and number of hidden neurons as well as the training algorithm. The designed network is then trained using the training data set to compute model weights and biases. The measured top-oil temperature is applied as a target of the training process. The network inputs are:

- Last-state of measured top-oil temperature
- Load current
- Ambient temperature
- Operating states of pumps
- Operating states of fans

After the training process, the top-oil temperature is calculated with the test data set applied in the designed network. The set of investigated data used for the training process and for the testing process (top-oil temperature calculation) can be seen from Table 5.1.

	Training data set	Test data set
Tr1	January 2004 – May 2004	June 2004 – December 2004
Tr2	January 2003 – May 2003	June 2003 – December 2003
Tr3	January 2003 – December 2003	January 2004 – December 2004

Table 5.1 Set of investigated data

5.6.1 Software Development

A network design program is developed for Feed-forward and Elman Recurrent network in MATLAB using the *Neural Network Toolbox* [Demuth, 1992]. Function *newff* is used to create a Feed-forward network and function *newelm* is used for an Elman Recurrent network. The numbers of hidden neurons are varied from 1 to 20 neurons and the networks are trained with 12 training algorithms. Consequently, 240 network structures with five inputs and one target output are examined. Results show that the three-backpropagation training algorithms: Lavenberg-Marquardt, Scaled conjugate gradient backpropagation, and Automated Bayesian Regularization achieve better performance than the others do. Therefore, these three training algorithm are chosen for the discussion.

The available training functions may be found in Appendix C. The maximum number of training epochs is set to be 100. An *epoch* is each time when the training data sets are presented to the model between updates of neural weights [Garson, 1998]. Training stops mostly when the

maximum number of epochs is reached or the performance has been minimized according to the goal. There are two training performance functions available from MATLAB; Performance function with SSE (sum squared errors) and Performance function with MSE (mean squared errors) obtained by dividing the SSE by the number of observations.

In the top-oil temperature calculation process, the designed neural network structure is interpreted into a mathematical model. Weights and biases obtained from the training process are transformed to be the coefficients of the model. The deviation between the measured and calculated temperature is then determined. Results from the network design program show the number of performed epochs, training time in seconds, and average top-oil temperature deviation from the training and testing process. The results are obtained corresponding to the number of hidden neurons, varied from 1 to 20 neurons, and the 16 different training functions. The performance of the network is defined by the average temperature deviation. The 20 best performance network structures are also presented with the monthly results and the weights and biases. In addition, the average deviation for each month and the average deviation of the whole data set for the 20 best performance models are also determined.

5.6.2 Mathematical Models

In general, each neuron in the hidden layer is transformed with a nonlinear transfer function, while in the output layer, the transfer function may be either nonlinear (a nonlinear-nonlinear network) or linear (a nonlinear-linear network). In this work, the Sigmoid nonlinear function (*logsig*) is applied as the transfer function for the hidden layer, which limits the outputs of the layer with small range. Since the calculated top-oil temperature can take values from a continuous set, thus, the linear function (*purelin*) is applied as the transfer function for the output layer.

Sigmoid functions are the most popular type of activation function used in many neural networks. They are continuous, differentiable everywhere and rotationally symmetric about some point. They approach their saturation values asymptotically. *Logsig* is one of the Sigmoid functions that may take any value between the limits of the output between 0 and 1.

The mathematical forms of the *logsig* and *purelin* function may be defined as in Eq. (5.4) and (5.5), respectively. The diagrams of both functions are shown in Figure 5.3 [Demuth, 1992].

$$f_k(s_k) = \frac{1}{1+e^{-s_k}} \tag{5.4}$$

Where f_k is a transfer function of input s_k.

$$f_k(s_k) = \begin{cases} 1 & s_k \to +\infty \\ 0 & s_k \to -\infty \end{cases}$$

$$f_k(s_k) = s_k \tag{5.5}$$

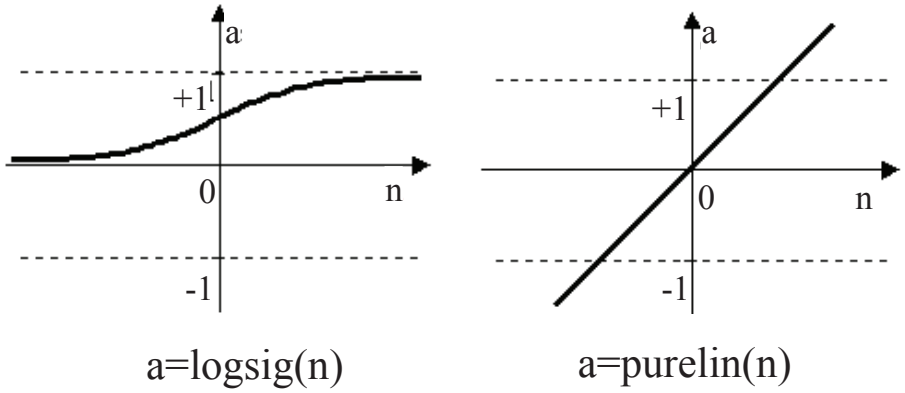

Figure 5.3 Transfer functions

Feed-forward Network

The one-hidden layer and the two-hidden layer feed-forward structures are illustrated in Figure 5.4 and Figure 5.5, respectively. The inputs i_1 - i_5 are the 5 measured input values, w is the weight for the corresponding neurons, b is the bias and y is the output for the network. The input delivered to the transfer function consists of the weight vector multiplied by the input vector summed with the bias.

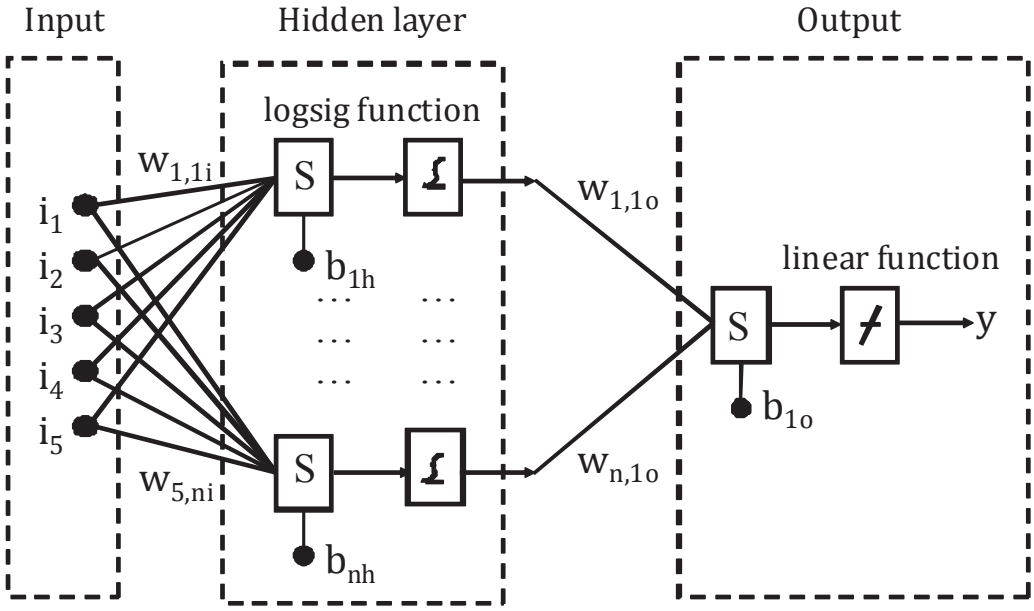

Figure 5.4 One hidden layer feed-forward structure with weights and biases

The output y can be calculated as

$$y = logsig\left(I \cdot W_i + B_h\right) \cdot W_O + B_O \tag{5.6}$$

where: Input: $I = (i_1, i_2, i_3, i_4, i_5)$
Bias of hidden layer: $B_h = (b_{1h} \ldots b_{nh})$
Bias of output layer: $B_o = b_{1o}$
Weights of output layer: $W_o = (w_{1,o}, \ldots, w_{n,o})^T$
Weights of hidden layer:

$$W_i = \begin{bmatrix} w_{1,1i} & w_{1,2i} & \cdots & w_{1,ni} \\ w_{2,1i} & w_{2,2i} & \cdots & w_{2,ni} \\ . & . & . & . \\ w_{5,1i} & w_{5,2i} & \cdots & w_{5,ni} \end{bmatrix}$$

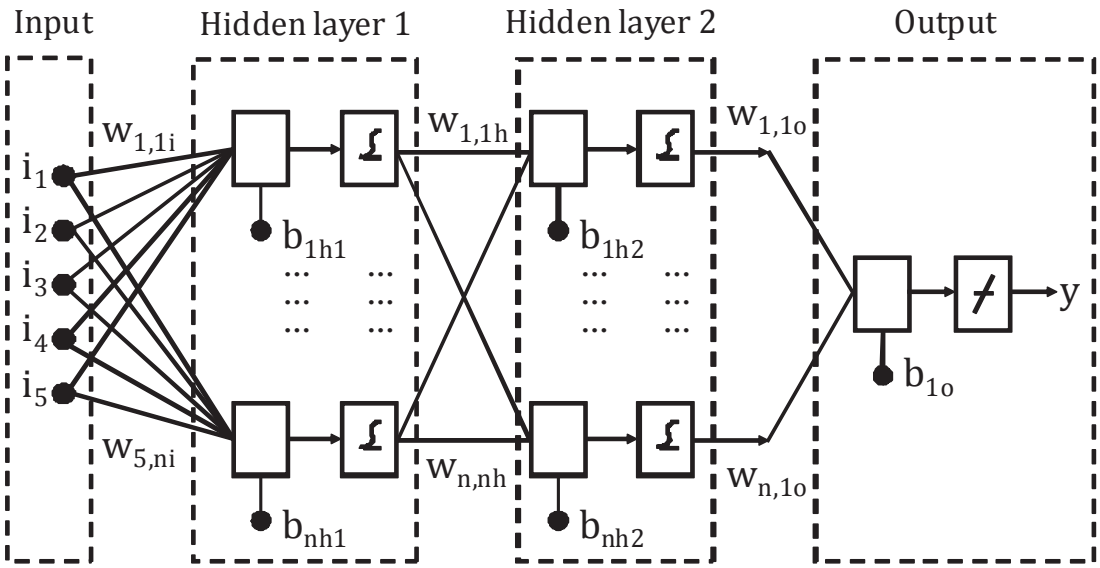

Figure 5.5 Two hidden layer feed-forward structure with weights and biases

The output y of the two-hidden layer network may be calculated as

$$y = logsig\left(logsig\left(I \cdot W_i + B_{h1}\right) \cdot W_h + B_{h2}\right) \cdot W_o + B_o \tag{5.7}$$

where: Input: $I = (i_1, i_2, i_3, i_4, i_5)$
Bias of first hidden layer: $B_{h1} = (b_{1h1} \ldots b_{nh1})$
Bias of second hidden layer: $B_{h2} = (b_{1h2} \ldots b_{nh2})$
Bias of output layer: $B_o = b_{1o}$
Weights of output layer: $W_o = (w_{1,1o}, \ldots, w_{n1o})^T$
Weights of the first hidden layer:

$$W_i = \begin{bmatrix} w_{1,1i} & w_{1,2i} & \cdots & w_{1,ni} \\ w_{2,1i} & w_{2,2i} & \cdots & w_{2,ni} \\ . & . & . & . \\ w_{5,1i} & w_{5,2i} & \cdots & w_{5,ni} \end{bmatrix}$$

Weights of the second hidden layer:

$$W_h = \begin{bmatrix} w_{1,1h} & w_{1,2h} & \cdots & w_{1,nh} \\ w_{2,1h} & w_{2,2h} & \cdots & w_{2,nh} \\ . & . & . & . \\ w_{5,1h} & w_{5,2h} & \cdots & w_{5,nh} \end{bmatrix}$$

Elman Recurrent Network

In the Elman network (Figure 5.6), the previous outputs of the first layer multiplied by the weight matrix are added to the input to the transfer function. The values stored at the previous time step is used to compute the values at the current time step. One requirement in the Elman network is that there has to be enough neurons in the hidden layer. More hidden neurons are needed as the overall input-output function for which a fit is required increases in complexity.

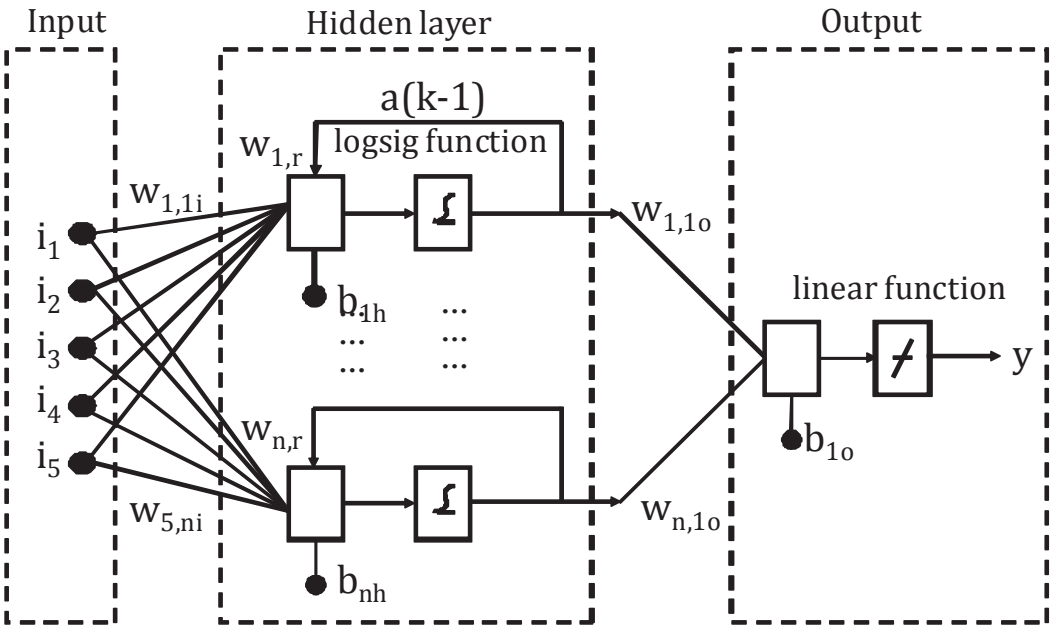

Figure 5.6 Elman network structure with weights and biases

The output y may be calculated by Eq. (5.8), Eq. (5.9) with weights of recurrent connection: $W_r = (w_{1r} \ldots w_{nr})$.

$$a(k) = logsig\left(I \cdot W_i + a(k-1) \cdot W_r + B_h\right) \tag{5.8}$$

$$a(k-1) = logsig\left(I \cdot W_i + a(k-2) \cdot W_r + B_h\right) \tag{5.9}$$

$$y = a(k) \cdot W_O + B_O \tag{5.10}$$

5.7 Calculation Results and Discussion

In this chapter, the performance of top-oil calculation from one-hidden layer and two-hidden layer feed-forward networks and recurrent network with various numbers of neurons are investigated for long-term operation with varying load current and ambient temperature.

5.7.1 Training Time

The speed of the network training process may range from a few seconds to many hours, depending on factors such as the number of weights in the network, the number of training sets considered and the setting of various learning algorithm parameters. As seen from Figure 5.7, the Levenberg-Marquardt training algorithm shows the shortest training time for the investigated transformers and the Bayesian Regularization presents the longest training time. The training time is proportional to the number of neurons in the hidden layer and to the number of data points.

Although ultimately the training time does not affect the monitoring system, since training time of the Bayesian Regularization can be up to 20 minutes, it is important that such times would be acceptable for an industrial situation.

5.7.2 Learning Algorithms and Number of Neurons

Figure 5.8 shows a comparison of the average top-oil temperature deviations from one-hidden layer feed-forward networks. The number of hidden neurons varies from 1 to 20 neurons. The networks are trained with three training algorithms as mentioned previously.

It may be seen that for all transformers, on average, the Bayesian regularization-training algorithm shows better performance than the other training algorithms with average deviations less than 6 K. The Levenberg-Marquardt-training algorithm shows a deviation higher than 10 K in some network structures. Furthermore, good performance in top-oil temperature calculation may also be found in all models with a small number of neurons. An average temperature deviation between the measured and the calculated top-oil temperature less than 2 K is achieved.

The best performance models for each transformer are shown with their average temperature deviations in Table 5.2. The temperature deviations are in the range of 1.4 – 1.9 K.

	Number of neurons	Training function	Deviation [K]
Tr1	8	Bayesian Regularization	1.9
Tr2	10	Bayesian Regularization	1.4
Tr3	5	Bayesian Regularization	1.5

Table 5.2 Results from the best performance network structures

The worst results for each transformer may be seen from the Table 5.3. The average temperature deviations are rather high and ranged from 23 K to 73 K. The results are all from Levenberg-Marquardt-training algorithm. These worst results may also be found in all models with small (6) or large (16) number of neurons.

	Number of neurons	Training function	Deviation [K]
Tr1	7	Levenberg-Marquardt	73.3
Tr2	16	Levenberg-Marquardt	23.7
Tr3	6	Levenberg-Marquardt	94.1

Table 5.3 Results from the worst performance network structures

The implication for the monitoring system implementation is that a lower number of neurons results in a less complicated system, which generally can be considered advantageous. Therefore, the smallest acceptable number of neurons should be considered during the network design process. Different transformers require their own individually designed network.

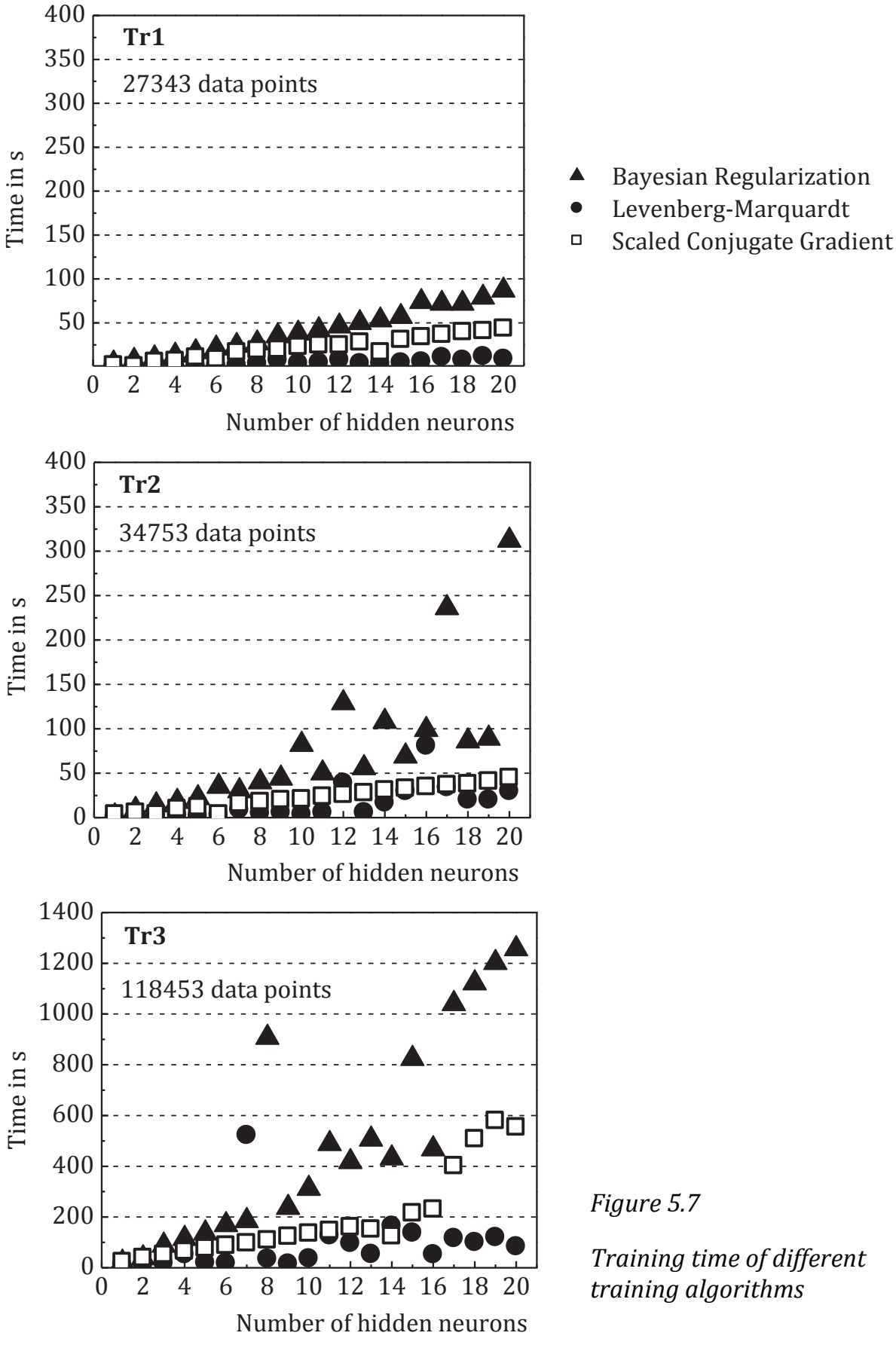

Figure 5.7

Training time of different training algorithms

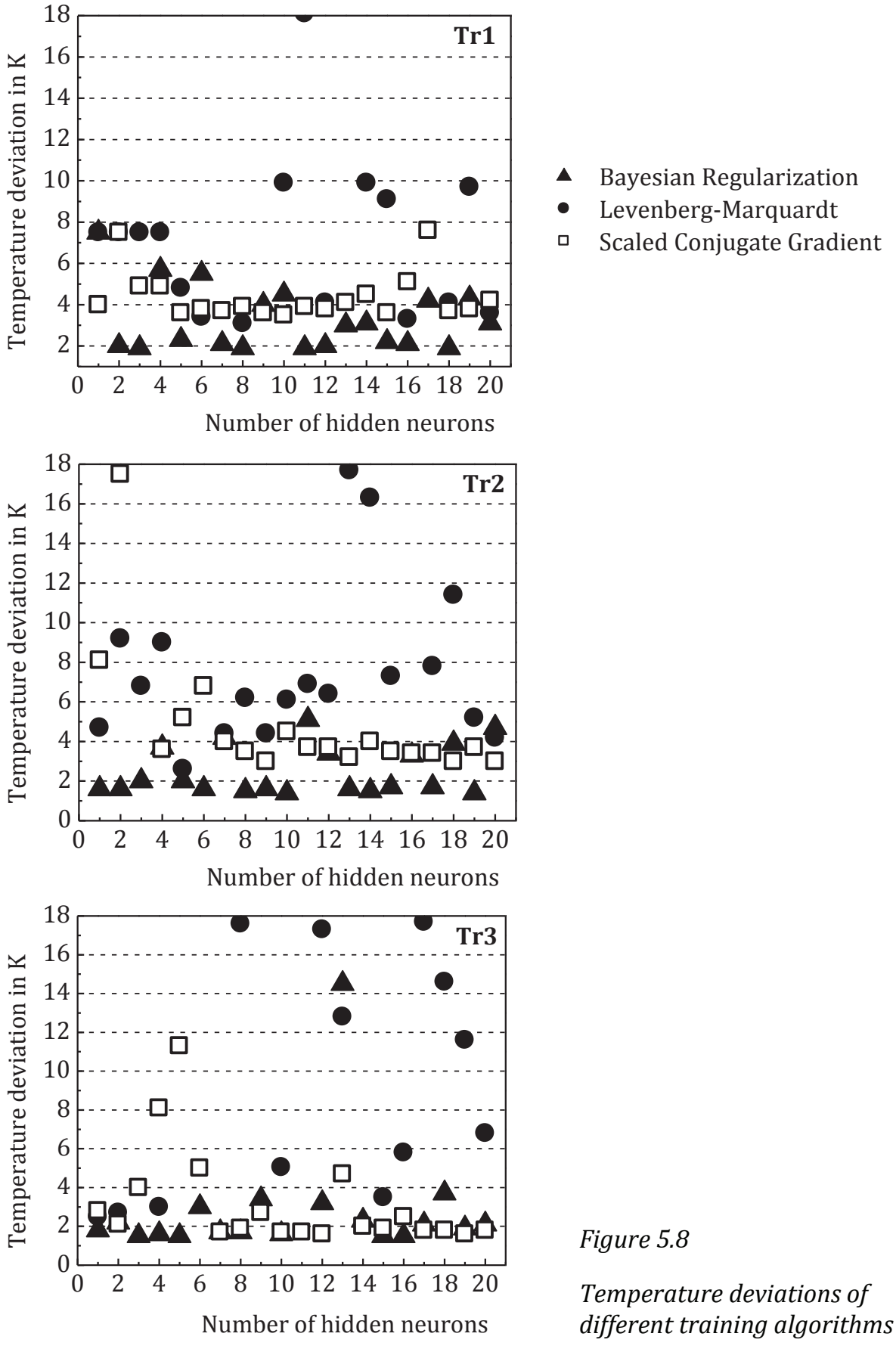

Figure 5.8

Temperature deviations of different training algorithms

5.7.3 Number of Hidden Layers

In this section the influence of the number of hidden layers on the model performance is observed. Because of the preferential performance described in the previous section, the Bayesian Regularization is further applied as the training algorithm for the investigation with two-hidden layer Feed-forward networks. The Sigmoid function is applied as the transfer function in both the first and second hidden layer. The number of hidden neurons is varied from 1 to 10 in both hidden layers. Consequently, 99 different network structures are investigated. The linear transfer function is applied in the output layer.

Figure 5.9 shows various average temperature deviations calculated by two-hidden layer networks with different numbers of neurons. The numbers in the first and second position of the network structure labels show the number of neurons in the first hidden layer and the second layer respectively. The results do not show any clear relation between the number of hidden neurons and the performance of the network. They are in fact seemingly random results. The lower temperature deviations are found for networks with a small number of hidden neurons, both in the first hidden layer and second hidden layer.

The models with the lowest temperature deviation are presented in Table 5.4. Though the two-hidden layer network has a more complex structure than the one-hidden layer network, results from all transformers show that its performance is not better than the performance from the one-hidden layer network. The temperature deviations are in the range 1.5 – 1.7 K. The models with the worst performance are presented in Table 5.5. The temperature deviation is shown to be in range 10 - 35 K.

	Number of hidden neurons		Deviation [K]
	First hidden layer	Second hidden layer	
Tr1	5	3	1.9
Tr2	1	9	1.5
Tr3	3	8	1.7

Table 5.4 Best performance results of two-layer feed-forward structures

	Number of hidden neurons		Deviation [K]
	First hidden layer	Second hidden layer	
Tr1	6	2	21.9
Tr2	6	3	10.5
Tr3	10	2	35.0

Table 5.5 Worst performance results of two-layer feed-forward structures

5.7.4 Performance of Elman Recurrent Neural Network

The Elman Recurrent network has a complex structure, which affects the calculating process. The training process of the Elman Recurrent network requires much longer times than the training process of the Feed-forward network. The investigation involving Tr3 with Elman Recurrent network (with the number of hidden neurons varied from 1 to 20 neurons and training with only one training function) needed over 3 hours, however the computer was found to hang before the calculation was complete. Therefore, in this section, only Tr1 and Tr2 are examined with the Bayesian Regularization and the Scaled Conjugate Gradient training algorithm.

Figure 5.10 shows how the temperature deviation for Tr1 and Tr2 varies according to the number of hidden neurons. Bayesian Regularization learning algorithm shows a better performance than the Scaled Conjugated Gradient. The lower temperature deviations may be also found in the small number of hidden neurons. The best performance results with each transformer can be seen from the temperature deviation results in Table 5.6. The average temperature deviations for both network topologies are found to be lower than 2 K for both Tr1 and Tr2. The deviations are in the same range as the deviations obtained from the Feed-forward network models.

	Number of neurons	Training function	Deviation [K]
Tr1	20	Bayesian Regularization	1.9
Tr2	16	Bayesian Regularization	1.3

Table 5.6 Results from the best performance models from Elman network

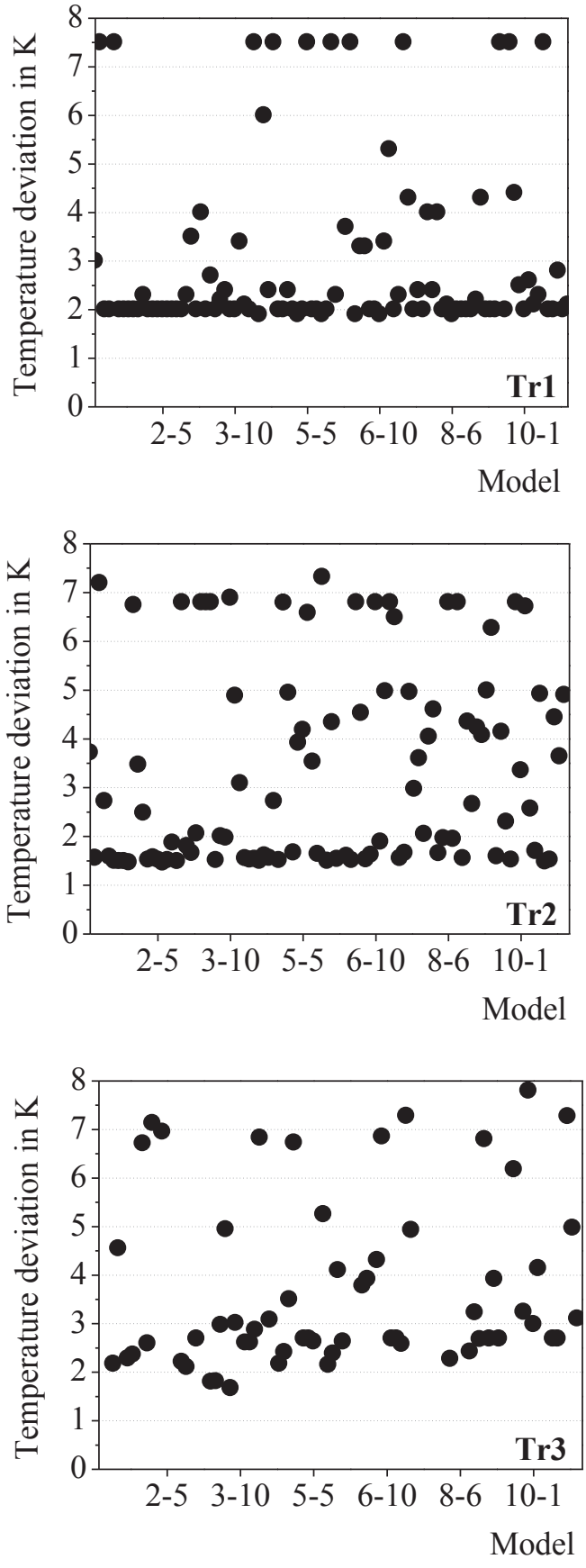

Figure 5.9

Temperature deviations of different two-hidden layer structures

According to the training time and the results of top-oil calculation, it may be said in conclusion that the Feed-forward network is more applicable for the top-oil prediction than the Elman Recurrent network. Therefore, in the next chapter, in which the applications of top-oil temperature prediction are investigated, the Feed-forward network type is applied in the neural network models.

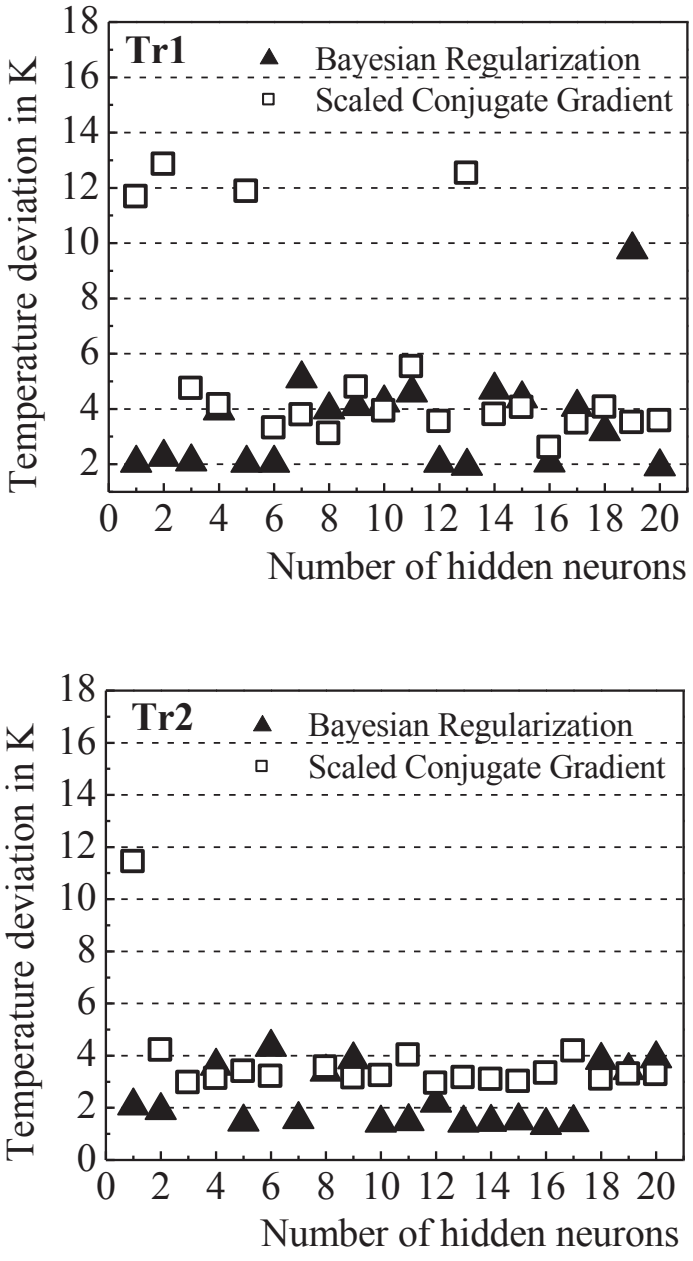

Figure 5.10 Temperature deviations compared for different training algorithms with Elman Recurrent network

6 Application of Top-oil Temperature Prediction

In order to apply the appropriate top-oil temperature model in the online monitoring system, some further conditions must be examined. In this chapter, first, the selection of the models and the performance of the chosen models under varied load and ambient temperature are presented. Later, the application of these top-oil temperature models in detecting malfunction of the cooling system is investigated.

6.1 Performance Comparison between the Physical and the Neural Network Top-oil Models

Table 6.1 presents the average temperature deviations between measured and calculated top-oil temperature from the best performance physical model (Model B) and the neural network models (Feed-forward networks) obtained from Chapter 3 and 4. They are trained by the Bayesian regularization-training algorithm. The networks have one hidden layer with 8 hidden neurons, 10 hidden neurons and 5 hidden neurons for Tr1, Tr2 and Tr3 respectively.

Transformer	Average temperature deviation [K]	
	Physical model	Neural network model
Tr1	1.6	1.9
Tr2	1.3	1.4
Tr3	3.3	1.5

Table 6.1 Best performance results of two-layer feed-forward structures

The transformers Tr1 and Tr2 have constant operating states of the cooling units. It is found that the results of the physical and the neural network models are not significantly different. For Tr1 the average temperature deviation from physical model and from neural network model is 0.3 K different. For Tr2 the difference between the average temperature deviations is also small (0.1 K). Transformer Tr3, with the varying operating states of the cooling units, shows a large difference of 1.8 K between the physical and the neural network model. In conclusion,

for these types of transformers, the neural network model has an advantage.

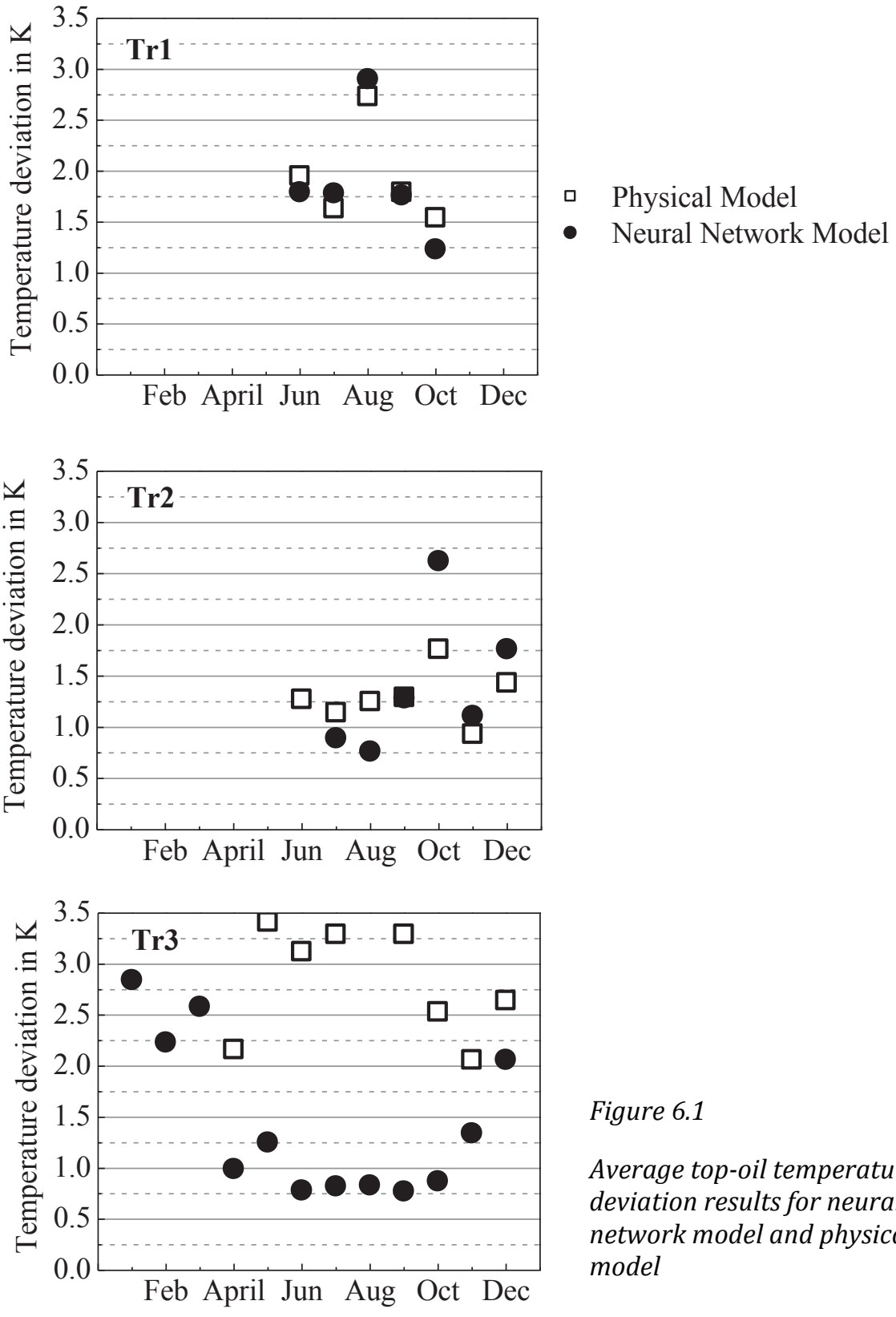

Figure 6.1

Average top-oil temperature deviation results for neural network model and physical model

In the physical model, different sets of estimated parameters must be determined for the different operating states of cooling units. Therefore, sufficient data of all available operating states of cooling units is necessary. The neural network model is able to accomplish this more easily as the number of operating state of pumps and fans can be used as input variables in the model. The accuracy of the neural network depends on the operating states available during the training process. But even if a particular state is not available, the neural network will still produce a result (coefficients) in this case. This is the advantage of the neural network model compared to the physical model that can only deliver results of already known states of operation. This explains the performance advantage shown to be evident for the neural network model over the physical model.

The monthly results of the temperature deviations between measured and calculated top-oil temperature from physical and neural networks models can be seen in Figure 6.1. Tr1 and Tr2 have the highest temperature deviation for both models in August and October, respectively. Figure 6.2 and 6.3 show the influence of load factor on the temperature deviations for Tr1 and Tr2 in this period. It can be seen that the fluctuation of load factor for Tr2 was quite severe in October. The high temperature deviation can be seen explicitly during the shutdown state. For Tr3, the temperature deviations of physical and neural network models for each month are obviously different. In almost every month, the temperature deviations for the physical model are higher than 2 K. However, for the neural network model, the higher temperature deviations appear in winter time.

The weekly results of top-oil temperature course will be compared for the physical model and neural network model during the fluctuation of the load factor in October and may be observed from Figure 6.4. It can be seen that on the 6 October, the measured top-oil temperature of Tr1 is much lower than the calculated top-oil temperature (around 5 K), both from the physical model and the neural network model. The measured top-oil temperature of Tr2 is also much lower than the calculated top-oil temperature (around 10 K). For Tr3 the fluctuation of calculated top-oil temperature course obtained from the physical model can be clearly observed over the period. The temperature course is totally different from the temperature course obtained from the neural network model and from the measured top-oil temperature.

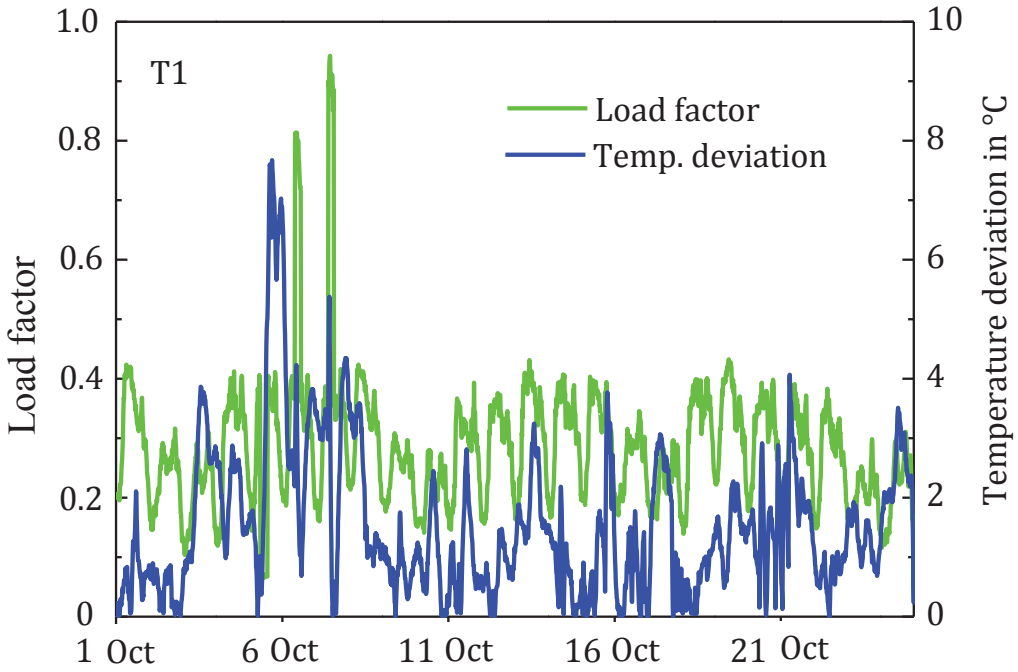

Figure 6.2 Relation of load factor and temperature deviation of Tr1

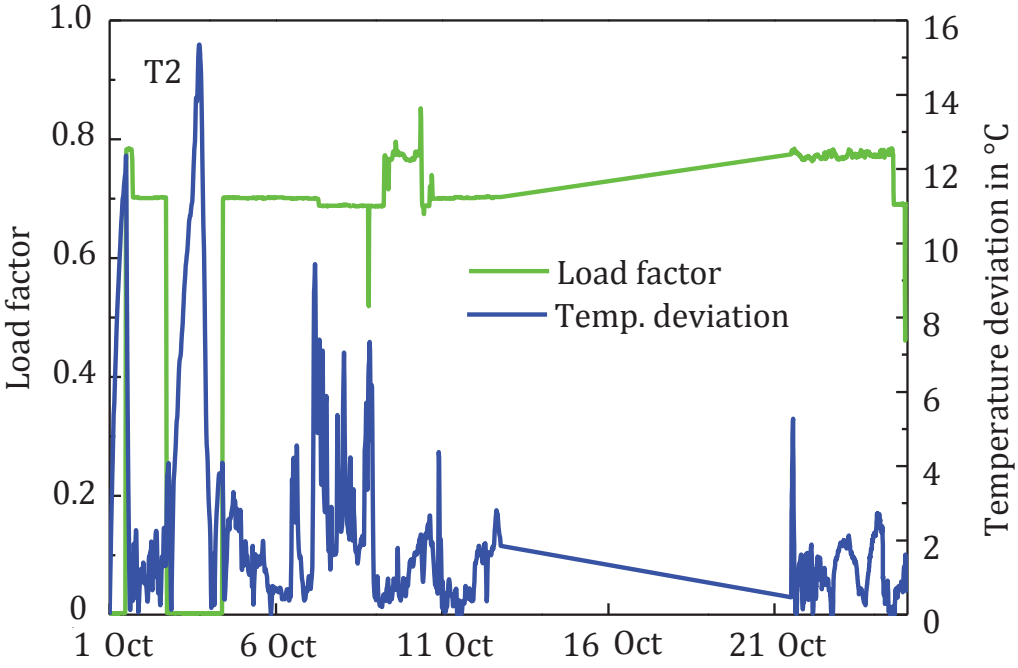

Figure 6.3 Relation of load factor and temperature deviation of Tr2

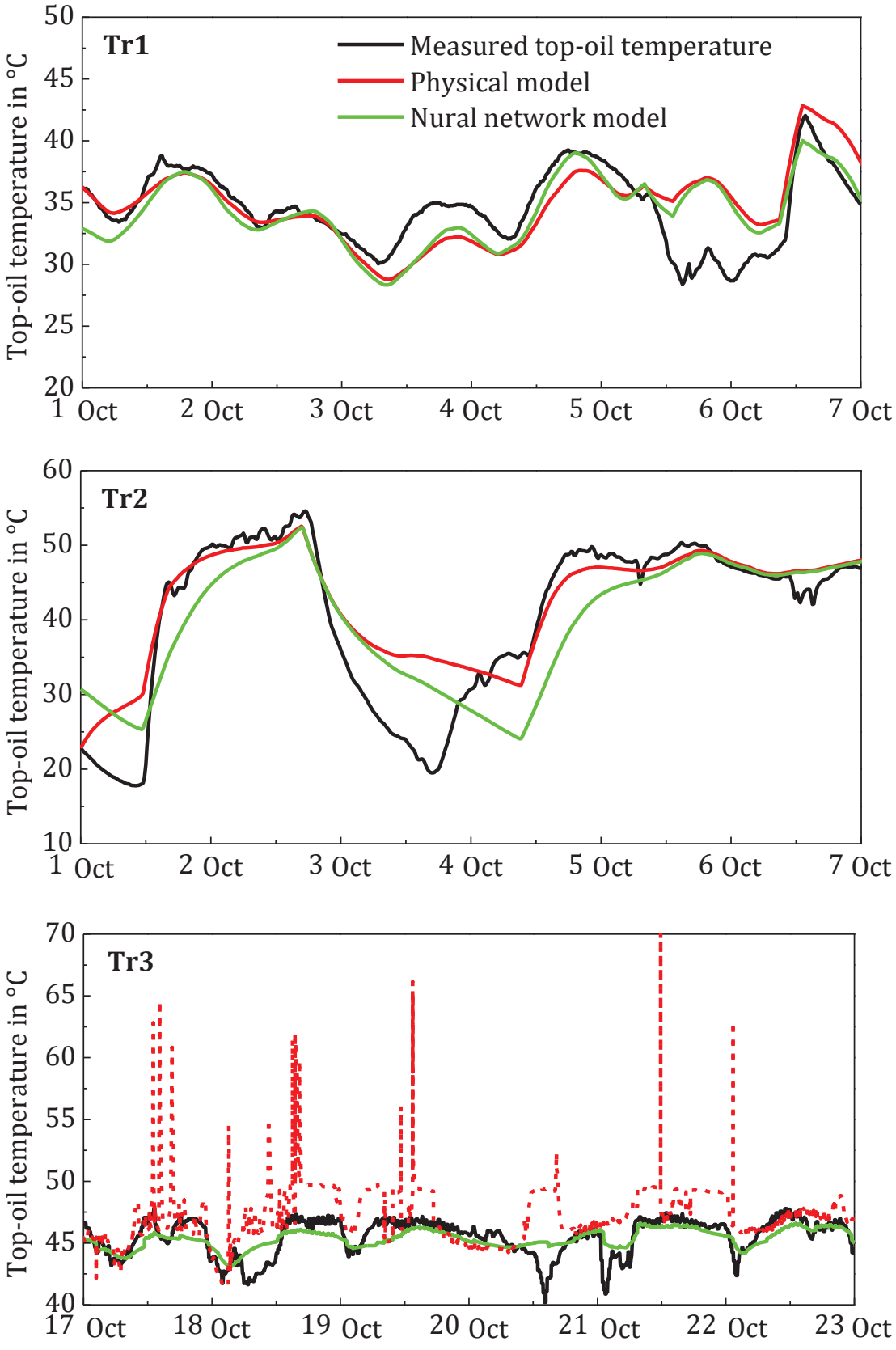

Figure 6.4 Temperature course from physical and neural network model

6.2 Reliability of the Model for Different Loading Conditions

As seen from section 6.1 load variation has an effect on the calculated top-oil temperature. In order to apply the top-oil temperature model in an online monitoring system for an operating transformer, this effect must be considered. In this section, the results of the top-oil temperature calculation during the sudden load change for Tr2 previously observed (section 6.1) is considered in particular. The results are calculated using the one-hidden layer feed-forward network with 10 hidden neurons.

Figure 6.5 shows the load factor and the temperature deviation between the measured and calculated top-oil temperature in the long-term observation during 15 – 21 September 2003. The shut-down state of the transformer (load factor equals 0) leads to a temperature deviation higher than 4 K. This temperature deviation remains for a certain period after the shut-down state is over. The time period of the shutdown state, 11:30 to 16:30, is analysed in Figure 6.6. In this period, the measured top-oil temperature is higher than the calculated top-oil temperature. The calculated top-oil temperature decreases immediately after shut-down. The measured top-oil temperature instead continues to increase for 1 hour. Then it starts to decrease too.

The same effect is observed during the change period from the shut-down state to the normal operating state but is vice versa. The calculated top-oil temperature increases directly after load is applied. The measured top-oil temperature instead decreases for another hour until it then starts to increase.

This physical effect of a delayed temperature change can be improved by applying an additional coefficient (a time constant) of the load factor in the model. For an online application the time constant must be determined for each transformer unit. However, it can be assumed that the here presented top-oil temperature model from neural network without considering the time constant is still proper to use in an online monitoring system.

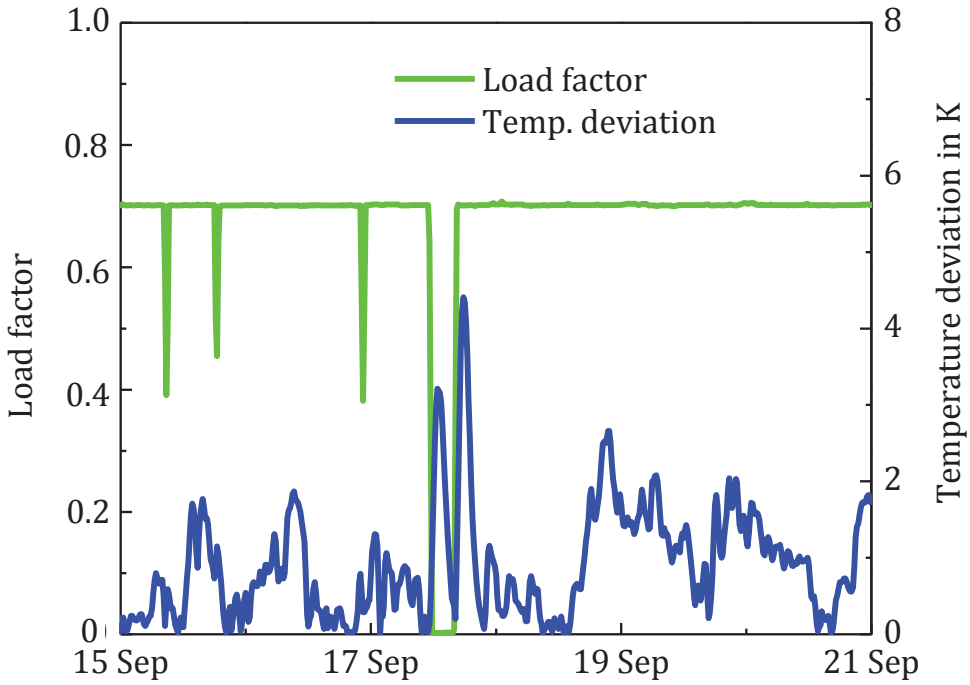

Figure 6.5 Influence of shut-down state of transformer on top-oil calculation

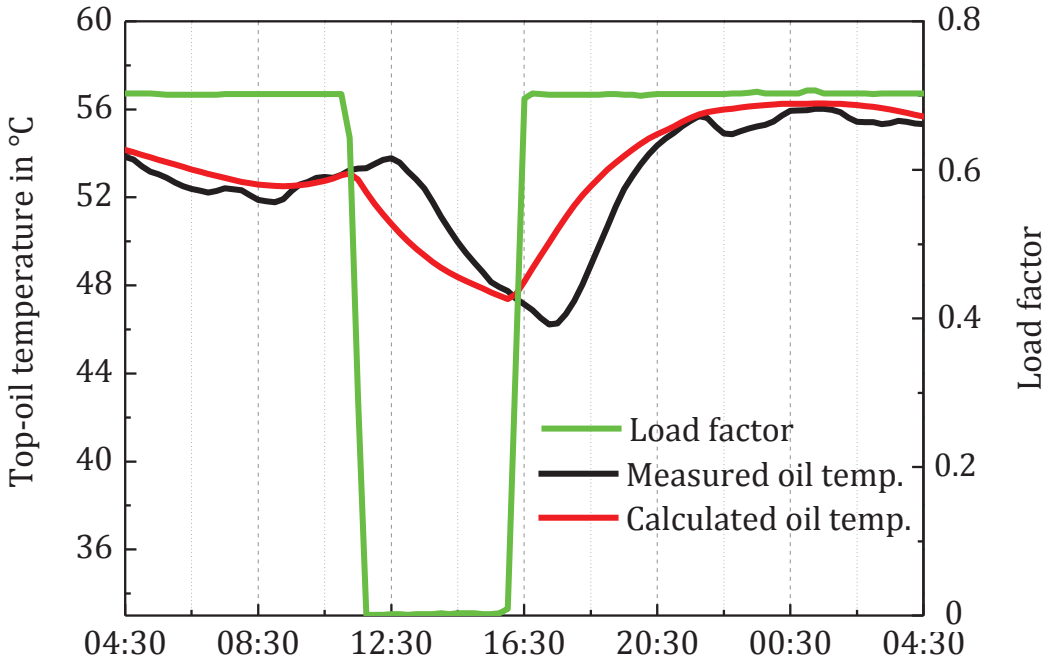

Figure 6.6 Temperature courses during the shut-down state of transformer

6.3 Effect of Transient-state of Ambient Temperature

The relation between transient-state of ambient temperature and temperature deviation is clearly seen in Figure 6.7. The dataset for Tr2 from 01 – 15 June 2003 was examined using a neural network model with one-hidden layer having 10 neurons trained by the Bayesian regularization. In this period, the ambient temperature appeared both in the steady state and in transient-state. It may be noticed that during the state of sudden drop in the ambient temperature (02 June), the temperature deviation increases up to 10 K, while the average temperature deviation of the normal period is not higher than 4 K. Thus, it may be concluded that the transient states of ambient temperature are significant for top-oil temperature calculation.

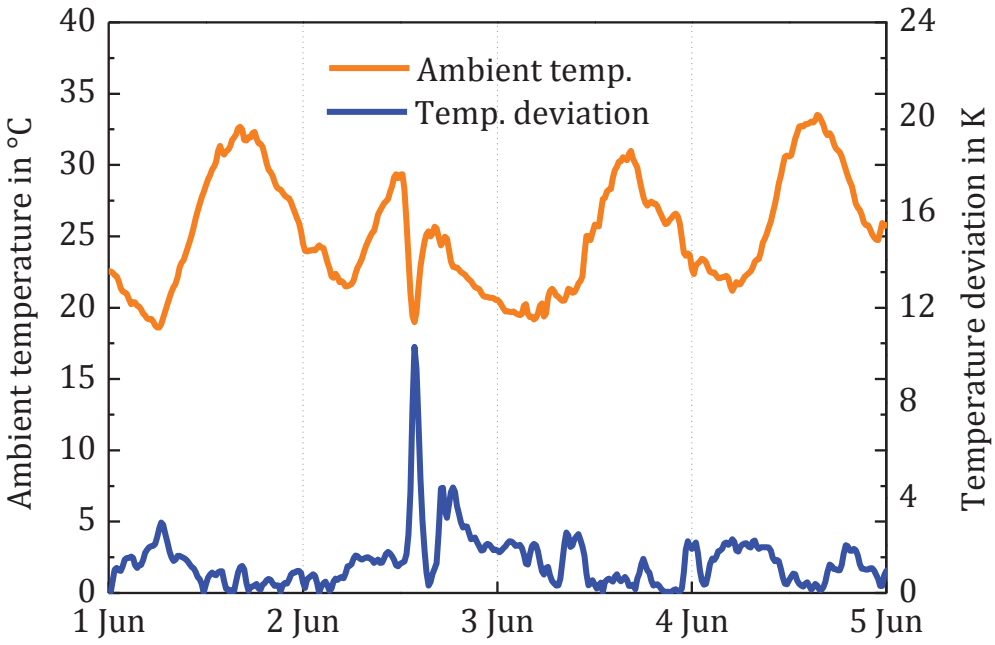

Figure 6.7 Influence of transient-state of ambient temperature

6.4 Detection of Malfunction of Fans

The task of the cooling system is to transfer the heat which is generated inside the active parts of the transformer to the ambient surroundings. Consequently, the top-oil temperature is determined by the operating of the pumps or fans. The top-oil temperature may be used as a trigger for the usage of the fans and pumps. The fans are turned on or turned off when the top-oil temperature exceeds or is below a set value. Usually, to avoid an excessive starting current of the power supply, only one group of fans is first turned on, and then a second group is automatically added in a few seconds later. The operating status of pumps or fans is monitored online by means of the auxiliary contacts of switching relays.

The failure of pumps or fans is the most frequent failure mode of the cooling system. Sources of these failures may be from the failure of pumps or fans themselves or from the electrical supply. The failure of pumps or fans may be checked by proving that they are on, when they are supposed to be on, and they are off, when they are supposed to be off. This can be done by predicting the actual number of operating pumps or fans using the top-oil temperature model. The calculating process is described in the following section.

6.4.1 Prediction of Number of Operating Fans

The number of operating fans was predicted for a 600 MVA grid coupling transformer. The transformer is OFAF-cooled with 6 fans in total. One-hidden layer Feed-forward neural network model with 10 hidden neurons was applied for the top-oil temperature calculation. The network was trained with the Bayesian regularization training function.

For each time interval, the top-oil temperature was calculated with every number of fans from 1 to 6. The calculation with the least deviation to the measured top-oil temperature in that time interval determines the best fit value for the number of operating fans.

Figure 6.8 illustrates the predicted and the monitored number of operating fans from 06 – 11 January 2004. During changing state a slight difference between the monitored and the predicted number of operating fans occurred. The monitored number of operating fans has changed immediately from 6 down to 4 fans on 09 January 2004. The predicted

number of operating fans has changed from 6 to 5 fans and after 4 hours from 5 to 4 fans.

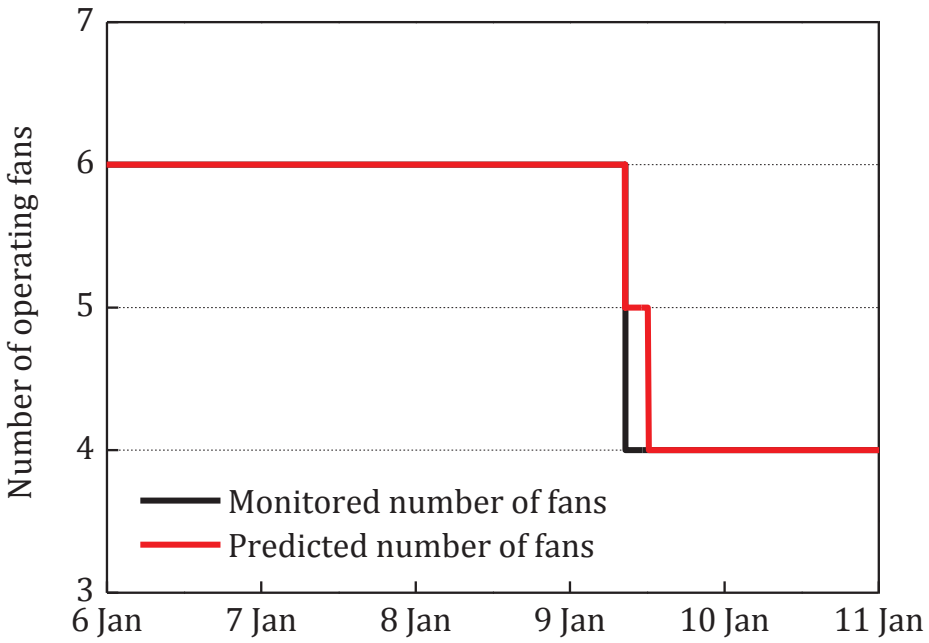

Figure 6.8 Monitored and predicted number of operating fans

The prediction was also performed on Tr3 for a period with quick changes of the operating state of fans as seen in Figure 6.9. Tr3 has 8 pumps and 8 fans in total. The number of operating pumps was kept constant. There were 8 datasets with the number of operating fans varying from 1 to 8 for the top-oil calculation. The neural network model with one-hidden layer and five hidden neurons was used on the dataset from 03:15 – 07:30 on the 25 October 2004.

The increasing number of fans over the studied period was predicted well by the model. Still there is a significant difference between the monitored and the predicted number of operating fans. Most times the calculation predicts one more fans operating than is actually measured. As the deviation is small and with increasing number of fans better predict ion is obtained, it can be assumed that with further improvement of the model a satisfactory prediction would be possible.

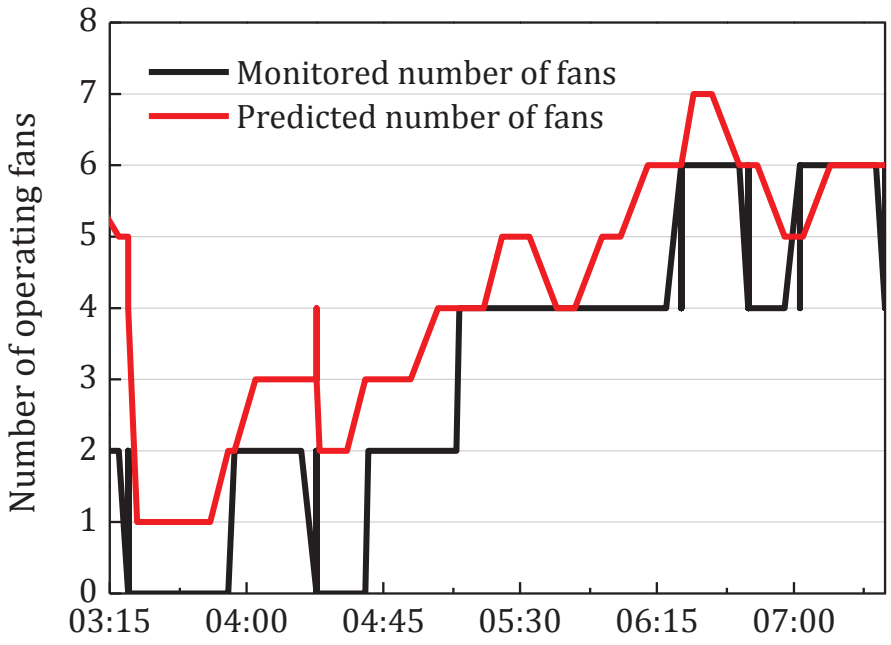

Figure 6.9 Monitored and predicted number of operating fans

6.4.2 Correlating the Calculated and the Measured Top-oil Temperature

An investigation is performed under the circumstances originally proposed in [Tenbohlen, 2003]. The studied transformer is a 420kV/600MVA grid-coupling transformer with ODAF cooling. The cooling unit consists of two parts with 3 fans each. Nominal cooling power is achieved by means of four running fans. The actual thermal resistance ($R_{th,act}$) was calculated from the difference between the top-oil temperature and ambient temperature and the power loss in the transformer, as can be seen from the following equation.

$$R_{th,act} = \frac{\vartheta_{TO} - \vartheta_{amb}}{P_N + P_S \cdot K^2} \tag{6.1}$$

The number of fans in operation has to be taken into account to calculate the thermal resistance (R_{thN}) for nominal condition as seen in (6.2).

$$R_{thN} = R_{th,act} \times number\ of\ fans/4 \tag{6.2}$$

The measured top-oil temperature, along with the nominal thermal resistance and the number of fans, during 07 January – 15 March 2002 are presented in Figure 6.10.

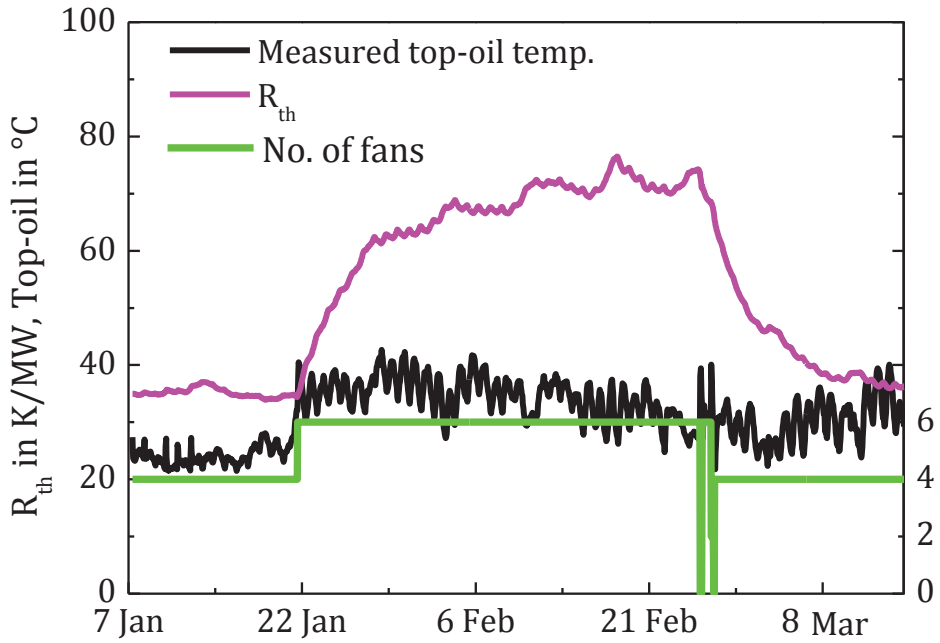

Figure 6.10 Abnormal condition of cooling unit detected by increase of thermal resistance R_{th}

After switching on two additional fans on 20 January 2002, a large increase in R_{thN} from approximately 35 K/MW to 70 K/MW was determined during 20 January – 26 February 2002.

The increase in R_{thN} indicates an abnormal condition of the cooling unit. A local check in the substation revealed that, due to a failure of the power supply in the cooling system, only three fans were running. This status was not in accordance with the information of the control system and led to the large increase of nominal thermal resistance.

This occurrence is examined further in this work. The top-oil temperature in this period is calculated using neural network model and the information of number of fans from the monitoring system. Then, it is compared with the measured top-oil temperature.

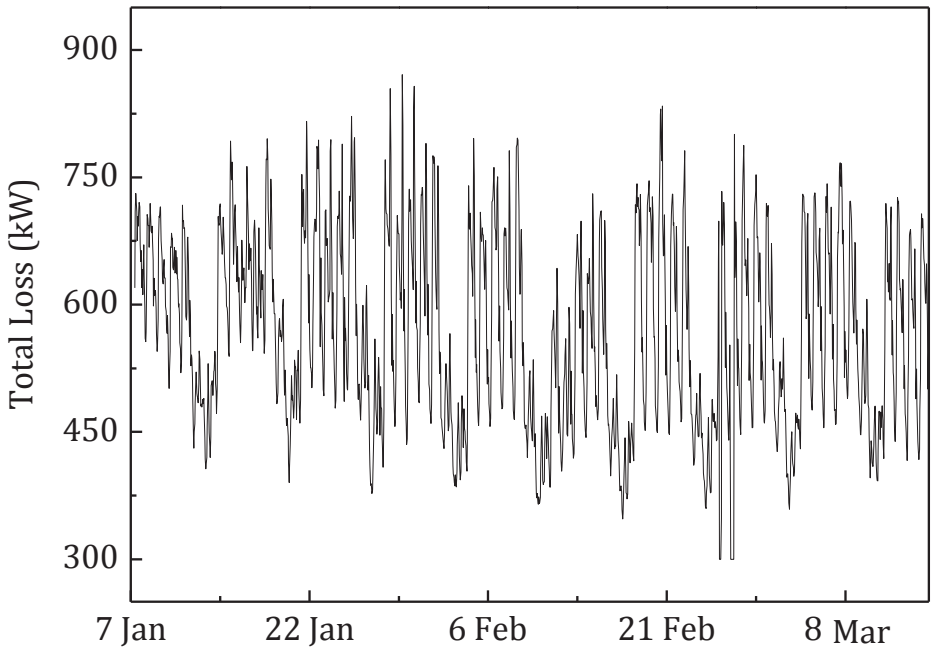

Figure 6.11 Losses of the investigated transformer during the examined period

In order to find a good model, a two-week dataset from normal operation conditions after the maloperation was used (01 March – 15 March 2002). In the case of the studied transformer unit, a one hidden layer Feed-forward network model with 10 hidden neurons trained by Lavenberg-Marquardt Backpropagation gives the best result for the top-oil temperature calculation. Weights obtained from the training process are later applied to the model using the whole dataset (07 January – 15 March 2002). Figure 6.12 shows the measured and the calculated top-oil temperature for comparison.

The results can be discussed in terms of three periods. The first period is from 07 – 20 January 2002. For this period the monitoring system predicts the correct number of 4 operating fans. A small deviation between measured and calculated top-oil temperature can be observed. The second period (20 January – 26 February 2002) is the period that the incorrect number of 6 operating fans is obtained from the monitoring system. For this period, the predicted top-oil temperature is based on 6 fans operating. However, the actual number of operating fans is only 3. Consequently, a large deviation between the measured and the calculated top-oil temperature is observed. The last period (27 February – 15 March 2002) was used for the training process and is therefore very accurate.

In conclusion, the malfunction of the pumps and fans can be well detected by comparing the measured top-oil temperature to calculated data from the neural network model.

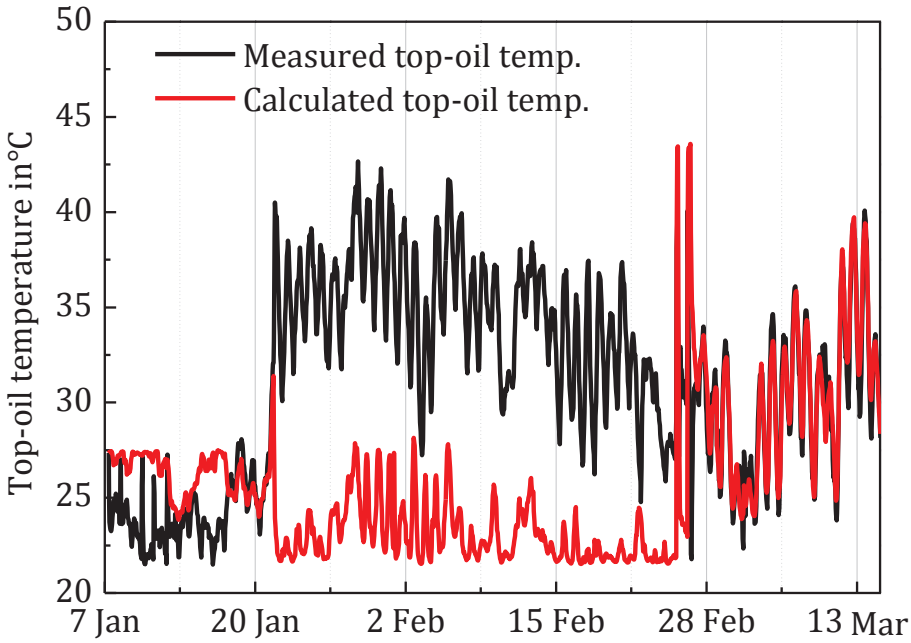

Figure 6.12 Measured and calculated top-oil temperature compared during the failure period of fans

6.4.3 Online Monitoring Criteria

The results in section 6.4.1 show that it is impossible to check the failure of cooling units by direct prediction of the number of fans operating. However, it can be seen from section 6.4.2 that by correlating the measured and calculated top-oil temperature, the information about the malfunction of the monitoring system may be examined. Therefore, the calculated temperature deviation may be used as an alarm criterion of an online monitoring system.

Figure 6.13 shows the actual and the average top-oil temperature deviations between the measured and the calculated top-oil temperature from the investigated period from section 6.4.2. The actual instantaneous temperature deviation fluctuates and can be up to 6 K in the normal period and up to 17 K during the failure period. Thus, consideration of the average temperature deviation is considered necessary. The average

temperature deviations are determined by filtering of the instantaneous temperature deviations. The filtering is done in MATLAB using the *Signal Processing Toolbox* with the function *filtfilt*. The number of points per cycle of the data is set to be 300. After the filtering of temperature deviation, it is obvious that the average deviation during the failure period increases by up to 12 K. However, during the normal period, the temperature deviation is less than 2 K. After the wrong signalling of the number of running fans on 20 January, the deviation was higher than 4 K. Consequently, a trigger of the alarm could be set for when the top-oil temperature deviation between the calculated and the measured temperature is higher than 4 K.

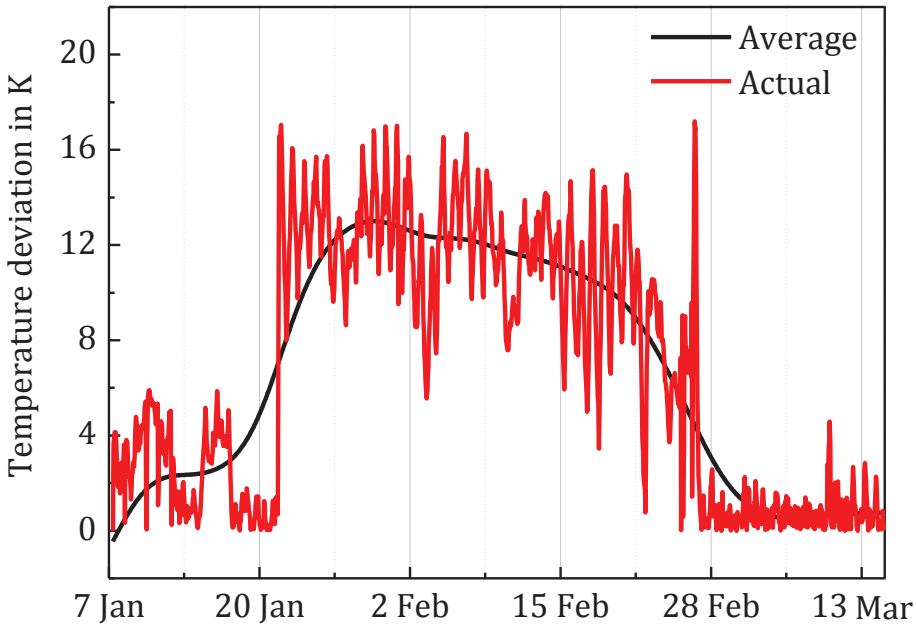

Figure 6.13 Average and actual temperature deviation during the failure of fans

However, the alarm criterion should be set with consideration of the other two conditions that have an influence on the top-oil calculation: shutdown state of the transformer and transient-state of ambient temperature. These influences must be precisely studied and considered for each transformer. For example, it is found from the investigation in section 6.2 and 6.3 that the average temperature deviation under the shutdown state of the transformer and transient-state of ambient temperature also appear clearly as being higher than 4 K with the time constant of 1 hour. Thus, in this case the temperature deviation higher than 4 K with the time constant of 1 hour can be set as an alarm for the monitoring system.

6.5 Implementation of a Neural Network Model in the Top-oil Temperature Monitoring System

The neural network model must be customised for any power transformer and weights must be set individually. However, it is recommended to use feed-forward neural networks with one hidden layer as explained in section 5.6.1.

In summary, to implement the model in the monitoring system, first, the model for each transformer must be designed by network design software, in this case using Matlab®. The data comprising at least one year of measured top-oil temperature, load current, ambient temperature and operating number of pumps or fans should be applied. The software will train different models (with number of hidden neurons varied from 1 to 20 neurons) with 12 different training algorithms. The weight and number of hidden neurons of these models are obtained. Then, the mathematical model as described in Eq. (5.6) is applied and the temperature deviation between measured and calculated top-oil temperature from different network models is determined. The results from these different models with their weights, number of hidden neurons and temperature deviations are then considered and analysed (using Excel).

The model with the lowest temperature deviation will be chosen as the model for the top-oil temperature calculation. Its weights and number of hidden neurons will be modified into a mathematical form for calculation and the model can then be applied in the monitoring system.

7 Monitoring and Diagnosis of On-load Tap Changers

On-Load Tap-Changers (OLTCs) are part of the voltage regulating systems in an electrical transmission network. They are connected to the transformers and are responsible for maintaining the voltage level under variable loading conditions. By changing a tapping on a winding, the OLTC allows the turns-ratio of the transformer and thus the level of its output voltage to vary. The selection of tapping on the transformer winding is done via the selector switch. Load current is then switched over a set of contacts by means of the diverter switch. The position of the electric contact is adjusted by a driving mechanism and a control unit, based on the comparison of an output voltage and a reference value.

7.1 Tap Changers Characteristics

During the tap changing, the current in a transformer winding is not allowed to be interrupted and the tap changing must be carried out without short circuit of two tapping points of the winding. This leads to the requirement of transition impedance during the transition stage. Such transition impedance is provided either with a resistor or with an inductor. The amount of impedance and the method of its connection in the circuit are determined by the following conflicting requirements: no excessive voltage fluctuations during the switching cycle and the circulating current between taps in the transition position.

7.1.1 Tap Changers Design Schemes

The tap changer of a transformer should meet the same normal and peak rating overload conditions as the transformer itself. The design schemes should consider the following points [Feinberg, 1979]:

- the maximum system voltage;
- step voltage and the number of steps;
- the maximum RMS test voltage to earth and across the tapping range;
- the maximum surge voltage to earth and across the tapping range;

- the maximum power-frequency and surge-test voltage between phases where applicable;
- current rating, both for normal full-load and peak rating conditions.

Moreover, type tests are necessary to determine the data for a particular tap changer to ascertain whether it is capable to meet supply authority specifications while conforming to international and national requirements.

7.1.2 Switching Principles

Two switching principles have been used for the load transfer in OLTC diverter switches; the slow-acting reactor and the high-speed resistor principles. Both principles provide reliable OLTCs for the full range of OLTCs. The reactor type OLTCs are in separate compartments that are normally welded to the transformer tank. The use of a reactor is to limit the circulating current during transition from one tap to the other. These reactor type OLTCs are now less used in Europe, however, they are still available and are frequently used in the USA.

The resistor type OLTCs tend to dominate, especially when they come to HV, HVDC and EHV OLTC transformers [Goosen, 1996]. They are installed inside the transformer tank. An advantage of this switching method is that the current interrupted and the re-striking voltage across the contact is in phase. Nowadays the high-speed resistor OLTC dominates a new application that allows designs that are more compact and the fast operation that the arc persists only about half a cycle. Therefore, contact erosion and oil contamination can be minimized [Feinberg, 1979].

There are two types of resistor tap changers in common use, as seen from designs and their switching schematics in Figure 7.1. They are different in current-transfer switching arrangements. These may be classified as the pennant switching cycle and the flag switching cycle. The term “pennant” and “flag” are derived from the appearance of the phasor diagrams that show the change of output voltage of the transformer in moving from one tapping to the next.

The *pennant-switching-cycle type* tap changer uses a selector switch that combines the functions of tap selection and current transfer. It is used for regulating transformers with small to medium output rates. Generally, a

single resistor is applied for giving an asymmetrical switching cycle. In one direction of movement, a circulating current is passing before the through current is interrupted. And in the reverse direction, the through current is broken before a circulating current starts to pass.

The *flag-switching-cycle type* tap changer uses a tap selector in conjunction with a separate diverter switch in the separate oil compartment. Two resistors are applied for giving a symmetrical switching. With this sequence, the through current is broken by the main contact before a circulating current starts to pass.

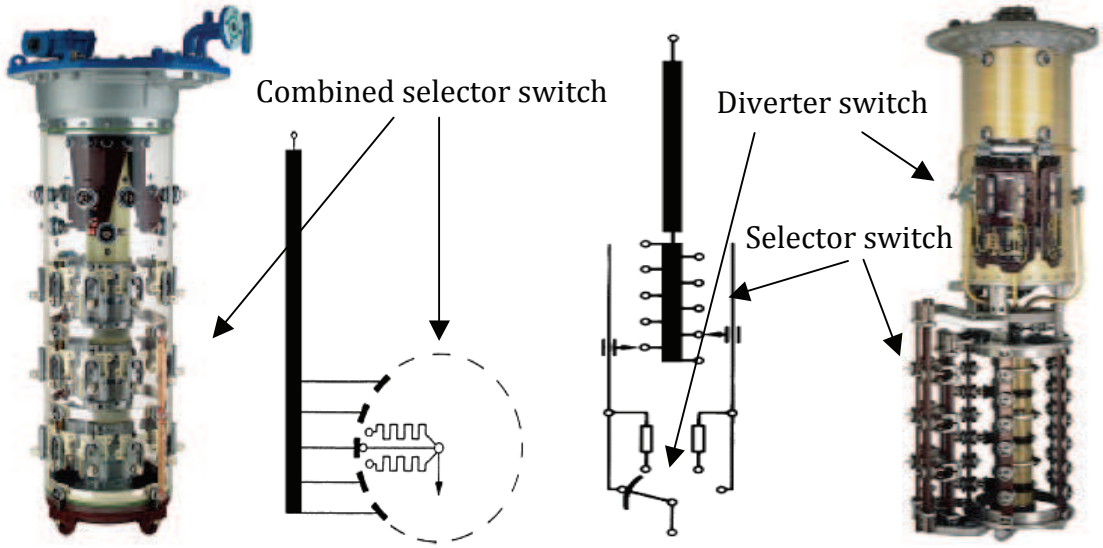

Figure 7.1 *Tap-change type: (left) pennant-switching cycle; (right) flag-switching cycle (Photos from Maschinenfabrik Reinhausen GmbH)*

The switching sequences of a tap changer operation of a selector switching type can be seen from Figure 7.2 [Krämer, 2000]. The fixed tapping contacts are spaced round the periphery of a circle and are indexed by a single rotary contact. Its insulated support arm also carries two transition resistor contacts.

Figure 7.3 shows the switching sequences of the tap selector-diverter switching type. The tap selector operation from Figure 7.3a to Figure 7.3c is a slow motion sequence actuated by the motor drive mechanism (3 to 10 seconds). The diverter switch operation from Figure 7.3d to Figure 7.3i is carried out in a rapid motion actuated by the spring loaded mechanism (40 to 60 milliseconds).

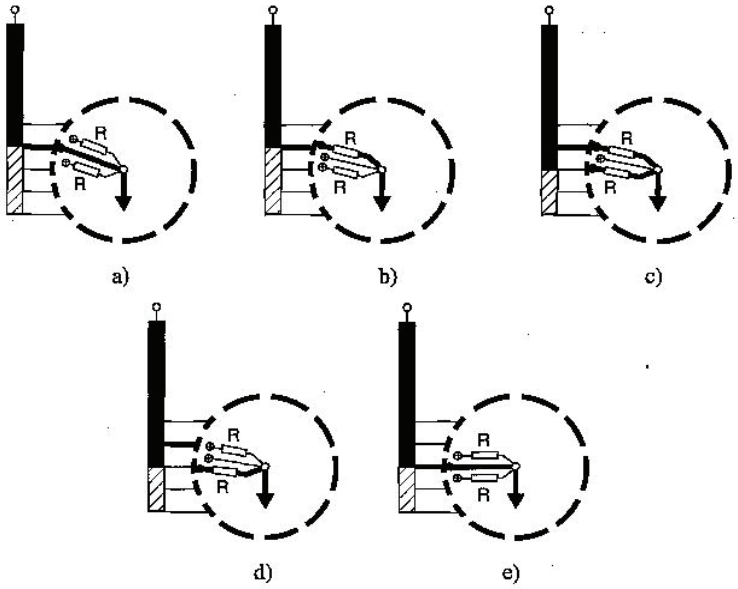

Figure 7.2 Principle switching sequence of a selector switching type (flag cycle)

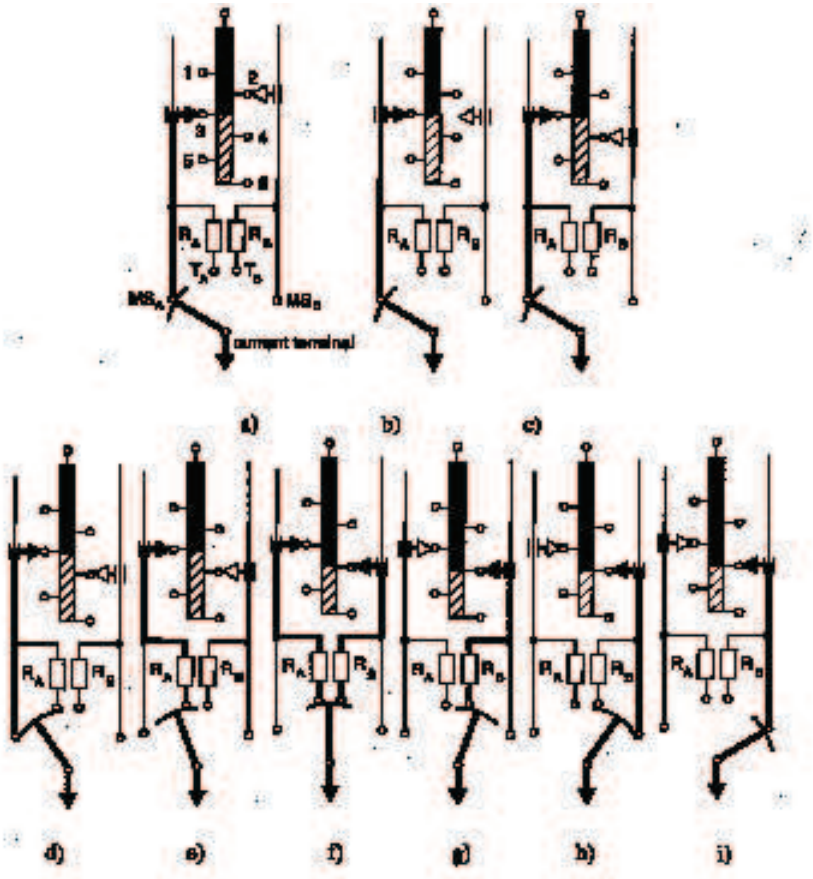

Figure 7.3 Principle switching sequence of a tap selector-diverter switch type (a-c: tap selector operation, d-i : diverter switch sequence)

7.1.3 Motor Drive Mechanisms

Either three-phase or single-phase induction motors may be used in the on-load tap changer drive units. Most of them are the capacitor start and run types. This motor drive mechanism must be capable of operating in both directions of rotation to satisfy the normal functioning conditions of the tap changer. The essential requirements for the control of these motors are the initiating components such as push buttons or switches and the maintaining contacts in the auxiliary equipment in order to make certain that a full tap-change sequence is completed once initiated. The limit switches are provided to prevent overrun.

Details of the motor drive mechanism are usually described in the manufacturer's maintenance manual or specific drawing. It is also usual for the motor drive mechanism to include the facility to allow the unit to be operated manually. If this facility is provided, it is essential that the electrical system is isolated automatically either before or at that time that the handle is inserted.

7.2 Failure Mechanisms in On-load Tap Changers

International publications [CIGRE, 1983] show that the on-load tap changers cause 40% of all transformer failures strongly affecting the quality of the energy delivered to the final consumer. In general, OLTC failures are categorized as electrical, mechanical and thermal faults. The major serious faults are mechanical faults. They appear from ageing, inadequate design, and missing quality control during manufacture or site erection. They may lead to loss of synchronization within the selector switch or between selector and diverter switch of the same phase. They may also lead to slow or incomplete diverter operation faults. The most frequent mechanical failures are contact problems and driving mechanism problems. The problems with contacts may be loosening on moving contacts from incorrect maintenance or reassembly, excessive wear, contact cracks on fixed contacts or moving contacts, erosion or weak spring wear from aged/deteriorated components. The driving mechanism problems may be drive mechanism malfunction, loose shafts or damaged shafts. They may cause slow or incomplete diverter operation faults.

Mechanical faults may lead to electrical faults such as burning of contacts or transition resistors and insulation breakdowns. The mechanical and electrical events can cause contacts erosion and the degradation of the dielectric oil strength. The electrical arcs (discharges) burn the oil causing carbon built-up. The contact's mechanical friction releases metal particles in the oil. A high concentration of carbon and metal particles change the dielectric oil characteristics leading to more intense electric discharges, in consequence, on extreme causes a transformer failure. The process of contacts erosion and oil degradation is described in Figure 7.4 [Simas F., 2005].

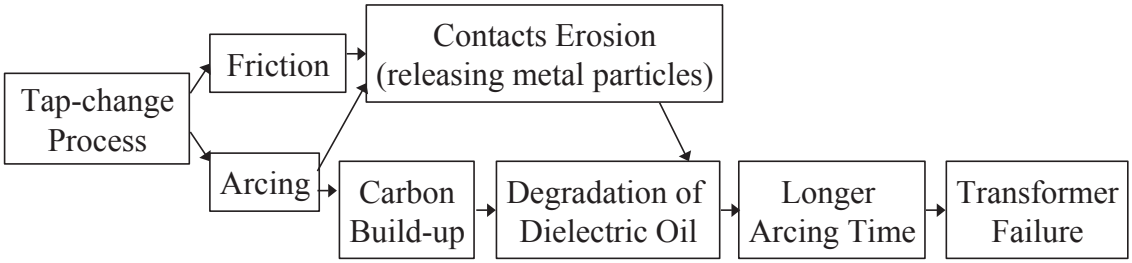

Figure 7.4 Contacts erosion and oil degradation process

7.3 Maintenance Strategy

At present, preventive maintenance is normally performed along with periodic inspection of the OLTCs and replacement of parts if necessary. The regularity of the maintenance work depends on the number of operations and total service time or when some kind of failure occurs. Periodical maintenance is suggested according to the number of operations, between 20,000 and 100,000, or after 4 to 7 service years, whichever comes first.

Generally, the information of the diverter switch unit obtained during the regular inspections includes oil quality (humidity and electric strength), oil leaks, and verification of transition resistors, contacts alignment and motor drive mechanism. The electrical contacts are examined for excessive wear or arcing. Normally, contacts are replaced before their wear limits just for safety reason. Furthermore, inspections are also carried out if the OLTCs were overstressed. For the in-tank tap changer, inspection is only possible after lifting the complete active part of the

transformer out of the tank. This maintenance procedure is a major expenditure both in time and in materials consuming, as it requires disconnection and substitution of the equipment. The selector switch is not regularly inspected. In some cases, if the operating numbers exceed 1,000,000 operations the manufacturer has to be contacted concerning a tap selector inspection.

Old designs of tap changers still present a significant problem for users since some have been in service for over thirty years and most are obsolete. This leads to the developments in alternative tap-changing technologies, the online condition monitoring systems and the possibility to change from periodic maintenance to condition-based maintenance. Today, tap changer status monitoring is becoming attractive to increase reliability and reduce the cost of maintenance by eliminating selector internal inspections and unacceptable deviations in diverter operation [Krämer 1996].

7.4 Online Monitoring Parameters

The most important parameters for measurement are those that detect mechanism movement, measure diverter timing and transition resistor current. Usual general diagnostic methods (analysis of transformer oil, measurement of terminal resistance, temperature measurement of the diverter switch oil, and a contact wear model in combination with measurement of load current) may not be able to detect such mechanical nature defects. The measurement and evaluation of mechanical parameters, i.e. forces, torques, switching supervision, velocities, accelerations within contact system and motor drive should also be considered.

7.4.1 Contact Resistance of Diverter Switch

Normally, the resistance between moving and fixed contacts is of the order of micro-ohms. Contacts with solid carbon layers have resistance values in milliohms. As the winding resistance of power transformers lies within a range of several hundred milliohms and a few ohms, it is necessary that the least possible number of winding turns is included in the measuring circuit in order to determine the contact resistance accurately.

One proposition for the resistance measurement is presented in [Krüger, 2007]. The winding resistance is measured for checking the loose connections, broken strands and high contact resistance in tap changers. A winding resistance test is carried out by injecting a DC current of approximately 1% of the rated current and measuring the DC voltage drop across the winding after the measurement has stabilized. By comparing the static winding resistance for each tap against the values measured at commissioning, the state of the selector as well as diverter contacts can be analyzed. Additionally, the dynamic resistance measurement enables an analysis of the transient switching operation of the diverter switch. The dynamic winding resistance test from one tap to the next yields a ripple and slope measurement, which will highlight any unwanted interruptions in the switching process of one tap to the next.

7.4.2 Drive Torque Measurement

A tap changer consists essentially of gears, insulated shafts and mounts fixtures as well as contacts and terminal surfaces. Mechanical malfunctions of on-load tap changers present untypical drive torque behaviours and mechanical vibrations, later accompanied by electrical failures. Mechanical and control problems can be detected from the additional friction, contact binding, extended changer operation times and drive motor torque or motor current information.

During the switching cycle of an OLTC, the required mechanical torque [Nm] increases considerably, depending on the action performed. The phenomena may be measured on the shaft of the driving motor by torque indicators [Krämer 1996]. However, this is not possible for OLTCs in service. The only way to measure the variable need for mechanical energy during a switching cycle is to measure the voltage and current from the electrical supply side. The active power of a motor is nearly proportional to the torque of the output shaft. However, the driving motor is not always a three-phase type; single-phase types and DC-motors are also used. From the comparison of torque and active power curve, it may be concluded that the detection of the active power of the motor drive unit may be used principally to monitor the OLTC torque.

The *drive torque* includes important mechanical forces of the selector and diverter switch. The mechanical forces at the selector switch come

especially from the contact springs and contact friction. The mechanical forces at the diverter switch come from the energy stored in the load switch. An evaluation of calculable value of torque dynamics from the *torque-time curve* (average value and average slope steepness) could give information about the adjustment of the selector contact and the condition of the contact surface.

Research has shown that when the contact springs are aged or broken, the torque dynamics, average value and average slope steepness decrease during the opening and closing of the contacts. When damage to contact surfaces occurs, during the opening and closing of the contacts, the torque dynamics, average value and average slope steepness increase. The load switching initiation also causes a large torque peak. The height of this peak depends on the switch adjustment and the condition of the energy store in the load switch. Generally, excessive values and oscillations in the torque-time function are caused by damaged motor drive elements, i.e. bearings and gearwheels [Marwitz 1992].

Initial current inrush and *starting torque* are related to mechanical static friction and backlash in the linkages. The monitoring of this peak value during the first fifty milliseconds of the event provides a useful diagnostic. Monitoring of *the average value of running current or torque* after initial inrush/start-up provides a measure of dynamic friction [Chu, 2000].

Motor current measurement is most effective when the motor directly drives the mechanical linkages. Most common tap changer designs employ a motor to charge a spring. The spring supplies energy to move the linkages during a tap change. In this case, motor current measurement is not very effective at detecting mechanical problems. Torque or force sensors measuring drive force will yield the desired information. The area under the motor current curve is called the *motor index* and is usually given in ampere-cycles, based on the power frequency. A similar parameter based on torque may be used. This parameter characterizes the initial inrush, average running conditions, and total running time. Not all types of tap changer operations have similar index values. Some monitoring characteristic parameters such as time of inrush current, total switching time and power consumption index for the mechanical conditions are also proposed in [Tenbohlen, 2003].

7.4.3 Selector Switch Monitoring

Before the diverter switch switches the current on to the selector switch, a monitoring system should be able to detect that the selector contacts are in the right positions. This can be done by monitoring drive shafts of the moving contact. These drive shafts generally are core of the tap selector tank and drive all three phases of the selector/change-over moving-contact arms. By monitoring the angular position of the moving contact drive shafts of the selector switch, an accurate indication of the position of the moving contacts may be obtained. [Kay 1997].

7.4.4 Temperature Difference between the Main Tank and Load Tap Changer Compartment

A variety of diagnostic algorithms for on-load tap changers may be implemented using temperature data. In the earlier days, temperature rise of oil in selector and diverter compartments may be used to detect overheating of fixed or moving switching contacts. When the tap changer is in a compartment separate from the main tank, it naturally results in larger temperature differences between main tank and the load tap changer compartment. Thus, the monitoring of this temperature difference is most effective for this external tap changer designs [Chu, 2000].

However, smaller differences are expected on tap changers that are physically located inside the main tank. This method is most suited for detecting coking contacts and problems of thermal/dielectric nature such as excessive losses caused by bad contacts. Under normal operating conditions, the main tank temperature will be higher than the temperature of the tap changer compartment. On the other hand, tap changer temperature may exceed main tank temperature periodically under normal conditions. Hourly variations in electrical load, weather conditions, odd tap position operation at low load for reactance type tap changers, and cooling bank activation may result in main tank temperatures below that of the tap changer. Reliable diagnostic algorithms must account for these normal variations in some way [Reason, 1993].

7.4.5 Dissolved Gas Analysis

Dissolved Gas-In-Oil monitoring has been recognized as an important tool for detecting incipient-fault conditions in the main tanks of transformers and is being applied to the OLTCs. The dissolved Gas-In-Oil analysis for OLTC has to be considered separately for the selector switch and the diverter switch. The oil of the selector switch is the same oil as the oil in the main tank. Dissolved gases in the oil in the main tank are the result of discharges or heating.

The oil of the diverter switch is in a separate enclosed compartment. Thus, the interpretation of gases in the diverter switch compartment is different from that of gases in the main tank of the power transformer. The aim of the interpretation is to distinguish between normal gassing behaviour and abnormal behaviour, which may caused by be excessive contact wear. In the diverter switch, localized overheating of conductors and surrounding insulation may lead to carbonization and byproduct polymeric films forming on conductors, which create a thermal runaway condition. Carbonization and polymeric films increase the surface resistance of the contacts, thereby causing increased heating and further byproduct formation and accumulation, which causes more heating and eventually leads to failure unless the cycle is interrupted by maintenance. This behaviour involves a special problem of OLTCs named “coking”, which comes essentially from carbonized oil in the diverter and may be detected by observing the generation of hydrocarbon gases such as methane (CH_4), ethane (C_2H_6), ethylene (C_2H_4), and acetylene (C_2H_2). The correlation between dissolved gases and certain types of faults is still in the early stages of determination and will depend on the design and material used for the tap changer. Some research has introduced the artificial intelligence (AI) method for detecting OLTC “coking” problems [Wang[2], 2000].

However, in practical terms, arcs occur during the normal switching of diverter switches. These arcs dissolve *gas* in the oil of the diverter switch. Thus, it is complicated to distinguish between normal and the above mentioned abnormal gassing behaviour in the diverter switch. At present the dissolved gas analysis for the diverter switch is not sufficiently meaningful.

8 Online Monitoring of Tap Changers with Vibration Technique

Vibration analysis is a non-invasive and relatively inexpensive monitoring technique. It has been successfully applied in many industrial applications, mainly aeronautics and manufacturing. In the field of electrical equipment, it has been applied in circuit breakers by numerous investigators [Demjanenko et al, 1992], [Runde et al, 1992].

8.1 State of the Art

Vibration monitoring for tap changers considering various types of sensors and acquisition units has been a topic of investigation over the last 20 years. A method of measurement and evaluation of mechanical vibrations by means of acceleration sensors was presented by Marwitz [Marwitz, 1992]. The switching vibration signals along with the contact oscillogram were also shown in Marwitz's work. This evaluation of the acceleration is not a suitable method for transformer monitoring due to the disturbances affecting the measuring (background noises, arc noises from the load switching etc.).

Subsequently, an approach using online acoustic emission monitoring equipment has been proposed [Richardson, 1998]. An amplified vibration signal is fed to an envelope detector, which is used to perform a data reduction technique to produce a time envelope. A processor is used to give an alarm, warning or an output display. The occurrence of acoustic bursts is mentioned as the key to the tap changer's status.

Some research has shown that normal, detrimental and faulty behaviours such as prolonged characteristic times, contact bounces, worn contacts and loose shafts may be distinguished by acoustic diagnosis [Bengstsson T, 1996]. Consequently, there has also been an attempt to evaluate acoustic signals. Two methods for evaluating faults situations have been developed [Wright, 1997]. The first method was *Automatic Timing (AT)*, where the significant events in the vibration signature are identified and timed automatically. The second method is *Resolution Ratio (RR)*, where changes in the response of these significant events provided information regarding cracked, damaged or worn components. Moreover, some acoustic

emission parameters like accumulated energy under normal conditions and with defect simulations of the tap changer have been presented [Trindade, 2005].

The feature map method is also one of the methods for long term continuous monitoring [Kang, 2000][2]. The continuous monitoring can be achieved by correlating induced faults on a real tap-changer with changes in the vibration signatures. The corresponding location of the signature on the map gives indication of actual condition of the equipment. By applying a set of signatures corresponding to both healthy and faulty conditions to obtain the trained map, the trajectories showing the transition of equipment from healthy to unhealthy conditions can be visualized.

More recently [Simas, 2005] has developed a data-conditioning unit to collect the vibration signal during a tap change. The recorded data has been processed using a Genetic Algorithm (GA) and a Recursive Least Square (RLS) filter. A system using the method of envelope extraction by the Hilbert convolution procedure with adaptive parameters has also been proposed [Foata, 2000].

8.2 Transition Sequence Investigation

In this work, the studies of the transition process are conducted during no-load situation on a tap changer without insulating oil in the laboratory. The tap changer is a diverter-switch type with series voltage up to 220 KV, current intensity from 400 to 1000 A and mounted in the laboratory for experimental purposes (Figure 8.1). During the investigations, it was manually operated from tap 1 to tap 19. The technical details of contacts in the diverter switches depend on the type of tap changer.

Figure 8.2 shows a photograph of the contacts in the studied diverter switch. The contacts are held in place by extension springs. During the tap-change process, the tap selection is firstly done via the selector switch. Then the diverter switch operates in order to transfer the current from one tap position to another tap position. The left set and the right set of contacts in the diverter switch represent the odd-tap or even-tap position of the tap changer. Thus, the set of contacts at odd-tap position and the set of contacts at even-tap position are always separately considered in the investigation of the tap changer.

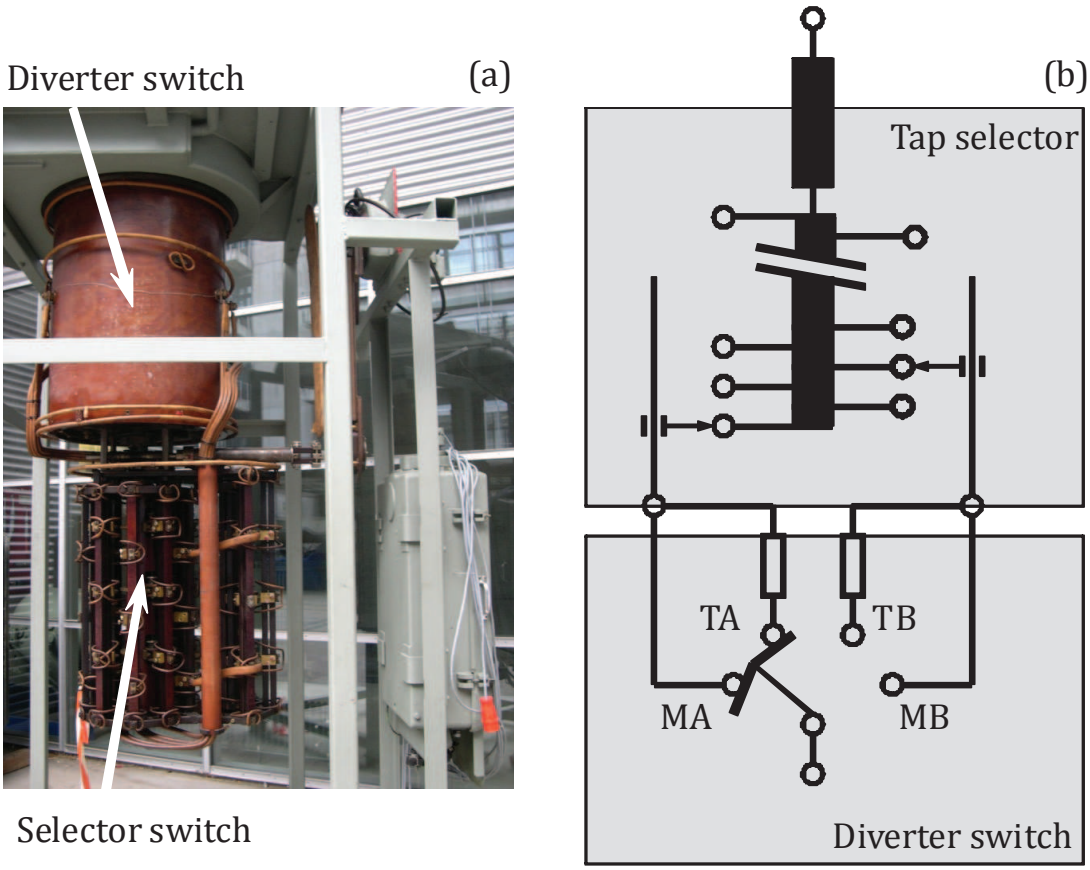

Figure 8.1 Investigated tap changer in laboratory: (a) photo; (b) schematic

The diverter switch is normally equipped with transition resistors to avoid short-circuit under operation; the set of contacts is therefore composed of main contacts (M) and transition contacts (T). The sequence of the transition process of the type of tap-changer from one tap position (A) to another tap position (B) may be concluded in the following five phases. In Figure 8.1b, MA and TA represent the main and transition contacts at position A, respectively. MB and TB represent the main and transition contacts at position B, respectively.

Phase 1: MA and TA are closed (load current via MA)
Phase 2: TA is still closed; MA is being opened (load current via TA)
Phase 3: TA is still closed; TB is being closed (load current via TA)
Phase 4: TA is being opened; TB is still closed (load current via TB)
Phase 5: TB is still closed; MB is being closed (load current via MB)

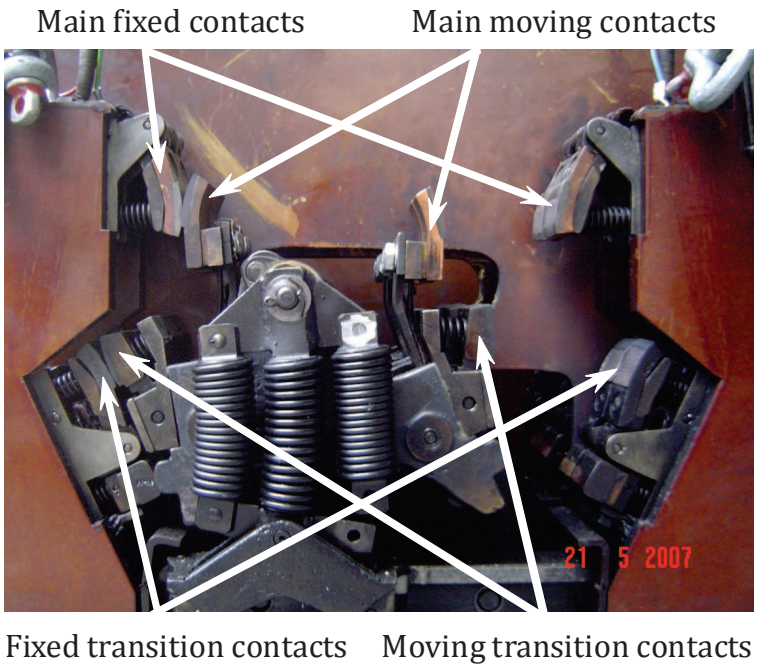

Figure 8.2 One-phase contact set of a diverter switch

In this work, the switching period of the transition process was studied from the sequence of the acoustic signal. The piezoelectric sensor type EPZ-27MS44 from EKULIT was fixed onto the top of the tap changer. In order to observe the phase of tap changer process, different resistors were additionally connected at the end of each contact set in the diverter switch (Figure 8.3). By applying a voltage across the contacts and additional resistors, different current levels were detected during different phases of the contact movement in order to get information about the current phase of the tap changing process.

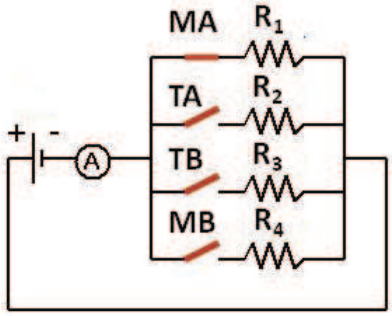

Figure 8.3

Tap change process measuring circuit

The voltage signal measured during the five-phase transition process and the complete vibration signatures captured by an oscilloscope are shown in Figure 8.4. The figures show the signals appear like a burst with a series of different peaks. The signatures are horizontal symmetric. They were captured during the switching upwards from tap 2 to tap 3 (odd-tap

position) and from tap 9 to tap 10 (even-tap position). Different current levels can be seen from these transition phases. Thus, Number 1 – Number 5 in the figures indicate the five phases of the transition process as described above. Furthermore, the switching period of each transition phase may be determined from the interval between doted lines. Figure 8.4a shows the tap transfer process of the contacts (TA and MA) from odd-tap position to even-tap position (TB and MB). It begins with phase 1 where MA and TA are closed and the load current is transferred via MA. The process ends with the closing of TB and MB in phase 5. Figure 8.4b presents the contact moving process from even-tap position (TB and MB) to odd-tap position (TA and MA). It begins with phase 5 where TB and MB are closed and the load current is transferred via MB.

Both signatures from the operating of odd-tap position and even-tap position show behaviour of a similar manner. Weak acoustic signals (noise) are obtained during the first phase before the contacts begin to move. This period takes around 60-65 ms. In phase 2, the transition contact is still closed and the main is being opened and no acoustic signal appears for a period of 40 ms. The higher amplitude signal is found during phase 3. This is the period that the transition contact is being closed. This phase is the shortest duration (around 16-20 ms). In phase 4, the period during which the transition contact is being opened and the main contact is still closed, the low amplitude signature can be detected. The highest and largest signature can be seen during phase 5, which is when the main contact is being closed. This takes a longer time than other phases (longer than 100 ms).

It is observed that the vibration signatures with the highest amplitude are found to mostly occur during the contact closing process. This is the period from the beginning of closing of the transition contact (phase 3) until the beginning of closing of the main contact (phase 5). The time interval between the beginnings of these two phases is visible as around 50 ms for odd-tap and 48 ms for even-tap. It is assumed that this closing time will be different when the tap changer is not in the normal condition. However, in practice, it is difficult to measure the time between the beginning of phase 3 and the beginning of phase 5. It is more feasible to measure the time between the first two highest peaks. This period is defined in this work as the *switching characteristic time* Δt (see Figure 8.4) and is used further as the monitoring criteria.

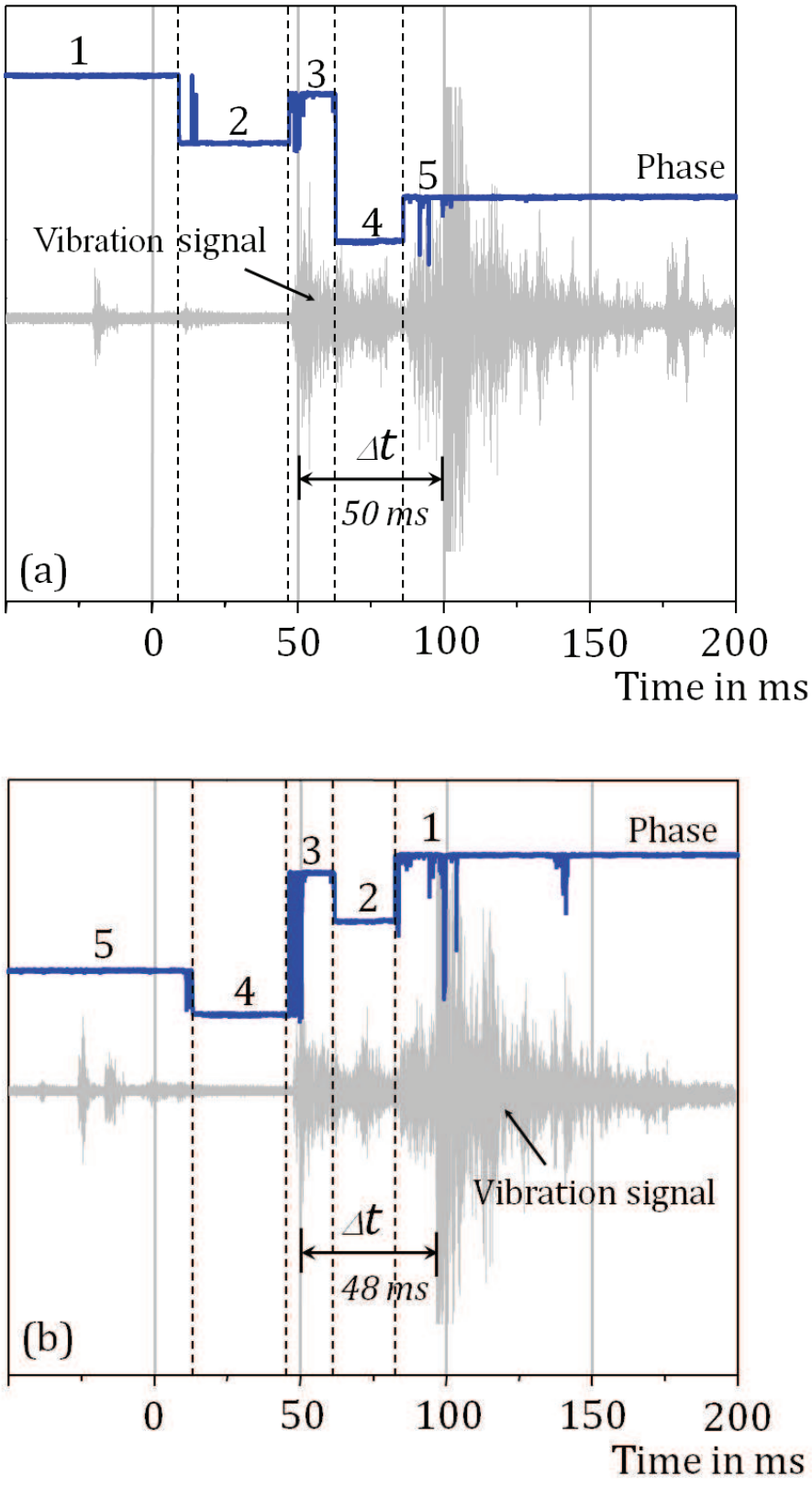

Figure 8.4 Vibration Signatures during tap-change in normal condition: (a) at odd-tap position; (b) at even-tap position

8.3 Simulation of Defects in Laboratory

In this section, the change of vibration signatures occurring with two types of defect in the diverter switch is studied. The characteristic time defined in the last section is observed and compared with that obtained in the normal condition. Figure 8.4 shows that under the normal condition of operation, there is no significant difference between the signals record during the switching of odd-tap position and even-tap position. Thus, in this section all simulations were done at the switching contact of odd-tap position.

The simulated defects were in the form of barriers between the contacts and the loss of main moving contacts of all three poles. Two different barrier types were investigated. The barriers were placed between the fixed and the moving contacts along the main and transition contacts. The first barrier (Figure 8.5a) was a plastic plate of 2 mm thickness. It covered all three poles of the diverter switch. The second barrier was a copper rod with a diameter of 5 mm (Figure 8.5b) which was placed only at the first pole of the diverter switch.

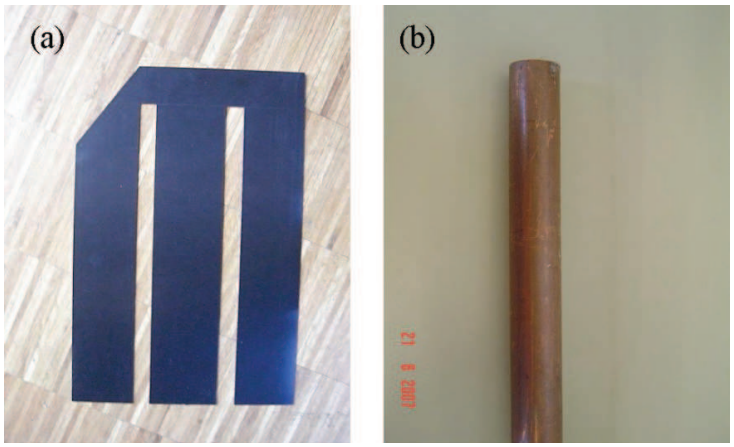

Figure 8.5

Samples for tap changer defect investigation

Figure 8.6 show the signals recorded during the simulation of defects. The phases of the signals are divided into the same series – dotted lines – as already presented in Figure 8.4a for the vibration signal of the diverter switch in normal state. For the comparison with the signatures from the normal status, four main features of the signatures can be focused on: form, amplitude, switching course and switching characteristic time.

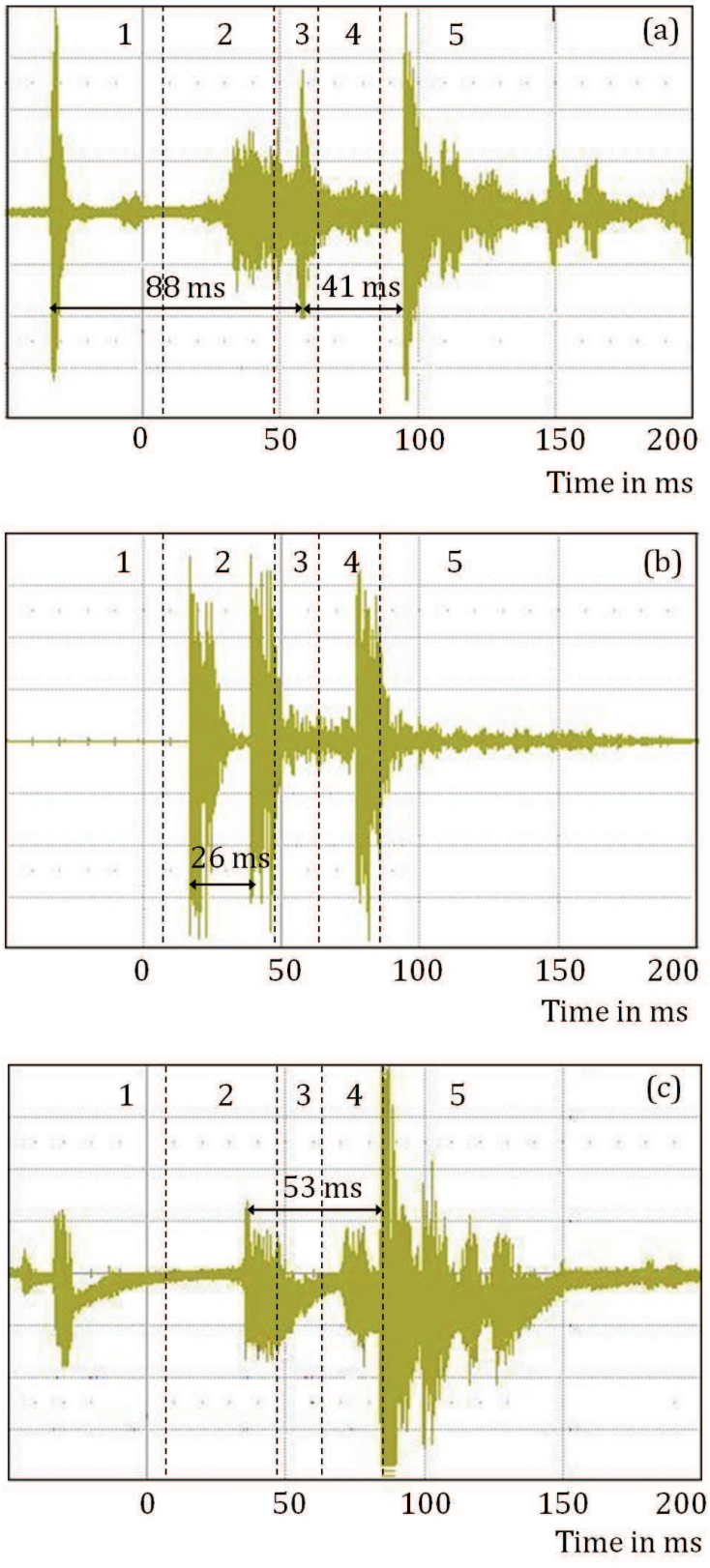

Figure 8.6 Vibrations signals at odd-tap from the failures investigations: (a) plastic plate; (b) rod; (c) loss of main moving contacts

In overall, the signature form and the signature course recorded when the plastic plate obstructed the contacts (Figure 8.6a) is not that different from the normal condition (Figure 8.4a). The signature is horizontal symmetric. The highest amplitudes are also found in phase 1 and phase 5. However, the highest amplitude in phase 3 does not appear directly at the beginning of the phase. The obstruction of the plastic plate can be assumed to cause this delay. Furthermore, unlike the normal condition, strong signals are clearly observed in first phase and second phase. The time between these strong signals is 88 ms. These noises may be from the vibration of the plastic plate during the switching process. The characteristic time between the highest peak in phase 3 and the highest peak in phase 5 is around 41 ms, which is much less than the characteristic time from normal condition which is 50 ms (Figure 8.4a).

Figure 8.6b shows the signatures captured during the operation of the tap changer with the copper rod between the contacts. The signature form and the signature course are totally different from the normal condition. The signature is horizontal symmetric and appears with three strong peaks in phase 2 and phase 4. There is no strong signal in phase 5 at all. It is impossible to match the closing time steps with those found under the circumstance of normal operation. When time between the first two highest peaks in phase 2 is measured, it is found to be around 26 ms, which is considerably less than the characteristic time in normal condition.

Figure 8.6c shows the signal recorded when all three poles of the main moving contacts of the diverter switch are lost. There is a strong noise with low amplitude in phase 1. A very high peak is observed in the beginning of phase 5. This is believed to be an acoustic signal from the stub of the lost contact. The time between the first two highest peaks in phase 2 and in phase 4 is measured to be 53 ms, which is very close to the characteristic time for the normal condition. However, the closing time steps are shifted forward.

In conclusion, it can be said that all signatures recorded from the defect simulations have differences in time phases. Consequently, the measured characteristic times under the defect conditions are different from the measured characteristic time under the normal condition. Thus, the results in this section show that the characteristic time can be selected as

for use in online measuring criteria to distinguish between normal operation and defective operation of a tap changer.

8.4 On-site Investigation

A compact measuring system was developed for online monitoring of the tap changer. The monitoring concept is to measure the characteristic time between the two strong peaks of the generated vibration signal. This measuring concept may be changed depending on the type of tap changer. A microcontroller is applied in the measuring system for the time determination. The advantage of using the microcontroller is that it can be reprogrammed for any future change in the measuring concept.

8.4.1 Measuring System

Figure 8.7 shows the diagram of the compact vibration measuring system. The vibration signal is detected by a piezoelectric sensor and is amplified by a preamplifier module. The amplified signal is then send to a measuring circuit for the characteristic time measurement, which has a microcontroller as a main component. The output of the measuring circuit is transferred to a digital to analogue converter. Finally, the characteristic time as a current output in a range of 4-20 mA is sent to a main online monitoring system. In case of the high disturbance from noise on site, a filter may be required. This can be applied as a modification to the measuring system or as an additional part.

Vibration Sensor and Preamplifier Module

The piezoelectric sensor type EPZ-27MS44 from EKULIT, as shown in Figure 8.8**,** is used to detect the vibration signal during the tap-change process. The sensor resonance frequency gives a bandwidth of about 40 kHz. The sensor uses the phenomenon of piezoelectricity to convert vibrations to an electrical signal.

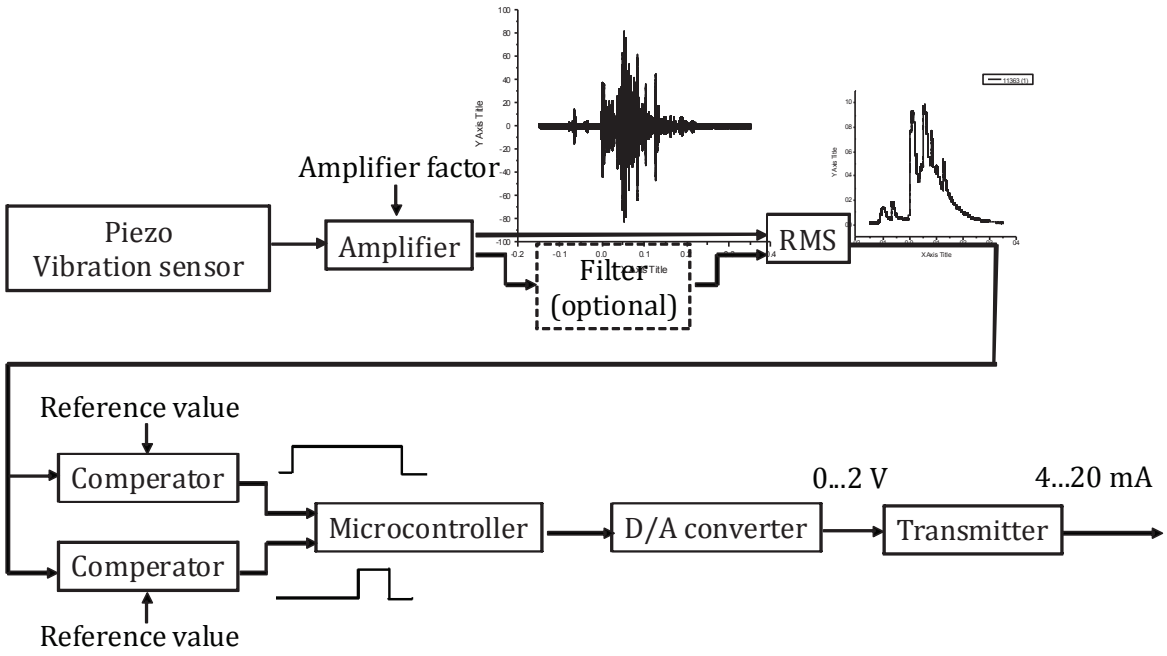

Figure 8.7 Vibration monitoring system

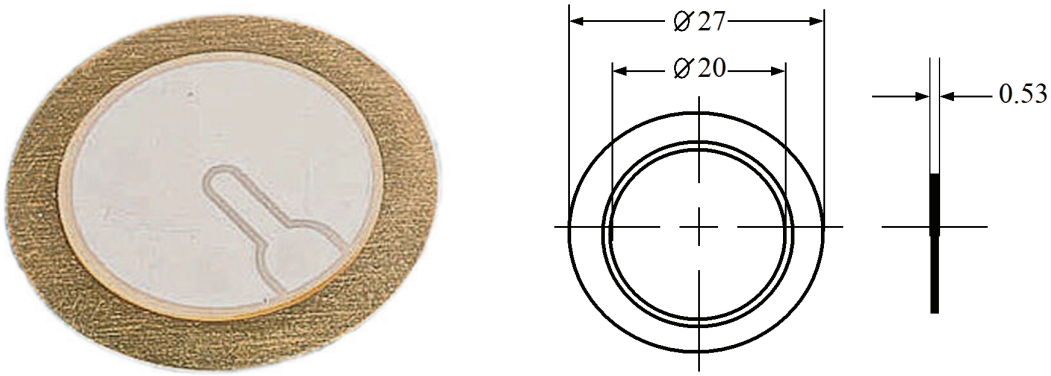

Figure 8.8 Piezoelectric sensor and its schematic diagram

The weak output signal of the piezoelectric vibration sensor is amplified to a voltage level within ± 5V using a linear inverting operational amplifier type TS921IN from ST Microelectronics. When no input signal appears, the positive input of the operational amplifier will be stabilized at 0 V via a 150kΩ resistor. The amplifier gain is determined by the ratio of two resistors (0-100kΩ and 2.40kΩ), which may be adjusted by the trimmer in the range of 1 to 42. The maximum gain can be calculated as follows:

$$Gain_{\max} = 1 + \frac{100k\Omega}{2.4k\Omega} \approx 42 \tag{8.1}$$

The preamplifier module is implemented on a separate board to allow for future developments. A new preamplifier module can be used as a replacement when a different sensor is required.

Characteristic Time Measuring Module

The envelope of the vibration signal is determined by considering the RMS (Root Mean Square) component. The RMS is used to form an averaged value for the squared signal. Two comparators are used to determine the time interval between the beginning of the first strong peak and the beginning of the final strong peak of the RMS signal. This time interval corresponds to the time during the transition process between the closing of transition contact and the closing of the main contact of the diverter switch. Two comparators are used to obtain a reliable measurement of the time interval. The signals from the comparators are formed by comparing the voltage of the input RMS signal with a fixed reference voltage. The microcontroller is used to calculate the time between the two changes in each comparator output signals. Further details of these system components can be found from the Appendix D. The circuit diagram of the measuring module is provided in Appendix E. Moreover, the flow chart of microcontroller programming can be defined as in Appendix F.

Mechanical Construction

The measurement module is placed in a compact 115 mm long, 65 mm wide and 55mm high aluminium case, as shown in Figure 8.9. There are two slots on the main board for two changeable components: the preamplifier and filter module. A 4-pole connector system is used for the power supply and signal transmission. The strap tape holds the piezoelectric sensor with an aluminium plate at the bottom of the case. The aluminium plate is used for pressing the sensor against the transformer tank. A thin foam sheet is inserted as insulation between the aluminium plate and the circuit board. Four strong magnets are built on the case of the box as well and these used for mounting the case on to the steel transformer tank. Consequently, the measurement can be made without screwing the case to the transformer tank.

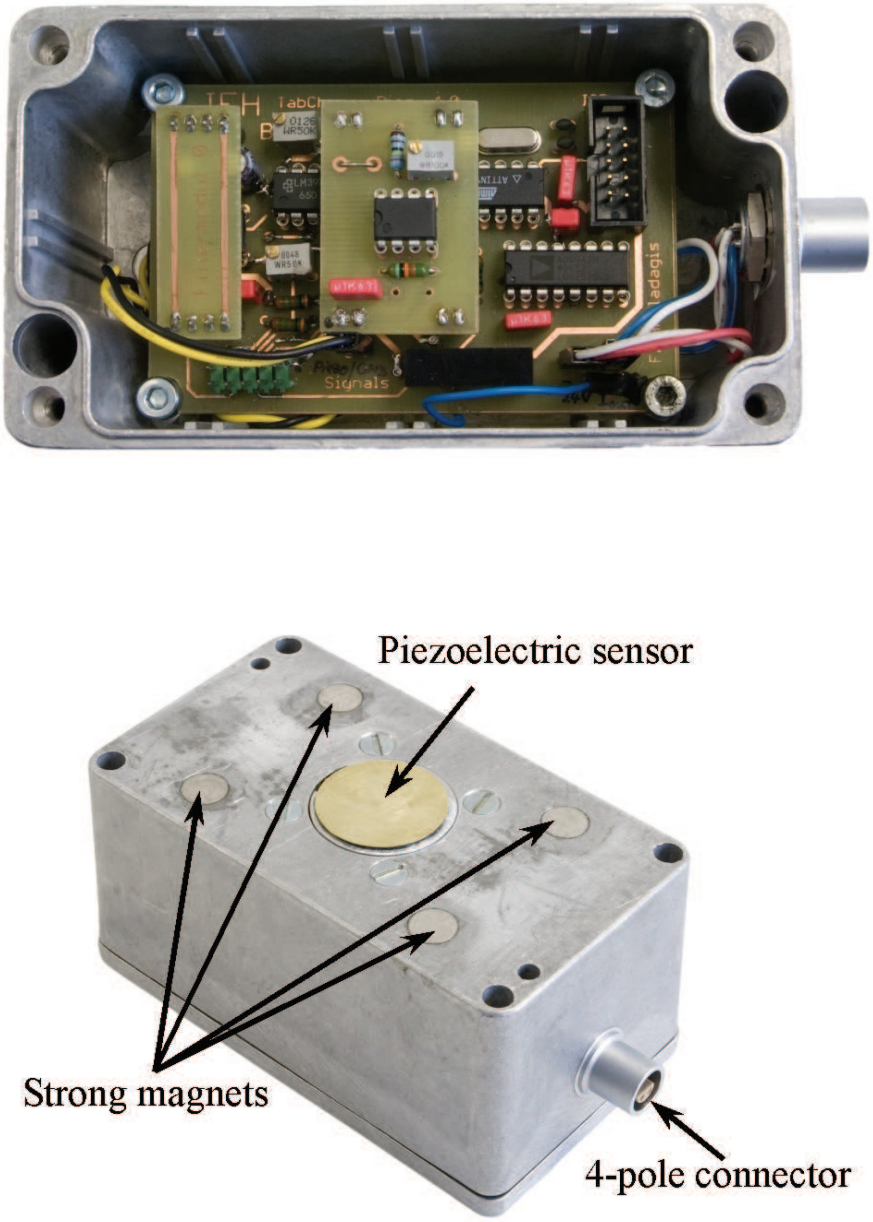

Figure 8.9 Measuring Module

8.4.2 Investigated Tap-changer

The investigations were performed with a tap changer type VACUTAP® VR 400Y–123/D–10191G with ± 9 tap positions from Maschinenfabrik Reinhausen. The tap changer was installed at a power transformer with a rated capacity of 40 MVA, ONAN and 107 kV ± 16.0% in stages ± 9 / 21 kV yn0d. For the investigation, the tap changer was manually operated during the no-load situation.

Figure 8.10 shows the position of the compact measuring system placed on top of the transformer tank next to the transformer cover and near the drive mechanism of the tap changer. It was ensured that the surface under the piezoelectric vibration sensor was as smooth and clean as possible for a good contact with the transformer tank.

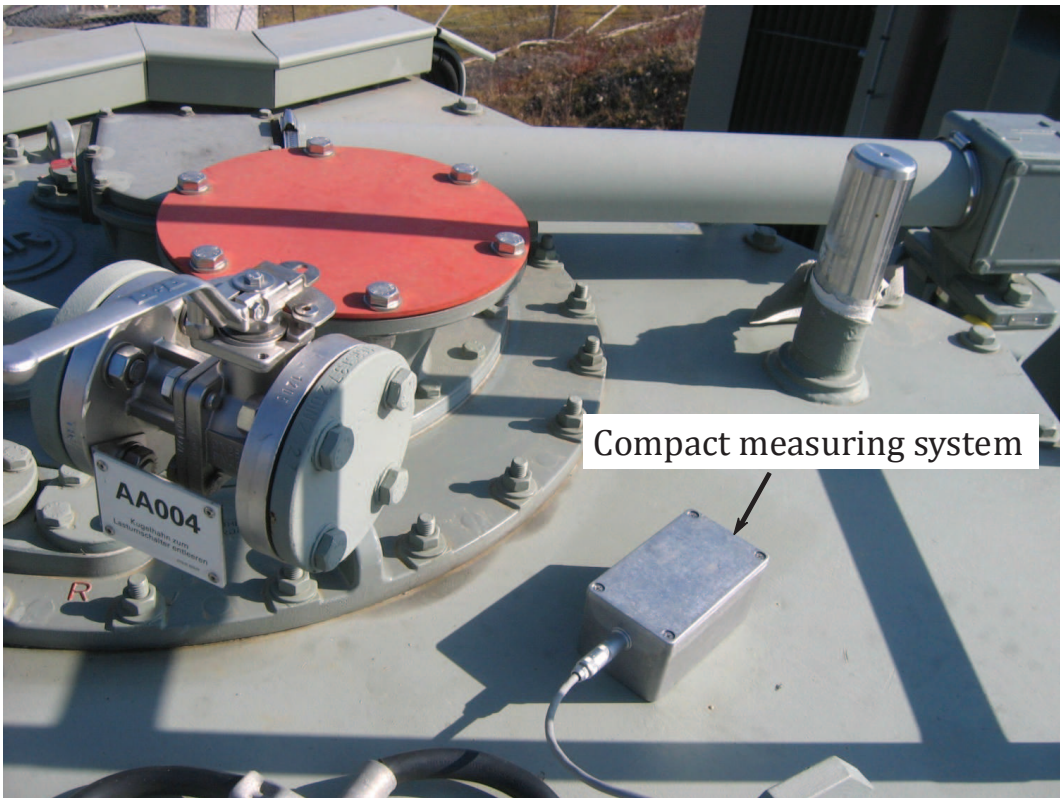

Figure 8.10 Measuring case on the investigated Siemens transformer

8.4.3 Results of the Measurement

The output current during the tap-change process was measured by a multi-meter. In addition, the vibration signals, the RMS signals and the signals from the two comparators were observed by an oscilloscope. First, the trimmer in the preamplifier module was adjusted to improve the amplitude and the quality of the vibration signals. Then the comparative values for the two comparators were adjusted to ensure correct measurement of the desired characteristic time. This was done by adjusting the resistors at the comparators.

Vibration signals (PREAMP) from the preamplifier module, signals (RMS) from the RMS module and signals (INT0 and INT1) from the comparators were recorded during the tap-change process from tap 4 to tap 3 (odd-tap position) and from tap 5 to tap 4 (even-tap position) as shown in Figure 8.11. Slight differences in shape and amplitude of the vibration waveforms measured at the even-tap and the odd-tap position may be seen. Also, it may be noticed that the measured characteristic times (Δt) from odd-tap and from even-tap position show a significant difference in range.

The characteristic times investigated during the tap-change process from tap 1 to tap 19 and from tap 19 to tap 1 are depicted in Figure 8.12. The characteristic time of the switching process is separated into two groups. The characteristic time of the odd-tap position averages around 124 ms and the characteristic time of the even-tap position averages around 110 ms.

It can be seen that the measured characteristic times vary within a tolerance band. The width of this tolerance band can be represented by the standard deviation, the value of which will depend on the type and condition of the tap changer. With a number of measurements K and the average characteristic time ($\overline{\Delta t}$), the standard deviation σ_t may be calculated from Eq. (8.2) and Eq. (8.3).

$$\overline{\Delta t} = \frac{\left(\Delta t_1 + \Delta t_2 + \Delta t_3 \ldots\ldots \Delta t_K\right)}{K} \tag{8.2}$$

$$\sigma_t = \sqrt{\frac{\sum\left(\Delta t - \overline{\Delta t}\right)^2}{K-1}} \tag{8.3}$$

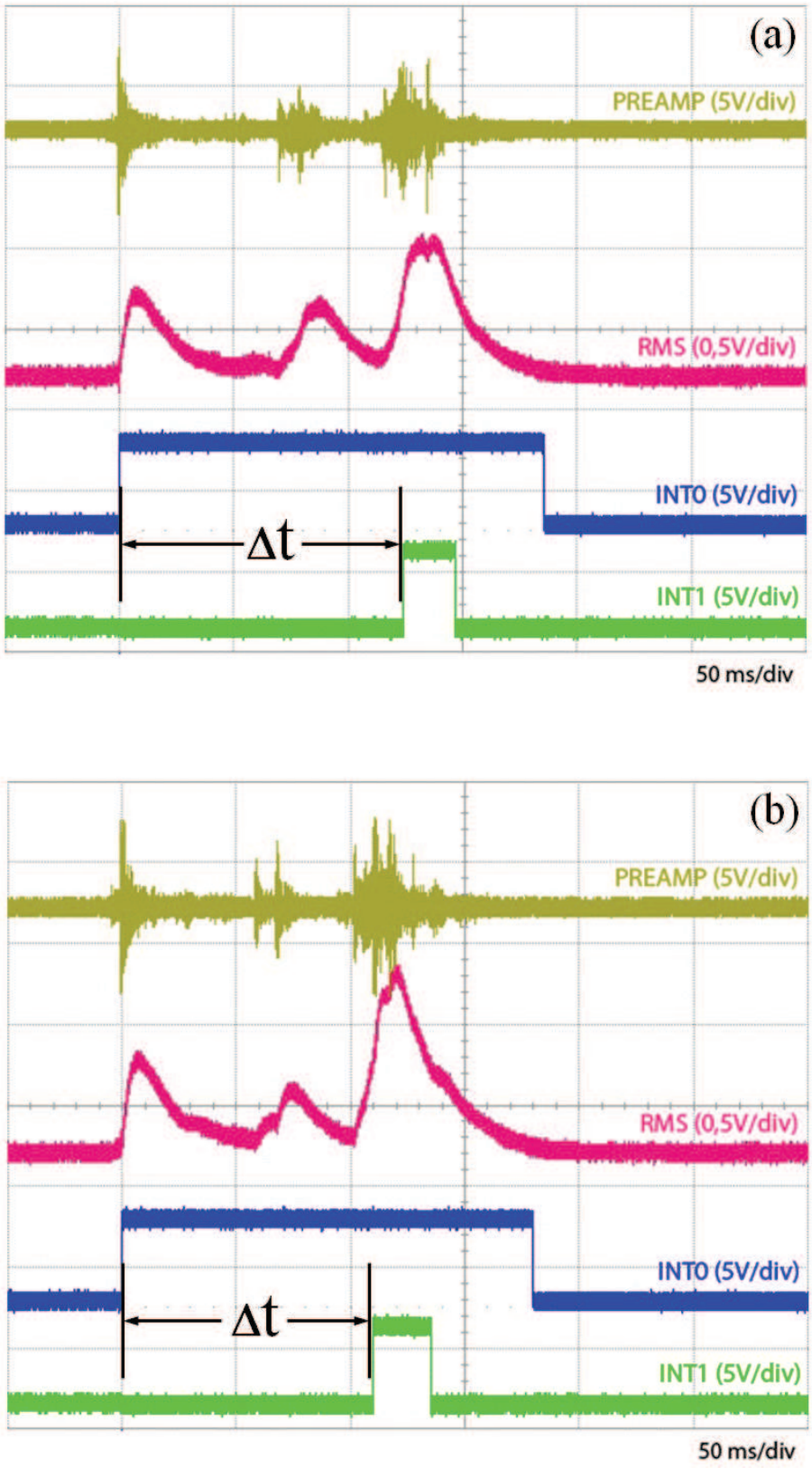

Figure 8.11 Signals from the measurements:
(a) odd-tap position; (b) even-tap position

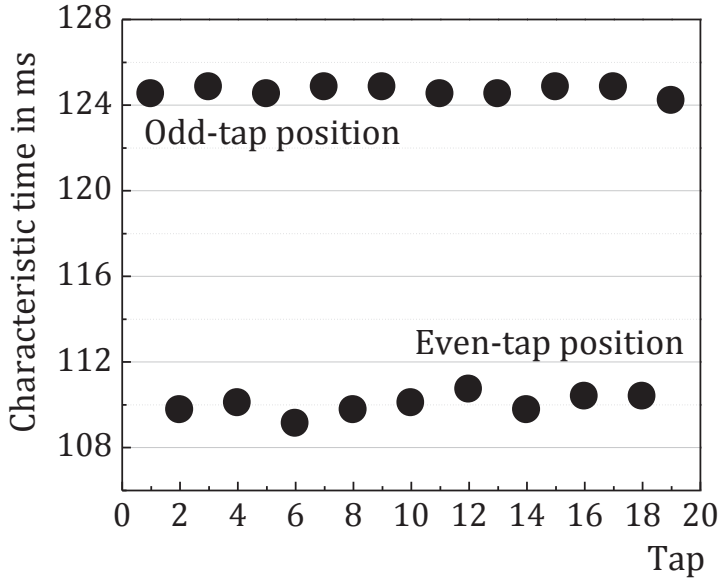

Figure 8.12
Measured characteristic time

The standard deviation indicates the distribution of the measured data set. The average characteristic time as well as the minimum, maximum and standard deviation at odd-tap position and even-tap position from the measurements described in 8.4.3 can be seen in Table 8.1. The results show that the characteristic time is repeatable with a low standard deviation: 0.2 ms for odd-tap position and 0.4 ms for even-tap position (less than 1). Therefore, the standard deviation of the characteristic time is considered as part of the criteria for monitoring the tap changer situation. From the statistic process control (SPC) theory it is known that a process is under statistical control as long as the new measured value is within 3 standard deviations of the historic process.

	Odd-tap position	Even-tap position
Average value (ms)	124.7	110.0
Minimum value (ms)	124.5	109.1
Maximum value (ms)	124.8	110.1
Standard deviation (ms)	0.22	0.48

Table 8.1 Measured characteristic time

8.5 Online Monitoring Criteria

To check if the process is under statistical control, a *control chart* may be used. Generally, the control chart is used to detect whether a process is statistically stable. It differentiates between variations: those that are normally expected of the process due to *chance* or *common causes* and those that change over time due to assignable or *special causes* [Xie, 2002].

The control chart is a specific kind of run chart that allows significant change to be differentiated from the natural variability of the measurement. It consists of:

- points representing a statistic of measurements of a quality characteristic in samples taken from the process at different times;
- a centre line, which is drawn at the value of the mean of the statistic;
- the standard deviation of the statistic;
- upper and lower control limit that indicate the threshold at which the process output is considered statistically 'unlikely' are drawn typically at 3 standard errors from the centre line.

The principles behind the application of control charts are based on the combined use of run charts and hypothesis testing. This method is a standard procedure in the industry to observe processes continually. The Shewhart procedure can be used for the hypothesis testing. It provides eight standard tests for special causes:

- One data point beyond 3 standard deviations from the centre line
- Nine data points in a row beyond one side of the central line
- Six data points in a row steadily increasing or steadily decreasing
- Fourteen data points in a row alternating up and down
- Two out of three data points in a row beyond two standard deviations
- Four out of five data points in a row beyond one standard deviations
- Fifteen data points in a row within the distance of one standard deviation from the central line
- Eight data points in a row with no data points within the distance of one standard deviation from the central line

The control chart can be applied to the online monitoring system and the eight tests of the Shewhart procedure can be used as the decision criteria. The control chart from the characteristic time measurement for the odd-tap position from section 8.4.3 is shown in Figure 8.13. There are 9 points for the measured data. It shows the mean line ($\bar{t}$) at 124.65ms. The upper limit (UCL) and lower limit (LCL) are set at 124.65 ± (3x0.22) ms, which are 125.31 ms and 123.99 ms, respectively. Figure 8.14 shows the control chart from even-tap position. The mean is 110ms. The UCL is set at 110 + (3x0.48), which is 111.44ms. The LCL is set at 110 - (3x0.48), which is 108.56ms.

When the eight tests are considered, both processes seem to be under control because none of the above cited tests take effect. It should be mentioned that usually more than 30 samples have to be taken to get reliable statistical information. The larger the sample size, the smaller is the standard deviation, as concluded from Eq. 8.3. As soon as one of the above mentioned tests take effect it may be observed in the monitoring system of a control room and electronic information may be send to the operator for example by e-mail or by short message service (SMS). This enables the operator to react promptly on the unusual process behaviour.

8.6 Implementation of the Tap-changer Acoustic Monitoring System

In conclusion, for the implementation of this acoustic monitoring system in the transformer unit, first, the vibration signature has to be recorded and the RMS signal must be created. Consequently, the range of the measured characteristic time may be defined by adjusting the compared values of the two comparators in the tap-change characteristic time measuring module. In the case of more than two significant pulses of vibration signals occurring, the program in the microcontroller must be modified. As the monitoring criterion, the characteristic time can be investigated by repeating the operation of each tap changer as many times as possible. When the repeatability of the characteristic time is found, then, the precise standard deviation can be defined and used to set the threshold value. Consequently, the monitoring alarm may be set.

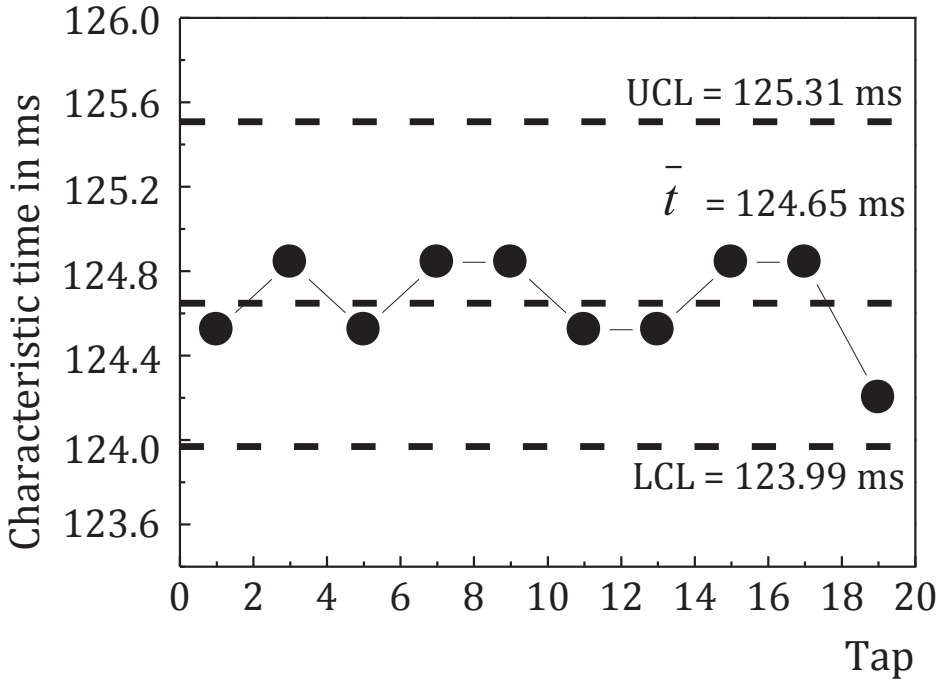

Figure 8.13 Control chart of the odd-tap characteristic time measurement

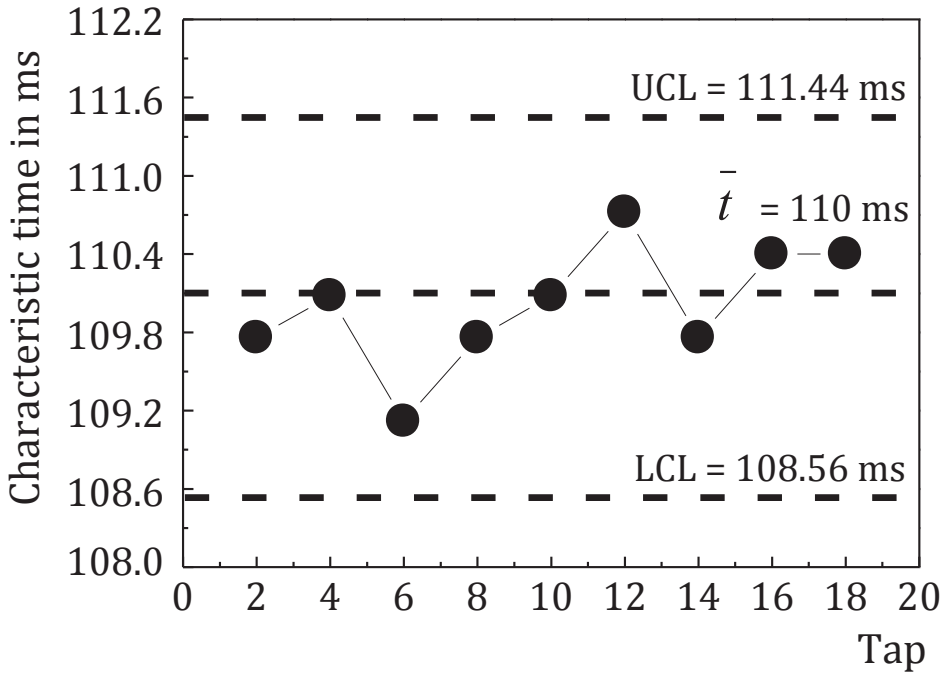

Figure 8.14 Control chart of the even-tap characteristic time measurement

9 Conclusion and Perspective

An attempt to find suitable on-line monitoring criteria for power transformers has been presented in this work. From the failure statistics of power transformer, two main topics: thermal behaviour and tap-changers have been chosen as the main focus of this work.

Thermal behaviour was studied with regard to top-oil temperature. Some simple and suitable dynamic top-oil temperature prediction models were considered for three different cooling types of transformer units (ONAN, ONAF and ODAF). The simple physical models based on the international standard and the Multilayer Feed-forward and Recurrent neural network models have been emphasized.

Last state of measured top-oil temperature, load current, ambient temperature and operating states of pumps or fans were selected as the input variables of both physical models and neural network models. The varying input measured data were provided by an existing online monitoring system supplied by AREVA Energietechnik GmbH. Some input constants in the physical models are optimized by the least square optimization technique.

Four top-oil temperature models were investigated. The first model was based on IEEE Std. C57.91. Its concept is that the change in top-oil temperature rise over ambient temperature is caused by the change in loading condition. The second model was developed by the MIT group. It is modified from the IEEE top-oil rise temperature by taking accounts of ambient temperature variations into calculations. The model is based on and supported by the linear regression technique. The third model was based on IEC60354 standard. The model considers the top-oil as a mixture of various oil flows, which have circulated along and/or outside the windings. The different types of cooling are treated separately in the calculation because of the differences in the oil flows. The last model was derived from the one-body equivalent circuit of thermal behaviour. This model is based on an assumption that all losses are transferred to the environment via a thermal resistance of the cooling equipment.

In long-term investigation, the semi-physical model from MIT group presents the best performance in top-oil temperature calculation for mentioned transformers. Results show the temperature deviation

between measured and calculated top-oil temperature of less than 2 K for the transformer cooling type ONAN and ONAF. The temperature deviation is around 3 K for the transformer cooling type ODAF with varying operating states of the fans.

The top-oil temperature neural network models were designed by varying the following characteristics: network topologies, training algorithms, number of hidden layers and numbers of hidden neurons. The one-hidden layer and two-hidden layer were investigated for the Feed-forward network type. Only one-hidden layer is modelled for the recurrent networks, due to their more complex structures.

The network structure (number of neurons and set of weights) can be achieved from network design software, which was developed in this work using the Neural Network Toolbox in Matlab. The numbers of hidden neurons was varied from 1 to 20 neurons. The networks were trained with 16 training algorithms. Consequently, 120 network structures with five inputs and one target output were examined. The designed networks with their training weights were compiled to mathematical models for top-oil temperature calculation. Weights and biases obtained from the training process were transformed to be the coefficients of the model. At the end, the network structure with the best performance in top-oil temperature calculation was reported.

The best results were obtained using the Levenberg-Marquardt, Scaled conjugate gradient and Automated Bayesian Regularization training algorithms. All investigated transformers showed that the multilayer feed-forward network has a better performance than recurrent neural network for top-oil temperature prediction. The training calculation process for the recurrent neural network needed much more time than for the feed-forward network. Low average temperature deviations were also obtained with the one-layer Feed-forward network structure with a low number of neurons. This network structure also gave slightly better performance than the two-hidden layer networks. Compared with the Lavenberg-Marquardt and the Scaled conjugate gradient backpropagation, results from Bayesian regularization-training algorithm showed the lowest average temperature deviations between measured and calculated top-oil temperature. However, the Levenberg-Marquardt method requires the shortest time for training the network.

Good performance with average temperature deviations less than 2 K may be obtained from both Feed-forward neural network model and physical model. This performance is sufficient for applying the model in the online monitoring system. However, the neural network model is more accurate in the top-oil temperature prediction for the transformer with the varied operating states of the cooling units. Results also show that the transient-state of ambient temperature has a negative effect on top-oil temperature prediction. Moreover, the unsteady-state behaviour of load current, such as the shut-down state of the transformer has a negligible effect on the accuracy of the investigated neural network model.

The ability of the model to detect malfunctions of the cooling units is proved by the actual case investigation. The difference of the measured and calculated top-oil temperature is observed during the period of the malfunction of fans. Therefore, top-oil temperature prediction using the neural network model is applicable in an online monitoring system.

To implement the model in the monitoring system, the network design for each transformer unit is required. The network should be trained with numerous qualitative measured data, especially the data of numbers of operating cooling units. The accuracy of the model should be improved by using the statistical data analysis. The input measured data, the model coefficients and the calculation errors should be analysed.

In the second part of the work, a reliable vibration measuring system for online condition monitoring of the tap changer is described. The sequences of movable main contacts and transition contacts in the diverter switch during the transition phase are studied. The vibration signal during the tap change process is detected by a piezoelectric sensor and is amplified by a preamplifier module. The amplified signal is then sent to a measuring circuit for the transition time measurement. A microcontroller is a key component in this measuring circuit. The microcontroller has an advantage for application to various transformers when the concept of measuring the characteristic time must be changed. The measuring system can be automatically triggered by the vibration signal. An output from the measuring circuit is transferred to a digital to analogue converter. Finally, the characteristic time is obtained by means of a current output in the range 4-20 mA. It may be later applied in the control unit of the main monitoring system of the power transformer.

The significant differences in vibration signatures and characteristic times during the tap change process under normal condition and fault conditions are seen from the investigations in the laboratory. The mechanical simulated fault conditions of tap changer considered were foreign parts obstruction between the contacts and loss of contacts. In these cases, the characteristic time and its standard deviation value may be employed as the online monitoring criteria for the tap changer.

The on-site measurements were done with a tap changer type VACUTAP® VR 400Y–123/D–10191G. It was manually operated during no-load situation. Results show that the developed measuring system can measure the repeatable characteristic time under the normal operation of the tap changer. It is confirmed to occur with a low standard deviation of less than 1 (0.2 for odd-tap position and 0.4 for even-tap position). The process is proved by the control chart and the Shewhart procedure to be under statistical control.

The characteristic time and the criteria must be defined at the set-up phase of the implementations on different transformer units. A filter is an additional part, which may be added to the measuring system to avoid the effect of disturbance in the plant.

In conclusion, this vibration measuring system has a good potential to be part of a comprehensive condition monitoring system. However, all investigations in this work have been done under the no-load situation. Therefore, this measuring system needs to be implemented and tested in the noisy environment during the on-load situation. Different mechanical failure conditions should also be simulated. The reliability to distinguish other type of failures should be further proved.

Symbols and Abbreviations

A Symbols

C_{th}	thermal capacity, Wh/K
i	period index
K	ratio of actual load to rated load
m_{oil}	weight of oil, kg
m_{Cu}	weight of copper, kg
m_{Fe}	weight of iron, kg
m_{steel}	weight of steel, kg
P_N	no-load loss, kW
P_S	short circuit loss at rated load, kW
P_T	total loss, kW
R	ratio of total loss to no load loss
R_{th}	thermal resistance, K/W
U_N	rated Voltage, kV
n	oil exponent
x	oil exponent
y	winding exponent
$tan\delta$	dissipation factor
Δt	sampling period, h
τ_{TO}	top oil time constant, h
$\tau_{TO,R}$	top oil time constant at rated load, h
ϑ_H	winding hottest-spot temperature, °C
ϑ_{TO}	top-oil temperature, °C
$\vartheta_{TO,\infty}$	ultimate top-oil temperature, °C
$\vartheta_{TO,I}$	initial top-oil temperature, °C
ϑ_{amb}	ambient temperature, °C
ϑ_H	winding hottest-spot temperature, °C
θ_{TO}	top-oil temperature rise over ambient temperature, K
$\theta_{TO,I}$	initial top-oil temperature rise, K
$\theta_{TO,R}$	top-oil temperature rise at rated load, K
$\theta_{BO,R}$	bottom-oil temperature rise at rated load, K
$\theta_{MO,R}$	average oil temperature rise at rated load, K
$\theta_{TO,\infty}$	ultimate top-oil temperature rise, K

B Abbreviations

EHV	**E**xtra **H**igh **V**oltage
HV	**H**igh **V**oltage
HVDC	**H**igh **V**oltage **D**irect **C**urrent
MLP	**M**ulti-**L**ayer **P**erceptron
MSE	**M**ean **S**quared **E**rrors
PD	**P**artial **D**ischarge
PT	**P**otential **T**ransformer
RMS	**R**oot **M**ean **S**quare
OD	**O**il **D**irected
ODAF	**O**il **D**irected **A**ir **F**orce
OF	**O**il **F**orce
OFAF	**O**il **F**orce **A**ir **F**orce
OLTC	**O**n-**L**oad **T**ap **C**hanger
ON	**O**il **N**atural
ONAF	**O**il **N**atural **A**ir **F**orce
ONAN	**O**il **N**atural **A**ir **N**atural
SOM	**S**elf-**O**rganizing **M**ap
SSE	**S**um **S**quared **E**rrors
UHF	**U**ltra **H**igh **F**requency
UHV	**U**ltra **H**igh **V**oltage

Appendix

A Deviation of Differential Equation (3.1)

$$\tau_{TO}\frac{d\theta_{TO}}{dt} = -\theta_{TO} + \theta_{TO,\infty}$$

$$\frac{d\theta_{TO}}{-\theta_{TO} + \theta_{TO,\infty}} = \frac{dt}{\tau_{TO}}$$

$$\frac{d\theta_{TO}}{\theta_{TO,\infty} - \theta_{TO}} = \frac{1}{\tau_{TO}}dt$$

$$-d\int\frac{\theta_{TO,\infty} - \theta_{TO}}{\theta_{TO,\infty} - \theta_{TO}} = \int\frac{1}{\tau_{TO}}dt$$

$$-\ln\left(\theta_{TO,\infty} - \theta_{TO}\right) = \frac{1}{\tau_{TO}}t + C$$

$$\ln\left(\theta_{TO,\infty} - \theta_{TO}\right) = -\left(\frac{1}{\tau_{TO}}t + C\right)$$

when $t = 0; -C = \ln\left(\theta_{TO,\infty} - \theta_{TO,I}\right)$

$$\ln\left(\theta_{TO,\infty} - \theta_{TO}\right) = -\frac{1}{\tau_{TO}}t + \ln(\theta_{TO,\infty} - \theta_{TO,I})$$

$$\ln\left(\theta_{TO,\infty} - \theta_{TO}\right) - \ln\left(\theta_{TO,\infty} - \theta_{TO,I}\right) = -\frac{1}{\tau_{TO}}t$$

$$\ln\frac{\theta_{TO,\infty} - \theta_{TO}}{\theta_{TO,\infty} - \theta_{TO,I}} = -\frac{1}{\tau_{TO}}t$$

$$e^{-\frac{1}{\tau_{TO}}t} = \frac{\theta_{TO,\infty} - \theta_{TO}}{\theta_{TO,\infty} - \theta_{TO,I}}$$

$$e^{-\frac{1}{\tau_{TO}}t}\left(\theta_{TO,\infty}-\theta_{TO,I}\right)=\theta_{TO,\infty}-\theta_{TO}$$

$$\theta_{TO}=\theta_{TO,\infty}-e^{-\frac{1}{\tau_{TO}}t}\left(\theta_{TO,\infty}-\theta_{TO,I}\right)$$

$$\theta_{TO}=\theta_{TO,\infty}-e^{-\frac{1}{\tau_{TO}}t}\theta_{TO,\infty}+e^{-\frac{1}{\tau_{TO}}t}\theta_{TO,I}$$

$$\theta_{TO}=\left(\theta_{TO,\infty}-\theta_{TO,I}\right)\left(1-e^{-\frac{1}{\tau_{TO}}t}\right)+\theta_{TO,I}$$

B Deviation of Differential Equation (4.1)

$$\tau_{TO}\frac{d\vartheta_{TO}}{dt} = -\vartheta_{TO} + \vartheta_{amb} + \vartheta_{TO,\infty}$$

$$\tau_{TO}\frac{\vartheta_{TO}[i]-\vartheta_{TO}[i-1]}{\Delta t} = -\vartheta_{TO}[i]+\vartheta_{amb}[i]+\vartheta_{TO,R}\left(\frac{K[i]^2R+1}{R+1}\right)$$

$$\frac{\tau_{TO}\vartheta_{TO}[i]}{\Delta t} - \frac{\tau_{TO}\vartheta_{TO}[i-1]}{\Delta t} = -\vartheta_{TO}[i]+\vartheta_{amb}[i]+\vartheta_{TO,R}\left(\frac{K[i]^2R+1}{R+1}\right)$$

$$\frac{\tau_{TO}\vartheta_{TO}[i]}{\Delta t}+\vartheta_{TO}[i] = \vartheta_{amb}[i]+\vartheta_{TO,R}\left(\frac{K[i]^2R+1}{R+1}\right)+\frac{\tau_{TO}\vartheta_{TO}[i-1]}{\Delta t}$$

$$\vartheta_{TO}[i]\left(\frac{\tau_{TO}}{\Delta t}+1\right) = \frac{\tau_{TO}\vartheta_{TO}[i-1]}{\Delta t}+\vartheta_{amb}[i]+\vartheta_{TO,R}\left(\frac{K[i]^2R+1}{R+1}\right)$$

$$\vartheta_{TO}[i]\left(\frac{\tau_{TO}+\Delta t}{\Delta t}\right) = \frac{\tau_{TO}\vartheta_{TO}[i-1]}{\Delta t}+\vartheta_{amb}[i]+\left(\frac{\vartheta_{TO,R}K[i]^2R}{R+1}\right)+\left(\frac{\vartheta_{TO,R}}{R+1}\right)$$

$$\vartheta_{TO}[i] = \frac{\tau_{TO}}{\tau_{TO}+\Delta t}\vartheta_{TO}[i-1]+\frac{\Delta t}{\tau_{TO}+\Delta t}\vartheta_{amb}[i]$$
$$+\frac{\Delta t\,\vartheta_{TO,R}R}{(\tau_{TO}+\Delta t)(R+1)}(K[i])^2+\frac{\Delta t\,\vartheta_{TO,R}}{(\tau_{TO}+\Delta t)(R+1)}$$

C Training algorithm in MATLAB Neural Network Toolbox

Training function	Used for
trainbfg	BFGS quasi-Newton backpropagation.
trainbr	Bayesian regularization.
traincgb	Powell-Beale conjugate gradient backpropagation
traincgf	Fletcher-Powell conjugate gradient backpropagation
traincgp	Polak-Ribiere conjugate gradient backpropagation.
traingd	Gradient descent backpropagation.
traingda	Gradient descent w/adaptive lr backpropagation.
traingdx	Gradient descent w/momentum & adaptive lr backprop.
trainlm	Levenberg-Marquardt backpropagation.
trainoss	One step secant backpropagation.
trainrp	Resilient backpropagation (Rprop)
trainscg	Scaled conjugate gradient backpropagation.

D Characteristic Time Measuring Module

RMS Converter

A precise *True RMS-to-DC Converter* type AD736JNC by Analog Devices is used for smoothing the signal from the preamplifier. It is a high rectification for the AC voltage with low pass filter. The RMS value is defined as the following U_{rms} [Kitchin, 1986]:

$$U_{rms} = \sqrt{\overline{u(t)^2}}$$

The response time constant may be calculated from the value of two capacitors, which are connected to the RMS component. According to the recommendation for general purpose in the data sheet of RMS component [AD736], the 15 µF and 1 µF capacitors are chosen, consequently, the response time is 36 ms. By the selection of these capacitors, the low frequency cut-off (-3 dB) is adjusted to 200 Hz. Thus, the low frequency of vibrations and zero-frequency component are weakened.

Comparators

A dual Comparator type LM393N is applied. Two different reference values are adjusted through 0-50 kΩ potentiometers in the range from 0 to 5 V. Consequently, the first comparator is switched when the first edge of the strongest vibration signal appears higher than the first reference value. The second comparator is switched when the next edge of the strongest vibration signal appears higher than the second reference value.

Microcontroller

The time between the two edges of the comparator outputs is calculated with a microcontroller. A compact 8-bit AVR RISC microcontroller Model ATtiny2313 from Atmel is applied in the circuit. The microcontroller is driven with an external quartz type LF A120K from Rakon. The quartz operates as a clock with a frequency of 4 MHz for a precise timing.

The microcontroller operates mostly in a waiting state and becomes active only after the occurrence of an interrupt or a timer event, which makes a precise time measurement possible. A 16-bit timer in the microcontroller is executed with an adjustable clock pulse. The minimum measurable time t_{min} (resolution) and the maximum measurable time t_{max} are determined

via a selection of prescaler. Selecting a prescaler of 64 and a process of 4 MHz clock thus:

$$t_{\min} = \frac{64}{4MHz} = 16\mu s$$

$$t_{\max,timer} = t_{\min} \cdot 2^{16} = 16\mu s \cdot 65536 = 1.048576s$$

The determination of the characteristic time starts at the beginning of the first comparator signal and stopped at the beginning of the second comparator signal. The characteristic time is always in the range of 500 ms, therefore, the maximum measurable time t_{max} is limited to the half in order to maintain the high accuracy of measurement.

$$t_{\max,mess} = t_{\max,timer} \cdot 0.5 = 524.288ms$$

The interrupt 0 and interrupt 1 at pin INT0 and pin INT1 of the microcontroller are executed by the positive edges of the signal from the two comparators. The “Interrupt 0” is responsible for the time save function and the “Interrupt 1” is for the time calculation. In case of time overflow, the 20mA default value is shown when there is no other values in the save function, otherwise the value is shown as before.

The microcontroller is programmed in C language. The program is based on interrupt and timing. The flow chart of the microcontroller configuration can be seen in Appendix E. The program composed of main three source code files. The first source code file is the main function program. The second source code file serves to declare the variables of the main program. The third source code file contains the control routine for D/A converter (www.mikrocontroller.net).

Transferring Signal

A 12-bit D/A converter type LTC1257 by Linear Technology carries out the measured time as an analogue value. A 100 Ω resistor and 100 nF capacitor are adopted as the recommendation from the datasheet to stabilize the output voltage. The output voltage ranges from 0 to 2.048 V. The resolution of the 12-bit D/A converter is up to

$$\Delta U = \frac{2.048V}{2^{12}} = 500\mu V$$

The current output is obtained from a voltage to current converter type AD694 by Analog Devices. It converts an input voltage from 0 to 2 V in an output current from 4 to 20 mA. The characteristic time may be calculated from the measured output current by

$$t_{char} = \frac{I_{out} - I_{\min}}{I_{\max} - I_{\min}} \cdot t_{\max,mess}$$

However, the output voltage of D/A converter may reach the voltage level of 2.048 V> 2 V, consequently, results in a measuring are maximum of 20.23 mA. Therefore, the characteristic time t_{char} may be obtained from the output current I_{out} with I_{min} = 4mA, I_{max} = 20.23 mA and $t_{max,\ mess}$ = 524.288 ms.

$$t_{char} = \frac{I_{out} - 4mA}{16.23mA} \cdot 524.288ms$$

Power Supply System

A 1-watt DC/DC converter type IA2405S from XP Power is applied for the power supply. This DC converter has an input voltage range of 21.6 V to 26.4 V (DC) and a bipolar output voltage with ±5 V. The bipolar voltage is used for the preamplifier and the RMS module. The microcontroller and the D/A converters are operated with the voltage of -5 V and ground. Whereas, the transmitter requires -5 V and +5 V for driving an additional load resistors.

E Circuit Diagram of the Characteristic Time Measuring Module

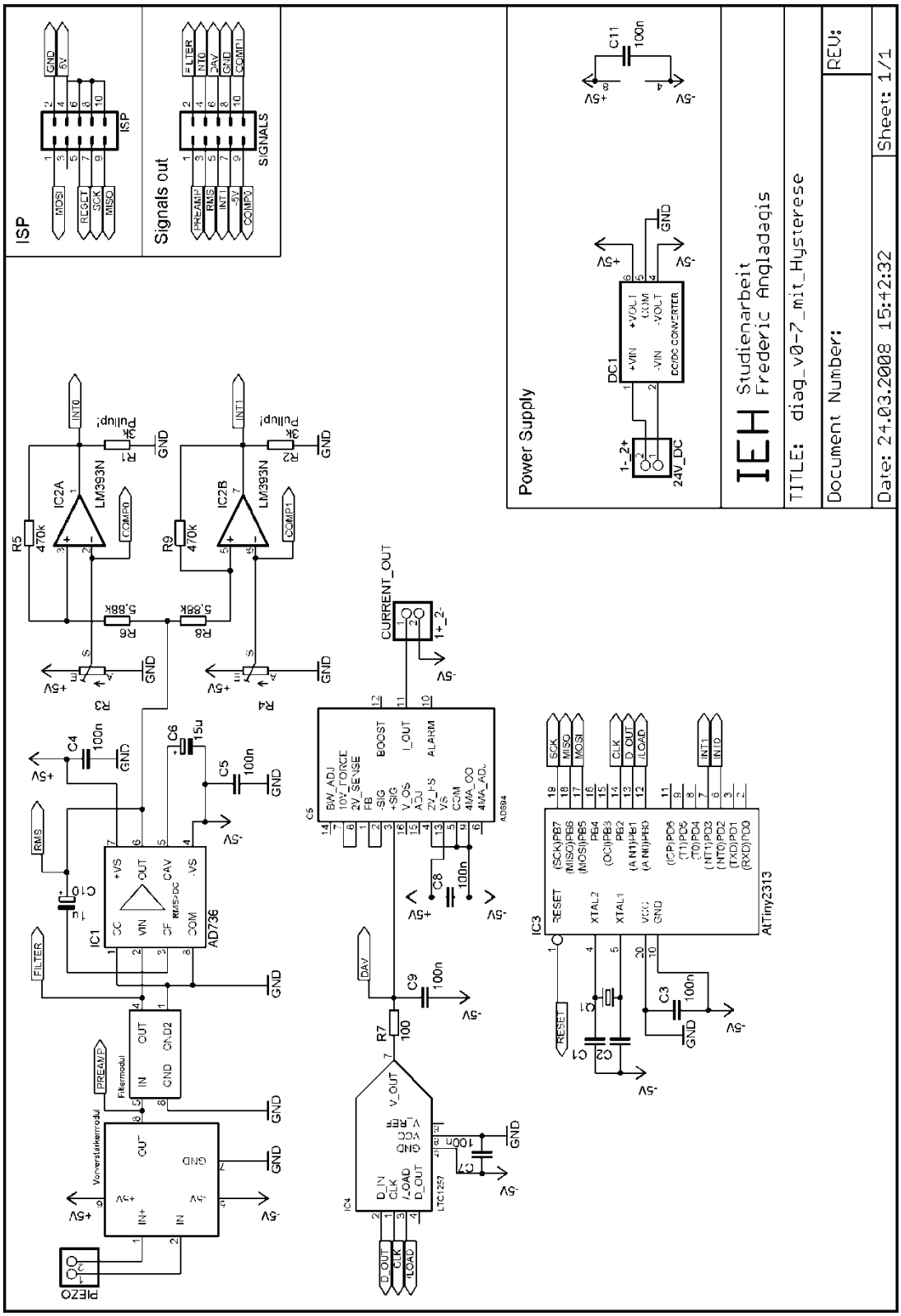

Bibliography

[AD736] **AD736 Data Sheet**
Analog Devices, USA, 2007, Rev. H

[Bengtsson C, 1996] **C. Bengtsson**
Status and Trends in Transformer Monitoring
IEEE Transactions on Power Delivery,
Vol. 11, No.3, July 1996, pp. 1379-1384

[Bengtsson T, 1996] **T. Bengtsson**
Acoustic Diagnosis of Tap Changers
CIGRE Session 1996, Paris, p. 12-101

[Berler, 2005] **Z. Berler, V. Sokolov&V. Prikhodko, D. Bates**
On-line Monitoring of HV Bushings and Current Transformers
Proc. Electrical Insulation Conference and Electrical Manufacturing Expo,
October 23-26, 2005, pp. 61-66

[Chu, 2000] **D. Chu, A. Lux**
On-line Monitoring of Power Transformers and Components: A Review of Key Parameters
Proc. Electrical Insulation Conference and Electrical Manufacturing & Coil Winding Conference, pp. 669-675, 2005

[CIGRE, 1983] **CIGRE Working Group 05**
An International Survey on Failures in Large Power Transformers in Service.
Electra, No. 88, May 1983, pp. 21-42

[Demjanenko et al, 1992] **V. Demjanenko et al**
A Noninvasive Diagnostic Instrument for Power Circuit Breakers
IEEE Transactions on Power delivery,
Vol.7, No.2, April 1992, pp.

[Demuth, 1992] **H. Demuth, M. Beale**
Neural Network Toolbox: For Use with MATLAB,
USA: The Math Works, Inc., 1992.

[Der Houhanessian, 1998] **V. Der Houhanessian**
Measurement and Analysis of Dielectric Response in Oil-Paper Insulation Systems
Dissertation, ETH No. 12832, Zurich, 1998

[Handley, 2001] **B. Handley, M. Redfern, S.White**
On load tap-changer conditioned based maintenance
IEE Proc. –Gener. Transm. Distrib.,
Vol. 148, No.4, July 2001, pp. 296-300

[He, 2000] **Q. He, J. Si, D. J. Tylavsky**
Prediction of Top-Oil Temperature for Transformers Using Neural Networks
IEEE Transactions on Power Delivery,
Vol. 15, No.1, January 2000, pp. 1205-1211

[Hell, 2007] **M. Hell, P. Costa, Jr., F. Gomide**
Recurrent Neurofuzzy Network in Thermal Modeling of Power Transformers
IEEE Transactions on Power Delivery,
Vol. 122, No.2, April 2007, pp. 904-910

[Feinberg, 1979] **R. Feinberg**
Modern Power Transformer Practice
Halsted Press, 1979, pp. 140-141

[Foata, 2000] **M. Foata, R. Beauchemin, C. Rajotte**
On-line Testing of On-load Tap Changers with Portable Acoustic System
Proc. 9th International Conference on Transmission and Distribution Construction, Operation and Live-Line Maintenance,
p. 31C-TRA-1

[Garson, 1998] **G. David Garson**
Neural Networks
An Introductory Guide for Social Scientists
SAGE Publications Ltd, London 1998

[Goosen, 1996] **P. V. Goosen**
Transformer Accessories
CIGRE Session 1996, Paris, pp. 12-104

[Großmann, 2002] **Ekard Großmann**
Akustische Teilentladungsmessung zur Überwachung und Diagnose von Öl/Papier-isolierten Hochspannungsgeräten
Dissertation, University of Stuttgart, Germany, 2002

[IEC 60354, 1991] **IEC 60354**

Loading Guide for Oil-Immersed Power Transformers
International Electrotechnical Commission Standard Geneve, Suisse, 1991

[IEEE Std. C57.91, 1995] **IEEE Std. C57.91**
IEEE Guide for Loading Mineral-Oil-Immersed Transformers, 1995

[Jagers, 2007] **R.N. Jagers, J. Khosa, P.J. De Klerk and C.T. Gaunt**
Transformer Reliability and Condition Assessment in a South African Utility,
Proc. 15th ISH International Symposium on High Voltage Engineering,
Ljubljana, August 2007, p. T6-442

[Kang, 2000] **P. Kang, D. Birtwhistle, J. Daley, D. McCulloch**
Non-Invasive On-Line Condition Monitoring of On-Load Tap Changers
IEEE Power Engineering Society Winter Meeting, 23-27 Jan 2000, Vol.3, pp. 2223-2228

[Kang, 2000] **P. Kang, D. Birtwhistle**
On-line Condition Monitoring of Tap Changer – Field Experience
Proc. 16th International Conference and Exhibition on Electircity Distribution, Part 1 : Contributions, 2001, paper no. 1.52

[Kay, 1997] **A.G. Kay**
Tap changer Condition Monitoring and Protection System
IEE Colloq. Condition Monitoring and Life Assessment in Power Transformers,
1994, pp. 8/1-8/3

[Kay, 1997] **A.G. Kay**
The monitoring and protection of on load tap changers
IEE Colloq. Condition Monitoring of Large Machines and Power Transformers,
1997, pp. 7/1-7/3

[Kitchin, 1986] **C. Kitchin, L. Counts**
RMS to DC Conversion Application Guide
Analog Devices USA 1986, 2nd Edition

[Kogan, 1988] **V.I. Kogan, J.A. Fleeman, J.H. Provanzana,**
Failure Analysis of EHV Transformers
IEEE Transactions on Power Delivery,
Vol. 3, No. 2, April 1988, pp. 672-683

[Krämer, 1996] **A. Krämer, J. Meyer, J. A. J. Pettinga**
Monitoring Methods for On-load Tap-changers.
An Overview and Future Perspectives
CIGRE Session 1996, Paris, p. 12-108

[Krämer, 2000] **A. Krämer**
On-load Tap-Changers for Power Transformers
Operation Principles, Applications and Selection
Regensburg: MR-Publication, 2000, pp. 10-11

[Krüger, 2007] **M. Krüger, A. Kraetge**
New Diagnostic Tools for Power Transformers
Proc. 15th ISH International Symposium on High Voltage Engineering,
Ljubljana, August 2007, p. T10-177, 2007

[Küchler, 1996] **A. Küchler**
Hochspannungstechnik, Grundlagen – Technologie – Anwendungen
VDI-Verlag Düsseldorf, 1996

[Lachman, 2000] **M. F. Lachman, W. Walter, P. A. Guggenberg**
On-line Dianostics of High-Voltage Bushings and Current Transformers Using the Sum Current Method
IEEE Transactions on Power Delivery,
Vol. 15, No. 1, January 2000, pp. 155-162

[Lesieutre, 1997] **B.C. Lesieutre, W.H. Hagman, J.L. Kirtley Jr.**
An Improved Transformer Top Oil Temperature Model for Use in An On-Line Monitoring and Diagnostic System
IEEE Transactions on Power Delivery,
Vol. 12, No. 1, January 1997, pp. 249-256

[Leibfried, 1998] **T. Leibfried**
Online Monitors Keep Transformers in Service
IEEE Transactions on Computer Applications in Power, Vol. 11, No. 3, July 1998, pp. 36-42

[Leibfried, 1999] **T. Leibfried**
Online Monitoring of Power Transformers -

System Technology and Data Evaluation
Proc. 11th ISH International Symposium on High Voltage Engineering,
London, August 1999, p. 5.184.P5

[Leibschner, 2007] **M. Liebschner, K. Boehm, A. Reumann**
On-line Monitoring of Capacitance and Dissipation Factor of High Voltage Bushings at Service Temperature,
Proc. 15th ISH International Symposium on High Voltage Engineering,
Ljubljana, August 2007, p. T7-490

[Mackay1, 1992] **D. J. C. Mackay**
Bayesian Interpolation
Neural Computation, Vol. 4(3), pp. 415-447, 1992

[Mackay2, 1992] **D. J. C. Mackay**
A Practical Bayesian Framework for Backpropagation Networks
Neural Computation, Vol. 4(3), pp. 448-472, 1992

[Markalous, 2006] **S. M. Markalous**
Detection and Location of Partial Discharges in Power Transformers using acoustic and electromagnetic signals
Dissertation, University of Stuttgart,
Germany, 2006

[Marwitz, 1992] **K. Marwitz, D. Gorgius**
Technical Diagnostics on Tap Changers for Large Power Transformers
Proc. 8th International IMEKO Symposium on Technical Diagnostics, pp. 587-593

[Minhas, 1997] **MSA Minhas, PJ de Klerk, JP Reynders**
A Study of Failure Modes of Large Power System Transformers
Proc. 10th ISH International Symposium on High Voltage Engineering,
Montreal, August 1997, p. 3517

[Minhas, 1999] **MSA Minhas, JP Reynders, PJ de Klerk**
Failures in Power System Transformers and Appropriate Monitoring Techniques
Proc. 11th ISH International Symposium on High Voltage Engineering,

London, August 1999, p. 1.94.S23

[Moller, 1993] **M. F. Moller**
A Scaled Conjugate Gradient Algorithm for Fast Supervised Learning
Neural Networks, Vol. 6, 1993, pp. 525-533

[Pradhan, 2004] **M. K. Pradhan, T.S. Ramu**
On-line Monitoring of Temperature in Power Transformers using Optimal Linear Combination of ANNs
Proc. IEEE International Symposium on Electrical Insulation, 2004, pp. 70-73

[Pylvänäinen, 2007] **J. K. Pylvänäinen, K. Nousiainen, P. Verho**
Studies to Utilize Loading Guides and ANN for Oil-Immersed Distribution Transformer Condition Monitoring
IEEE Transactions on Power Delivery,
Vol. 22, No. 1, January 2007, pp. 201-207

[Runde et al, 1992] **M. Runde et al,**
Acoustic Diagnosis of high voltage circuit-breakers
IEEE Transactions on Power delivery,
Vol.7, No.3, July 1992, pp.

[Simas F., 2005] **E. F. Simas F., L. A. L. de Almeida, Antonio C. de C. Lima**
Vibration Monitoring of On-Load Tap Changers Using A Genetic Algorithm
Proc. Instrumentation and Measurement Technology Conference, Ottawa, 17-19 May 2005

[Stirl, 2004] **T. Stirl**
Online-Monitoring von kapazitiv gesteuerten Durchführungen an Leistungstransformatoren
ETG Diagnostik elektrotechnischer Betriebsmittel, Köln, 9-10 March 2004

[Stirl, 2006] **T. Stirl, R. Skrzypek, S. Tenbohlen, R. Vilaithong**
On-line Condition Monitoring and Diagnosis for Power Transformers their Bushings, Tap Changer and Insulation system
Proc. CMD Internal Conference on Condition Monitoring and Diagnosis, p. 661, 2006

[Susa, 2005] **D. Susa, M. Lehtonen, H. Nordman**
Dynamic Thermal Modelling of Power Transformers
IEEE Transactions on Power Delivery,
Vol. 20, No. 1, January 2005, pp. 197-204

[Swift, 2001] **G. Swift, T. S. Molinski, W. Lehn**
A fundamental Approach to Transformer Thermal Modelling
IEEE Transactions on Power Delivery,
Vol. 16, No. 2, April 2001, pp. 171-180

[Tang, 2004] **W.H. Tang, Q.H. Wu, Z.J. Richardson**
A simplified Transformer Thermal Model Based on Thermal-Electric Analogy
IEEE Transactions on Power Delivery,
Vol. 19, No. 3, July 2004, pp. 1112-1119

[Tenbohlen, 1999] **S. Tenbohlen, M. Schäfer**
Beurteilung der Überlastbarkeit von Transformatoren mit online Monitoringsystemen
Elektrizitätswirtschaft,
Jg. 99 (2000), H. 1-2, S. 26-32

[Tenbohlen[1], 2000] **S. Tenbohlen, F. Figel**
On-line Condition Monitoring of Power Transformers
IEEE Power Engineering Society Winter Meeting
Vol. 3, 23-27 Jan 2000, pp. 2211-2216

[Tenbohlen[2], 2000] **S. Tenbohlen, H. Borsi, U. Sundermann, H. Matthes**
Enhanced Diagnosis of Power Transformers using On- and Off-line Methods: Results, Examples and Future Trends
CIGRE Session 2000, Paris, p. 12-204

[Tenbohlen, 2001] **S. Tenbohlen, T. Stirl, M. Stach**
Assessment of Overload Capacity of Power Transformers by On-line Monitoring Systems
IEEE Power Engineering Society Winter Meeting
Vol. 1, 28 Jan-1 Feb 2001, pp. 329-334

[Tenbohlen, 2003] **S. Tenbohlen, T. Stirl, M. Rösner**
Benefit of Sensors for On-line Monitoring Systems for Power Transformers
Proc. of the 2nd European Conference on HV & MV

Substation Equipment, Lyon, November 2003

[Trindade, 2005] **M. B. Trindade, H. J. A. Martins and A. F. Cadilhe**
On-Load Tap-Changer Diagnosis Based on Acoustic Emission Technique
Proc. 14th ISH International Symposium on High Voltage Engineering, Beijing,
August 2005, p. G-033

[Tylavsky, 2000] **D.J.Tylavsky, Q. He, G.A. McCulla, J.R. Hunt**
Sources of Error in Substation Distribution Transformer Dynamic Thermal Modeling
IEEE Transaction on Power Delivery,
Vol. 15, No. 1, January 2000, pp. 178-185

[Tylavsky, 2000] **D.J.Tylavsky, Q. He, G.A. McCulla, J.R. Hunt**
Transformer Top-oil Temperature Modelling and Simulation
IEEE Transaction on Industry Applications,
Vol. 36, No. 5, September 2000, pp. 1219-1225

[Vilaithong, 2005] **R. Vilaithong, S. Tenbohlen, T. Stirl**
Improved Top-oil Temperature Model for Unsteady-State Conditions of Power Transformers
Proc. 14th ISH International Symposium on High Voltage Engineering, Beijing, August 2005, p. F-42

[Vujovic, 1994] **P. Vujovic, R. K. Fricker**
Development of an On-line Continuous Tan δ Monitoring System
Conference Record of the IEEE International Symposium on Electrical Insulation, pp. 50-53

[Wang1, 2000] **Z. Wang, Y. Liu, P. J. Griffin**
Neural Net and Expert System Diagnose Transformer Faults
IEEE Computer Applications in Power
Vol. 13, No. 1, January 2000, pp.50-55

[Wang2, 2000] **Z. Wang, Y. Liu, P. J. Griffin**
Artificial Intelligence in OLTC Fault Diagnosis Using Dissolved Gas-In-Oil Information
IEEE Power Engineering Society Summer Meeting, Vol. 4, 16-20 July 2000, pp. 2422-2427

[Wang, 2001] **P. Wang, M. R. Raghuveer**
A Digital Technique for the On-line Measurement of Dissipation Factor and Capacitance
IEEE Transaction on Dielectrics and Electrical Insulation, Vol. 8, No. 2, April 2001, pp. 228-232

[Wang, 2002] **M. Wang, A. J. Vandermaar, K.D. Srivastava**
Review of Condition Assessment of Power Transformers in Service
IEEE Insulation Magazine,
Vol. 18, No. 6, Nov :Dec. 2002, pp. 12-25

[Ward, 2001] **B. H. Ward**
A Survey of New Techniques in Insulation Monitoring of Power Transformers
IEEE Electrical Insulation Magazine,
Vol. 17, No. 3, May-June 2001, pp. 16-23

[Wright, 1997] **S. E. Wright, J. P. Bushby**
Development of A Diagnostic System for Non-continuously Operating Machines
Proc. 14th International Conference and Exhibition on Electricity Distribution, p. 1.14.1

[Xie, 2002] **M. Xie, T. Ngee Goh**
Statistical Models and Control Charts for High Quality Processes, Springer; 1 edition, 2002

[Xinhong, 2001] **H. Xinhong, L. Ruijin, H. Xuesong, S. Caixin**
Research on the On-line Monitoring of Dissipation Factor by Using Synthetic Relative Measuring Method
2001 Annual Report Conference on Electrical Insulation and Dielectric Phenomena,
pp. 118-122

[Zhu, 1988] **G. Zhu, J. Wang**
Measurement of tg δ and C of Single Phase Electrical Apparatus of Capacitive Insulation under Operating Voltage
Proc. 1988, Second International Conference on Properties and Applications of Dielectric Materials, 12-16 Sep. 1998, Vol. 2, pp. 701-703